Supporting Information

Dual phosphorescent emissions from conformers of iridium complex rotors.

Yu-Ting Hsu,[1] Chandni Bhagani,[1] Juan A. Aguilar,[1] Mark A. Fox,[1] Dmitry Yufit,[1] Ross Davidson,[1]* Andrew Beeby.[1]*

[1]Department of Chemistry, Durham University, South Rd, Durham, DH1 3LE, UK

*To whom correspondence should be addressed. Email: Ross Davidson (ross.davidson@durham.ac.uk) and Andrew Beeby (andrew.beeby@durham.ac.uk).

Table of Contents

S1. Synthetic details

General details. Proton and carbon-13 NMR spectra were recorded in deuterated solvent solutions on either \ Varian VNMRS-700 or -500 spectrometer and referenced against solvent resonances (^{1}H, $CHDCl_2$ = 5.33 ppm; ^{13}C, CD_2Cl_2 = 53.4 ppm). Proton and carbon-13 NMR peaks were assigned with the aid of 2D ^{1}H–^{1}H COSY/NOESY and ^{1}H–^{13}C correlation (HSQC and HMBC) NMR spectra.

Atmospheric pressure solids analysis probe (ASAP) ionization mass spectra were obtained using an LCT Premier XE mass spectrometer and an Acquity® UPLC from Waters Ltd at 350°C. Electrospray mass spectra (ES) data were recorded on a TQD mass spectrometer (Waters Ltd, UK) in acetonitrile or MALDI TOF MS data were recorded on a Bruker Autoflex II ToF/ToF. Microanalyses were performed by the Elemental Analysis Service, London Metropolitan University, UK.

The chemicals, 4-(triisopropylsilylethynyl)pyridine (**py-≡-TIPS**),[S1] 4-(trimethylsilylethynyl)pyridine (**py-≡-TMS**), [S2] di-μ-chlorotetrakis[2-(2-pyridinyl-κ*N*)phenyl-κ*C*]di-iridium [{Ir(ppy)$_2$(μ-Cl)}$_2$] [S3] were prepared according to literature methods. Other chemicals used in this study were purchased commercially.

4-(triethylsilylethynyl)pyridine (py-≡-TES). Triethylsilylacetylene (1.96 mL, 1.54 g, 11 mmol) was added to a solution containing 4-bromopyridinium chloride (2.00 g, 10.41 mmol), $PdCl_2(PPh_3)_2$ (700 mg, 1 mmol), CuI (190 mg, 1 mmol), Et_3N (5 mL) in THF (50 mL) degassed by three freeze-pump-thaw cycles. The solution was heated to reflux for 16 hours before the solvent was removed *in vacuo*. Purification was achieved using silica chromatography, using a solvent gradient from neat DCM to DCM:Et_2O (8:2), to give a yellow oil. **Yield**: 1.86 g (82%). **^{1}H NMR** (700 MHz; CD_2Cl_2): δ_H 8.62 (br, 2H, H2), 7.34 (br, 2H, H3), 1.05 (td, $^{3}J_{HH}$ = 7.9 Hz, $^{4}J_{HH}$ = 1.1 Hz, 9H, H_d), 0.71 (qd, $^{3}J_{HH}$ = 7.9 Hz, $^{4}J_{HH}$ = 1.1 Hz, 6H, H_c) ppm. **^{13}C{^{1}H} NMR** (176 MHz; CD_2Cl_2): δ_C 149.6 (C2), 131.0 (C3), 125.9 (C4), 103.2 (C^b), 97.3 (C^a), 7.1 (C^d), 4.1 (C^c) ppm. **MS(ASAP)**: m/z 218.122 $[M+H]^+$.

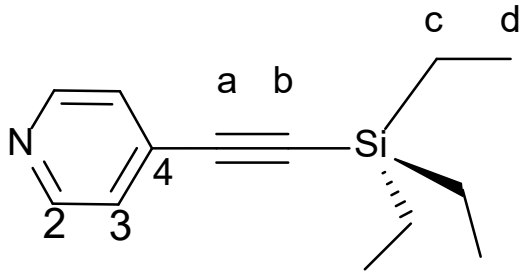

General synthesis of Ir(ppy)$_2$(pyX)Cl complexes

To a degassed solution of {Ir(ppy)$_2$Cl}$_2$ (200 mg, 0.187 mmol) in anhydrous dichloromethane (30 mL), the alkynyl pyridine (0.410 mmol) was added and the solution was stirred for 1 h at 30 °C. The solvent was removed in vacuo to leave a yellow residue. The solid was washed with hexane prior to being

purified on a silica column eluted by DCM to afford a bright yellow solid. Crystals were grown by evaporation of a DCM/MeOH solution.

Ir(ppy)$_2$(py-≡-TIPS)Cl (**1**). **Yield**: 246 mg (83%). **^{1}H NMR** (700 MHz; CD_2Cl_2, 25°C): δ_H 9.85 (d, $^3J_{HH}$ = 5.7 Hz, 1H, H^{B6}), 8.92 (v.br., FWHH = 400 Hz, 2H, $H^{E2/E2´}$), 8.11 (d, $^3J_{HH}$ = 5.6 Hz, 1H, H^{D6}), 7.95 (d, $^3J_{HH}$ = 8.1 Hz, 1H, H^{D3}), 7.80 (ddd, $^3J_{HH}$ = 7.3 Hz, $^3J_{HH}$ = 5.7 Hz, $^4J_{HH}$ = 1.6 Hz, 1H, H^{D4}), 7.79 (d, 1H, H^{B3}), 7.74 (ddd, $^3J_{HH}$ = 7.3 Hz, $^3J_{HH}$ = 5.7 Hz, $^4J_{HH}$ = 1.6 Hz, 1H, H^{B4}), 7.62 (dd, $^3J_{HH}$ = 7.8 Hz, $^4J_{HH}$ = 1.3 Hz, 1H, H^{C3}), 7.56 (dd, $^3J_{HH}$ = 7.8 Hz, $^4J_{HH}$ = 1.3 Hz, 1H, H^{A3}), 7.25 (ddd, $^3J_{HH}$ = 7.4 Hz, $^3J_{HH}$ = 5.8 Hz, $^4J_{HH}$ = 1.6 Hz, 1H, H^{B5}), 7.24 (br, FWHH = 16 Hz, 2H, $H^{E3/E3'}$), 7.09 (ddd, $^3J_{HH}$ = 7.3 Hz, $^3J_{HH}$ = 5.7 Hz, $^4J_{HH}$ = 1.4 Hz, 1H, H^{D5}), 6.91 (td, $^3J_{HH}$ = 7.4 Hz, $^4J_{HH}$ = 1.4 Hz, 1H, H^{A4}), 6.86 (td, $^3J_{HH}$ = 7.4 Hz, $^4J_{HH}$ = 1.4 Hz, 1H, H^{C4}), 6.81 (td, $^3J_{HH}$ = 7.4 Hz, $^4J_{HH}$ = 1.3 Hz, 1H, H^{A5}), 6.75 (td, $^3J_{HH}$ = 7.4 Hz, $^4J_{HH}$ = 1.3 Hz, 1H, H^{C5}), 6.34 (dd, $^3J_{HH}$ = 7.7 Hz, $^4J_{HH}$ = 1.4 Hz, 1H, H^{A6}), 6.18 (dd, $^3J_{HH}$ = 7.6 Hz, $^4J_{HH}$ = 1.5 Hz, 1H, H^{C6}), 1.11 (pseudo singlet, 21H, H^c+H^d) ppm. **^{13}C{^{1}H} NMR** (176 MHz; CD_2Cl_2, 25°C): δ_C 168.2 (C^{D2}), 167.7 (C^{B2}), 151.3 (br, FWHH = 12 Hz, C^{E2} + $C^{E2´}$), 150.8 (C^{B6}), 150.5 (C^{A1}), 149.0 (C^{D6}), 148.4 (C^{C1}), 144.1 (C^{C2} + C^{A2}), 137.1 (C^{B4}), 136.8 (C^{D4}), 132.2 (C^{E4}), 132.0 (C^{C6}), 131.3 (C^{A6}), 130.1 (C^{A5}), 129.1 (C^{C5}), 127.4 (br, FWHH = 3 Hz, C^{E3} + $C^{E3´}$), 124.2 (C^{A3}), 123.7 (C^{C3}), 122.4 (C^{B5}), 122.0 (C^{D5}), 121.2 (C^{A4}), 121.1 (C^{C4}), 119.1 (C^{D3}), 118.4 (C^{B3}), 103.2 (C^b), 100.2 (C^a), 18.3 (C^d), 11.1 (C^c) ppm. **HRMS (ES+)**: m/z 760.2719 $[M\text{-}Cl]^+$. **Anal. Calc.** for $C_{38}H_{41}ClIrN_3Si$: C, 57.37; H, 5.20; N, 5.28 %. **Found**: C, 57.19; H, 5.30; N, 5.37 %.

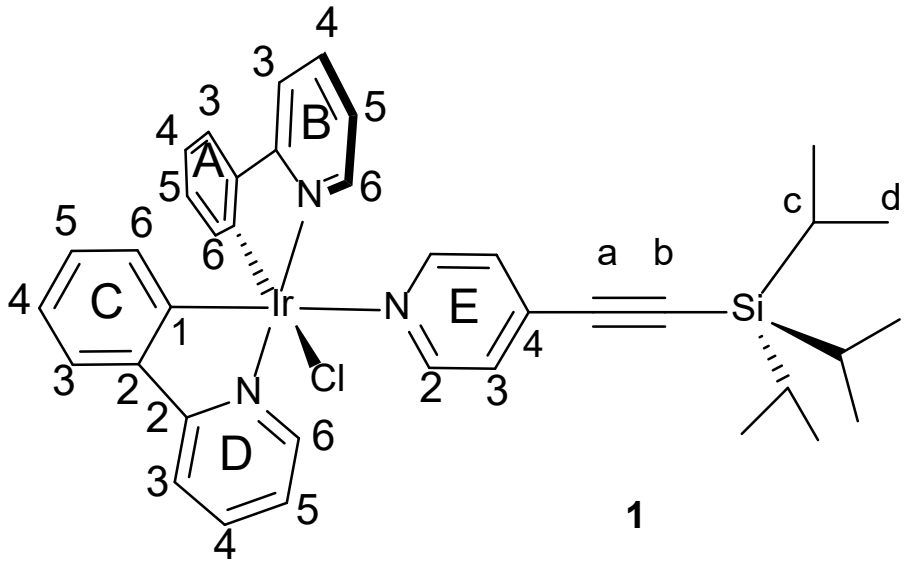

1

Ir(ppy)$_2$(py-≡-TES)Cl (**2**). **Yield**: 89 mg (32%). **^{1}H NMR** (700 MHz; CD_2Cl_2, 25°C): δ_H 9.83 (d, $^3J_{HH}$ = 5.5 Hz, 1H, H^{B6}), 8.92 (v.br., FWHH = 500 Hz, 2H, $H^{E2/E2´}$), 8.09 (d, $^3J_{HH}$ = 5.6 Hz, 1H, H^{D6}), 7.94 (d, $^3J_{HH}$ = 8.2 Hz, 1H, H^{D3}), 7.80 (ddd, $^3J_{HH}$ = 7.3 Hz, $^3J_{HH}$ = 5.7 Hz, $^4J_{HH}$ = 1.6 Hz, 1H, H^{D4}), 7.79 (d,

1H, H^{B3}), 7.73 (ddd, $^3J_{HH}$ = 7.3 Hz, $^3J_{HH}$ = 5.7 Hz, $^4J_{HH}$ = 1.6 Hz, 1H, H^{B4}), 7.61 (d, $^3J_{HH}$ = 7.7 Hz, 1H, H^{C3}), 7.55 (d, $^3J_{HH}$ = 7.7 Hz, 1H, H^{A3}), 7.24 (ddd, $^3J_{HH}$ = 7.4 Hz, $^3J_{HH}$ = 5.8 Hz, $^4J_{HH}$ = 1.6 Hz, 1H, H^{B5}), 7.22 (br, FWHH = 16 Hz, 2H, $H^{E3/E3´}$), 7.08 (ddd, $^3J_{HH}$ = 7.3 Hz, $^3J_{HH}$ = 5.7 Hz, $^4J_{HH}$ = 1.4 Hz, 1H, H^{D5}), 6.90 (td, $^3J_{HH}$ =7.5 Hz, $^4J_{HH}$ = 1.2 Hz, 1H, H^{A4}), 6.85 (td, $^3J_{HH}$ = 7.4 Hz, $^4J_{HH}$ = 1.2 Hz, 1H, H^{C4}), 6.80 (td, $^3J_{HH}$ = 7.4 Hz, $^4J_{HH}$ = 1.4 Hz, 1H, H^{A5}), 6.74 (td, $^3J_{HH}$ = 7.4 Hz, $^4J_{HH}$ = 1.3 Hz, 1H, H^{C5}), 6.33 (dd, $^3J_{HH}$ = 7.8 Hz, $^4J_{HH}$ = 1.2 Hz, 1H, H^{A6}), 6.16 (dd, $^3J_{HH}$ = 7.8 Hz, $^4J_{HH}$ = 1.2 Hz, 1H, H^{C6}), 1.01 (t, $^3J_{HH}$ = 7.9 Hz, 9H, H_c), 0.67 (q, $^3J_{HH}$ = 7.9 Hz, 6H, H_d) ppm. **$^{13}C\{^1H\}$ NMR** (176 MHz; CD_2Cl_2, 25°C): δ_C 168.1 (C^{D2}), 167.7 (C^{B2}), 151.3 (br, FWHH = 17 Hz, $C^{E2} + C^{E2´}$), 150.8 (C^{B6}), 150.4 (C^{A1}), 149.0 (C^{D6}), 148.3 (C^{C1}), 144.1 ($C^{C2} + C^{A2}$), 137.1 (C^{B4}), 136.8 (C^{D4}), 132.1 (C^{E4}), 132.0 (C^{C6}), 131.3 (C^{A6}), 130.1 (C^{A5}), 129.1 (C^{C5}), 127.4 (br, FWHH = 3 Hz, $C^{E3} + C^{E3´}$), 124.2 (C^{A3}), 123.7 (C^{C3}), 122.4 (C^{B5}), 122.0 (C^{D5}), 121.2 (C^{A4}), 121.1 (C^{C4}), 119.1 (C^{D3}), 118.4 (C^{B3}), 102.3 (C^b), 101.0 (C^a), 7.1 (C^d), 4.0 (C^c) ppm. **MS(MALDI)**: m/z 751.2 $[M]^+$, 536.0 $[M\text{-pyCCTES}]^+$, 718.4 $[M\text{-Cl}]^+$. **Anal. Calc.** for $C_{35}H_{35}ClIrN_3Si$: C, 55.80; H, 4.68; N, 5.58 %. **Found**: C, 55.65; H, 4.65; N, 5.54 %.

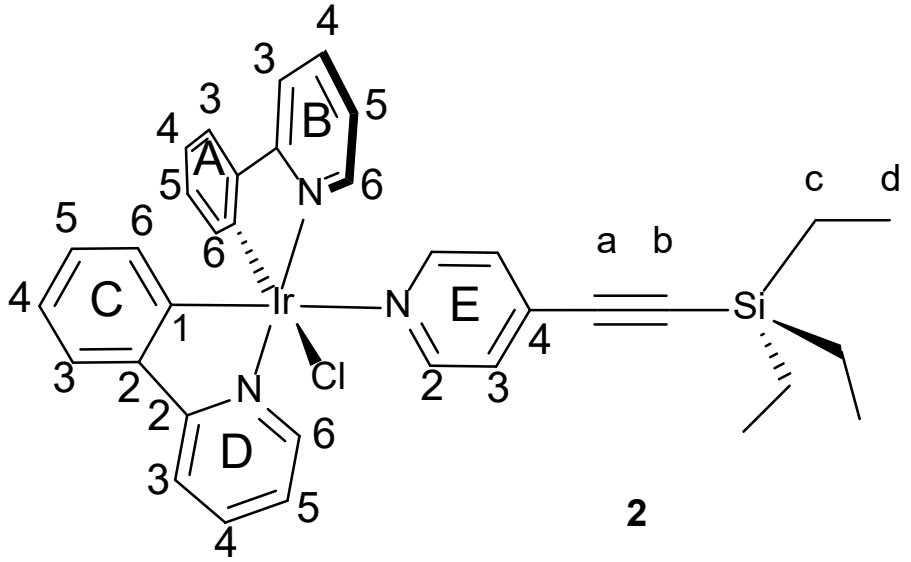

2

Ir(ppy)$_2$(py-≡-TMS)Cl (3). Yield: 60 mg (23%). **^1H NMR** (700 MHz; CD_2Cl_2, 25°C): δ_H 9.83 (d, $^3J_{HH}$ = 5.8 Hz, 1H, H^{B6}), 8.92 (v.br., FWHH = 300 Hz, 2H, $H^{E2/E2'}$), 8.08 (d, $^3J_{HH}$ = 5.8 Hz, H^{D6}), 7.94 (d, $^3J_{HH}$ = 8.2 Hz, 1H, H^{D3}), 7.80 (ddd, $^3J_{HH}$ = 7.3 Hz, $^3J_{HH}$ = 5.7 Hz, $^4J_{HH}$ = 1.6 Hz, 1H, H^{D4}), 7.79 (d, 1H, H^{B3}), 7.73 (ddd, $^3J_{HH}$ = 7.3 Hz, $^3J_{HH}$ = 5.7 Hz, $^4J_{HH}$ = 1.6 Hz, 1H, H^{B4}), 7.61 (d, $^3J_{HH}$ = 7.9 Hz, 1H, H^{C3}), 7.55 (d, $^3J_{HH}$ = 7.7 Hz, 1H, H^{A3}), 7.24 (ddd, $^3J_{HH}$ = 7.4 Hz, $^3J_{HH}$ = 5.8 Hz, $^4J_{HH}$ = 1.6 Hz, 1H, H^{B5}), 7.21 (br, FWHH = 16 Hz, 2H, $H^{E3/E3'}$), 7.08 (ddd, $^3J_{HH}$ = 7.3 Hz, $^3J_{HH}$ = 5.7 Hz, $^4J_{HH}$ = 1.5 Hz, 1H, H^{D5}), 6.90 (td, $^3J_{HH}$ = 7.5 Hz, $^4J_{HH}$ = 2.0 Hz, 1H, H^{A4}), 6.85 (td, $^3J_{HH}$ = 7.5 Hz, $^4J_{HH}$ = 2.0 Hz, 1H, H^{C4}), 6.80 (td, $^3J_{HH}$ = 7.5 Hz, $^4J_{HH}$ = 2.0 Hz, 1H, H^{A5}), 6.74 (td, $^3J_{HH}$ = 7.5 Hz, $^4J_{HH}$ = 2.0 Hz, 1H, H^{C5}), 6.33 (d, $^3J_{HH}$ = 7.6 Hz, 1H, H^{A6}), 6.16 (d, $^3J_{HH}$ = 7.7 Hz, 1H, H^{C6}), 0.23 (s, 9H, H^c) ppm. **$^{13}C\{^1H\}$ NMR** (176 MHz; CD_2Cl_2,

25°C): δ_C 168.1 (C^{D2}), 167.7 (C^{B2}), 151.3 (br, FWHH = 16 Hz, $C^{E2} + C^{E2'}$), 150.8 (C^{B6}), 150.4 (C^{A1}), 149.0 (C^{D6}), 148.3 (C^{C1}), 144.1 ($C^{C2} + C^{A2}$), 137.1 (C^{B4}), 136.8 (C^{D4}), 132.1 (C^{E4}), 132.0 (C^{C6}), 131.3 (C^{A6}), 130.1 (C^{A5}), 129.1 (C^{C5}), 127.3 (br, FWHH = 3 Hz, $C^{E3} + C^{E3'}$), 124.2 (C^{A3}), 123.7 (C^{C3}), 122.4 (C^{B5}), 122.0 (C^{D5}), 121.2 (C^{A4}), 121.1 (C^{C4}), 119.1 (C^{D3}), 118.3 (C^{B3}), 103.1 (C^{b}), 100.8 (C^{a}), -0.89 (C^{c}) ppm. **MS(MALDI)**: m/z 710.0 $[M]^+$, 536.0 $[M\text{-pyCCTMS}]^+$. **Anal. Calc.** for $C_{32}H_{29}ClIrN_3Si \cdot ¼CH_2Cl_2$: C, 52.87; H, 4.06; N, 5.74 %. **Found**: C, 52.85; H, 4.14; N, 5.54 %.

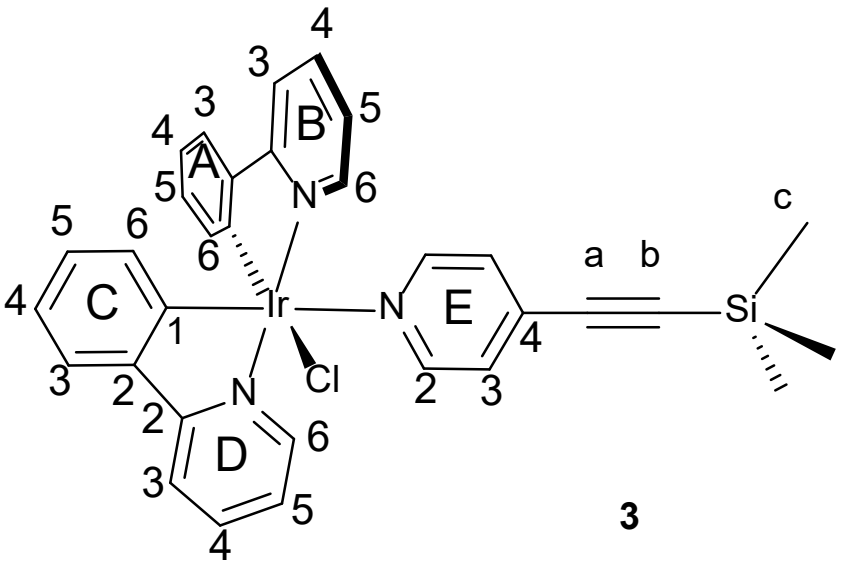

3

S2. Room temperature NMR spectra of new compounds

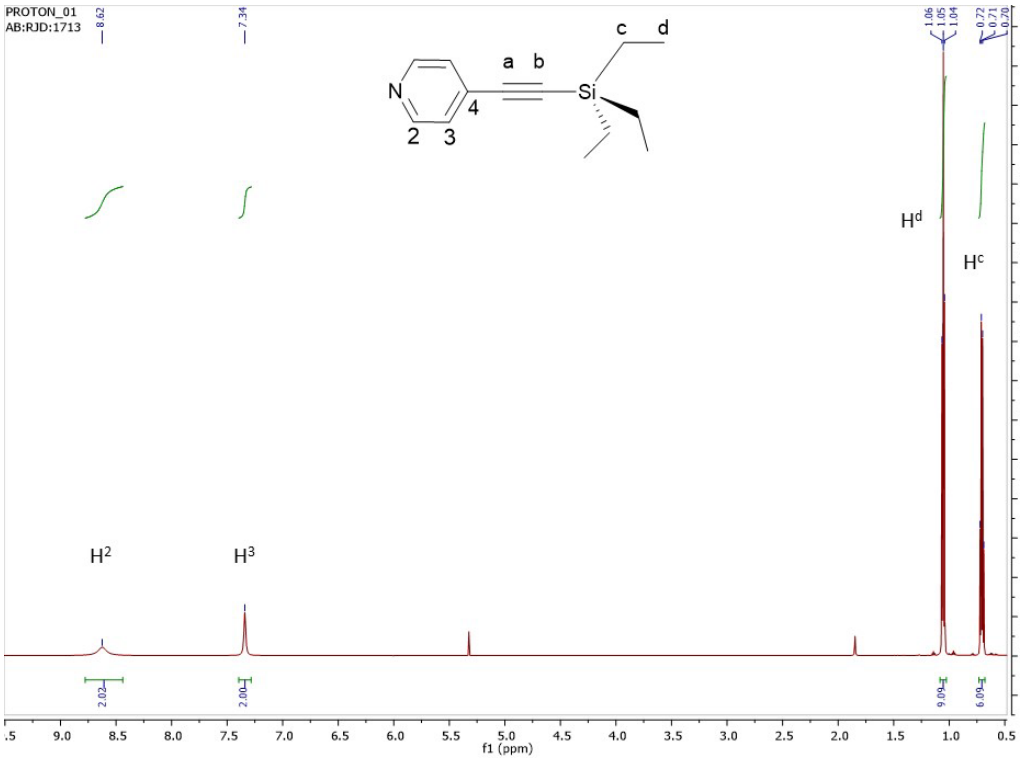

Figure S1. ^{1}H NMR spectrum of **py-≡-TES**, recorded in CD_2Cl_2 at 25°C.

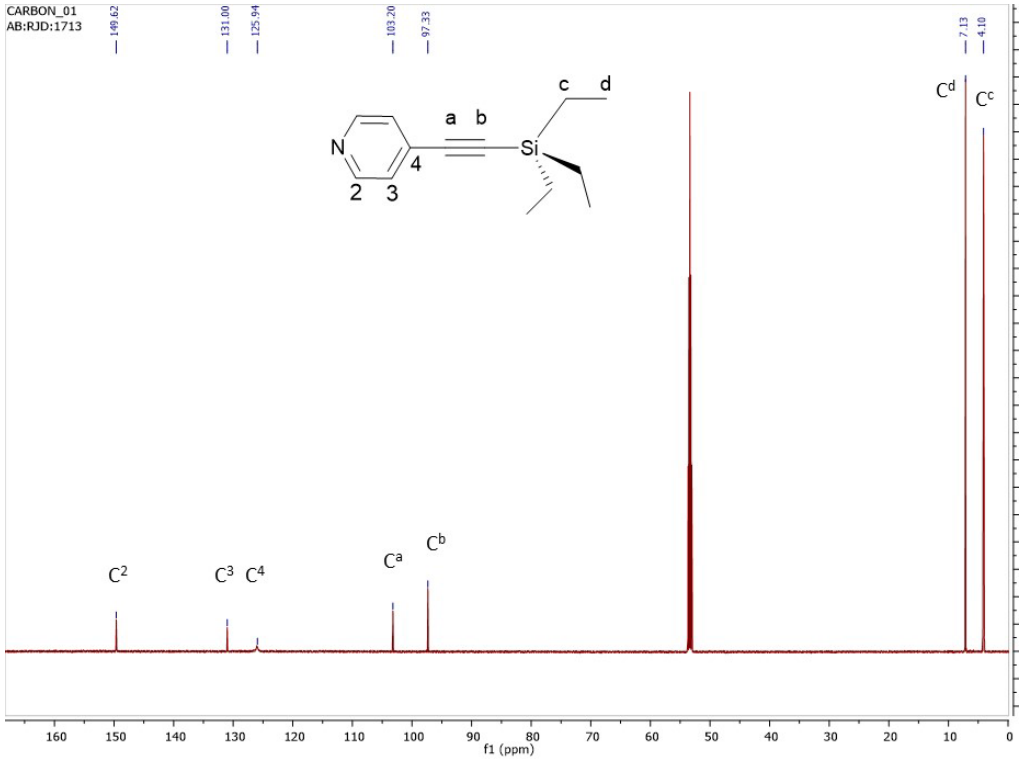

Figure S2. $^{13}C\{^{1}H\}$ NMR spectrum of **py-≡-TES**, recorded in CD_2Cl_2 at 25°C.

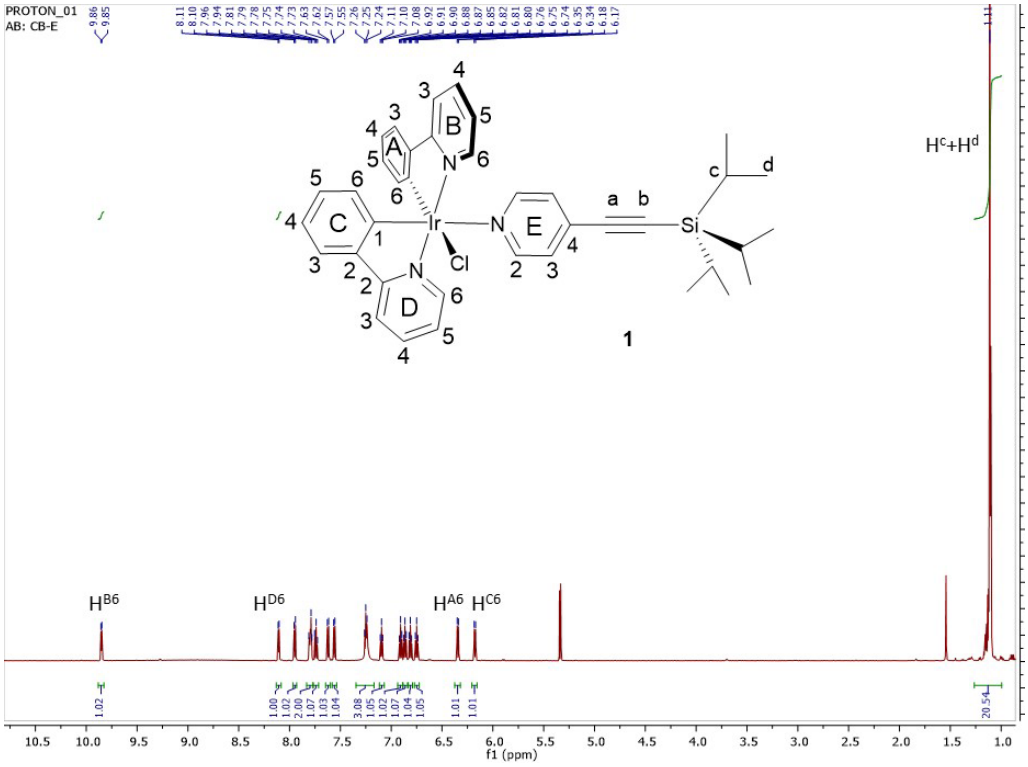

Figure S3a. ^{1}H NMR spectrum of **1**, recorded in CD_2Cl_2 at 25°C.

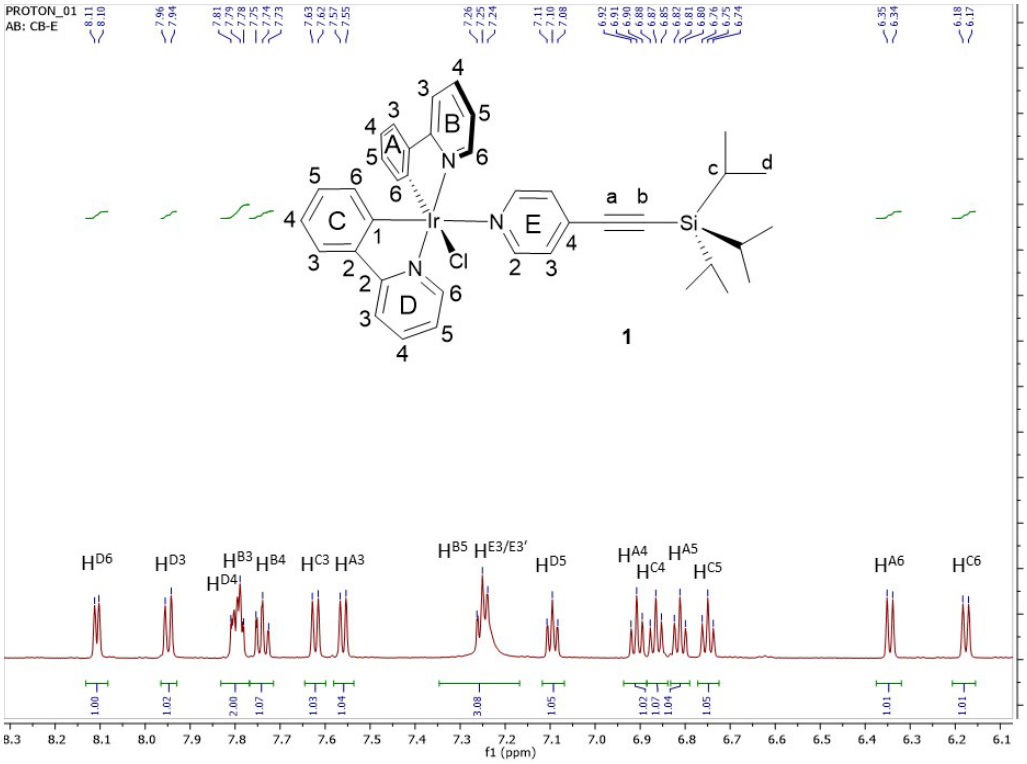

Figure S3b. ^{1}H NMR spectrum of **1**, recorded in CD_2Cl_2 at 25°C.

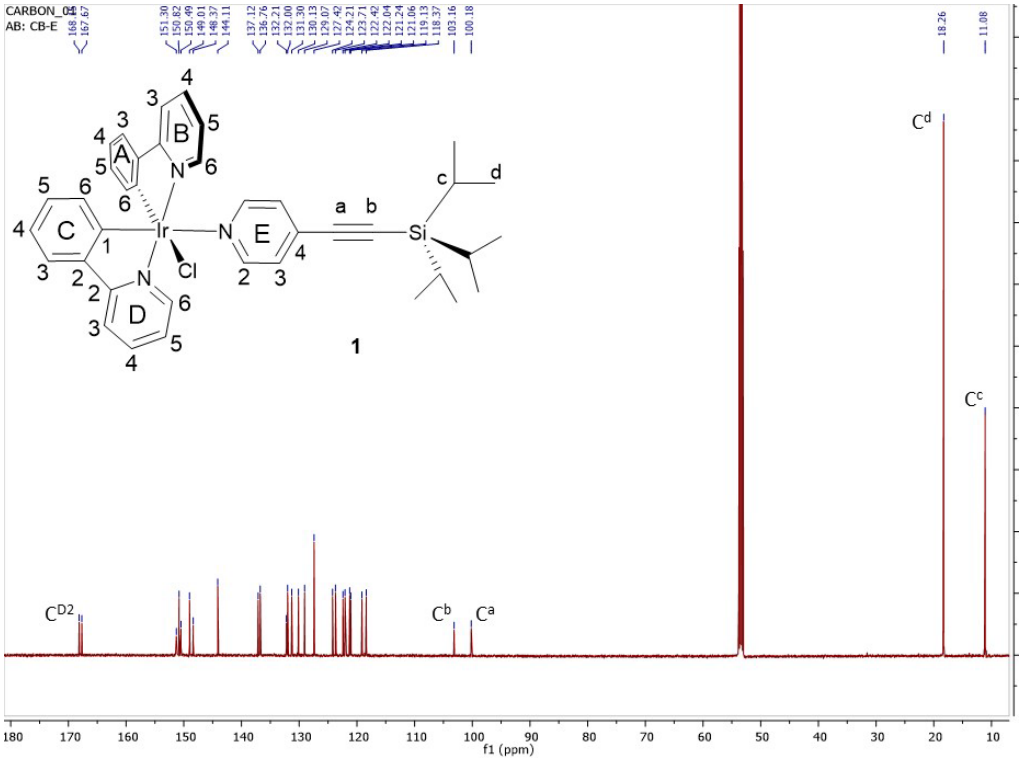

Figure S4a. $^{13}C\{^{1}H\}$ NMR spectrum of **1**, recorded in CD_2Cl_2 at 25°C.

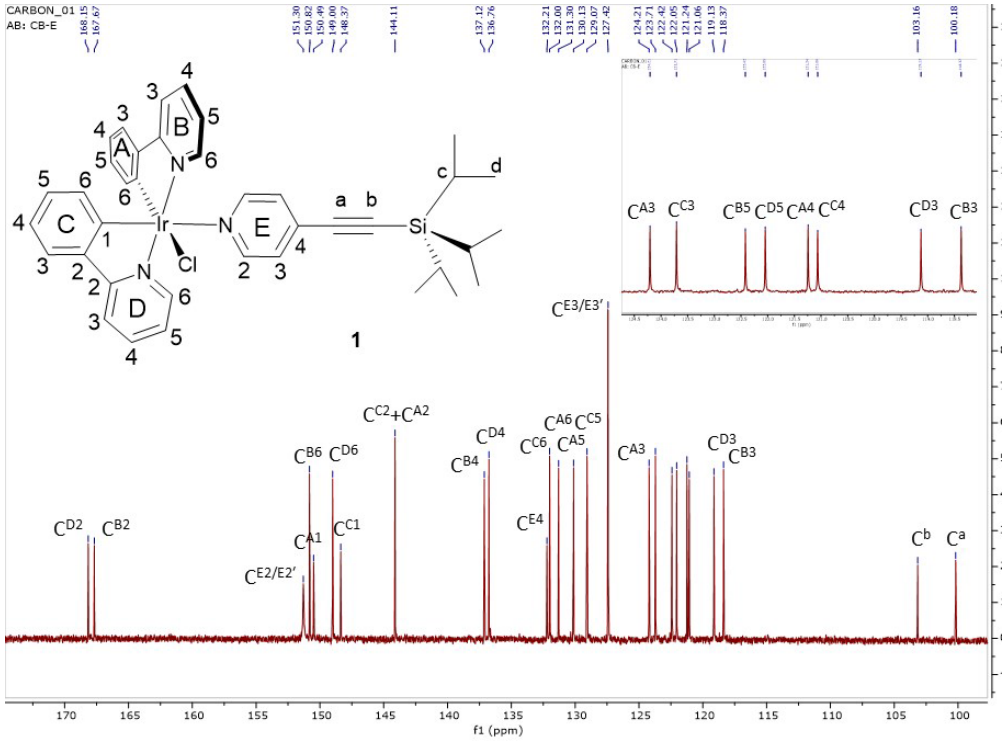

Figure S4b. $^{13}C\{^{1}H\}$ NMR spectrum of **1**, recorded in CD_2Cl_2 at 25°C.

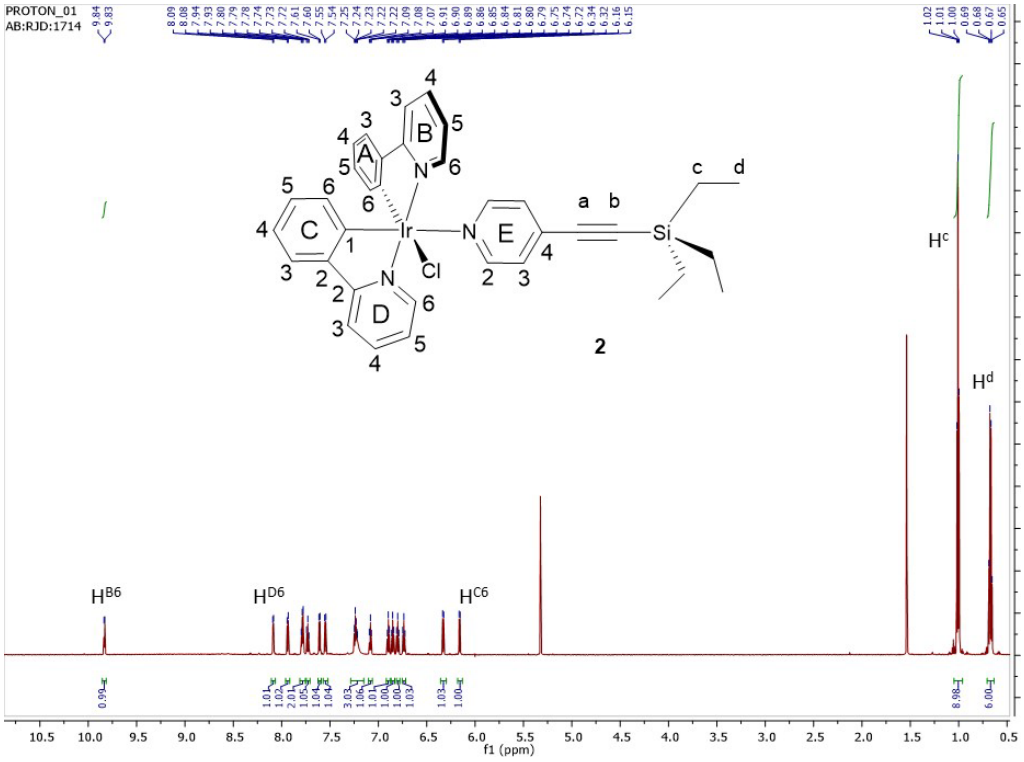

Figure S5a. ^{1}H NMR spectrum of **2**, recorded in CD_2Cl_2 at 25°C.

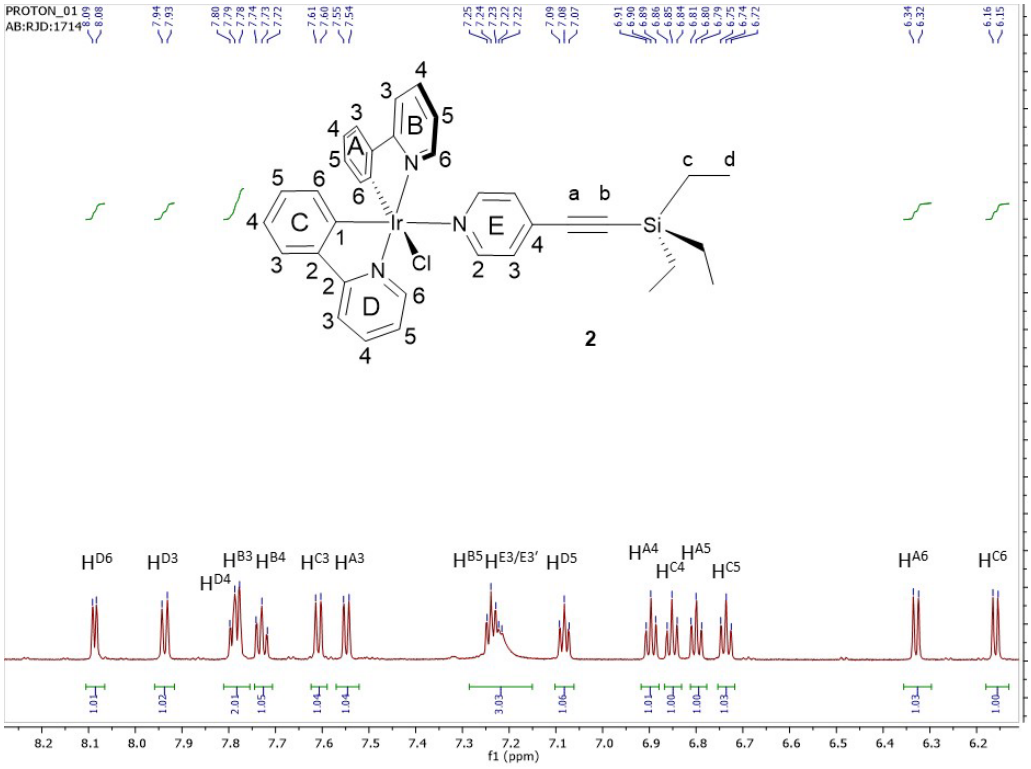

Figure S5b. ^{1}H NMR spectrum of **2**, recorded in CD_2Cl_2 at 25°C.

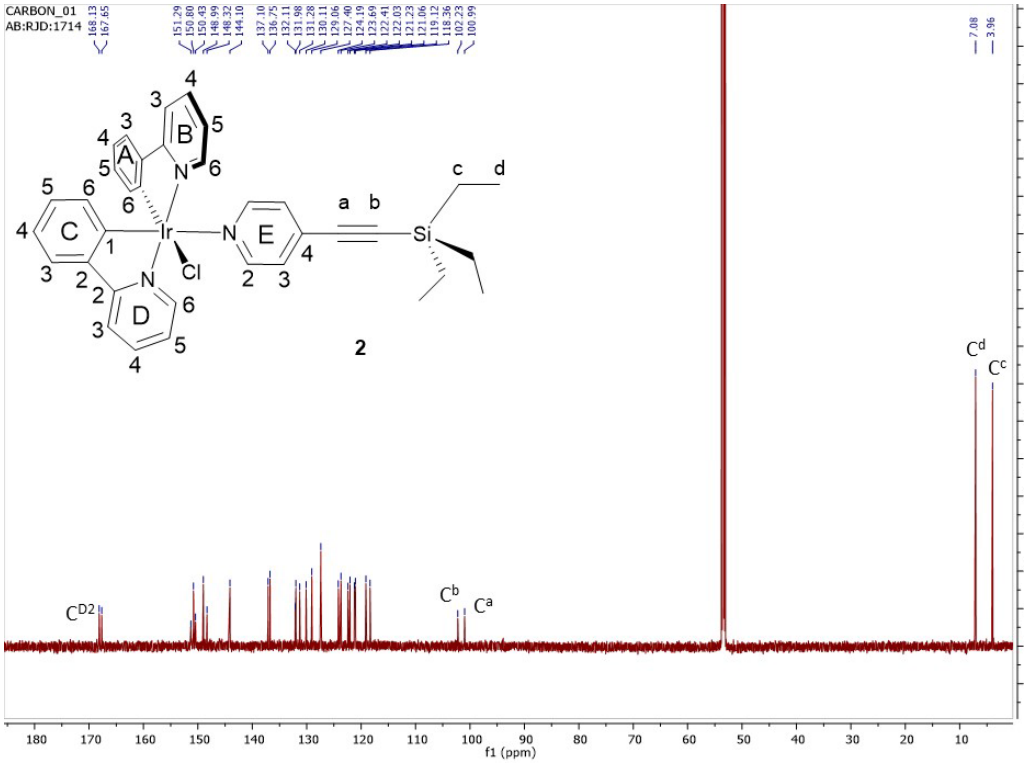

Figure S6a. $^{13}C\{^{1}H\}$ NMR spectrum of **2**, recorded in CD_2Cl_2 at 25°C.

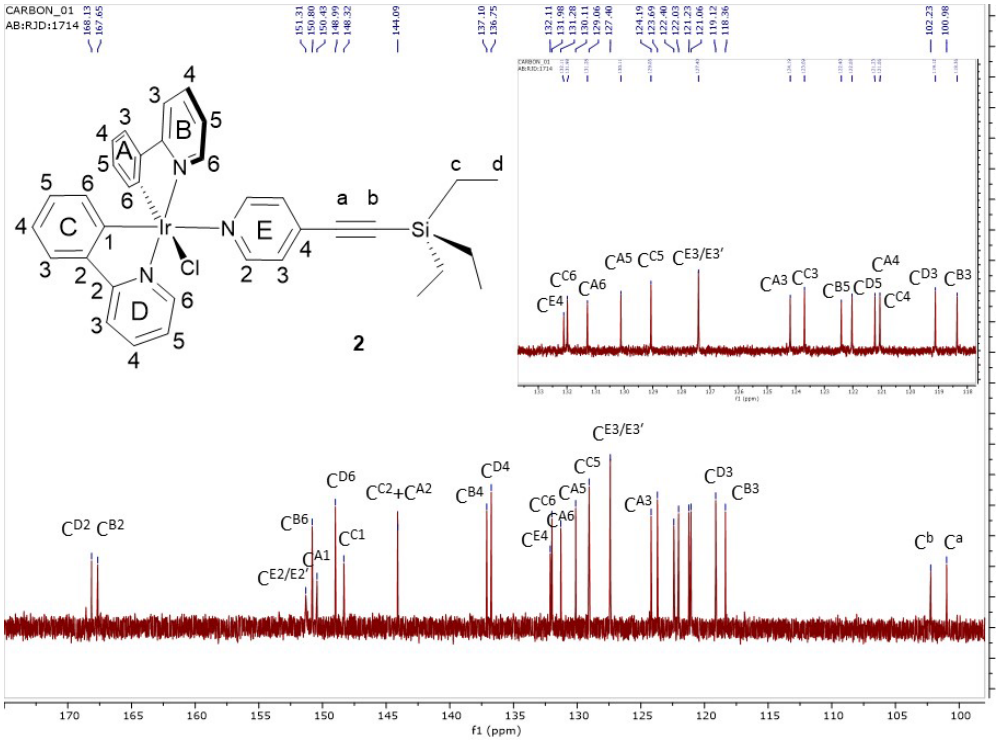

Figure S6b. $^{13}C\{^{1}H\}$ NMR spectrum of **2**, recorded in CD_2Cl_2 at 25°C.

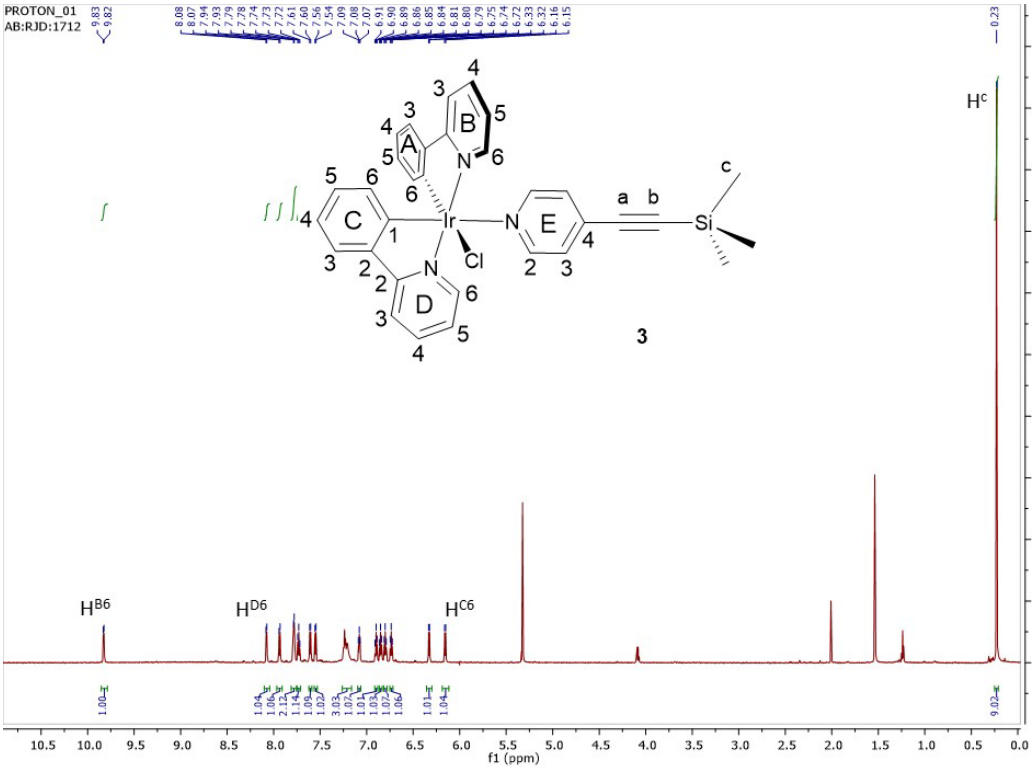

Figure S7a. ^{1}H NMR spectrum of **3**, recorded in CD_2Cl_2 at 25°C.

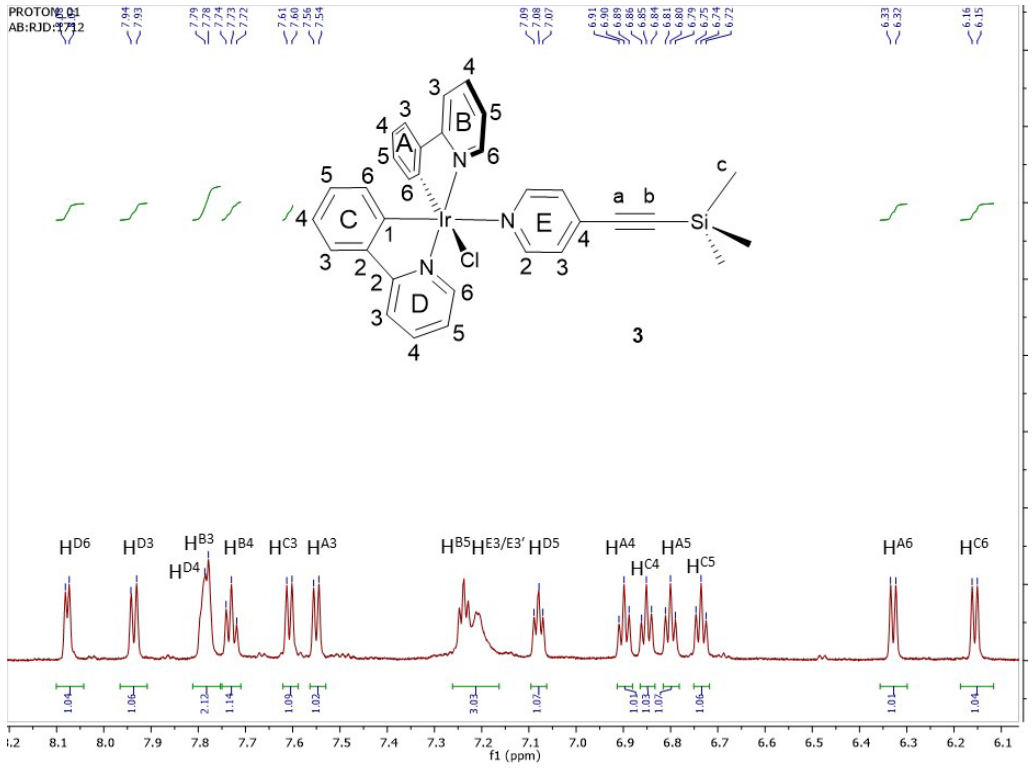

Figure S7b. ^{1}H NMR spectrum of **3**, recorded in CD_2Cl_2 at 25°C.

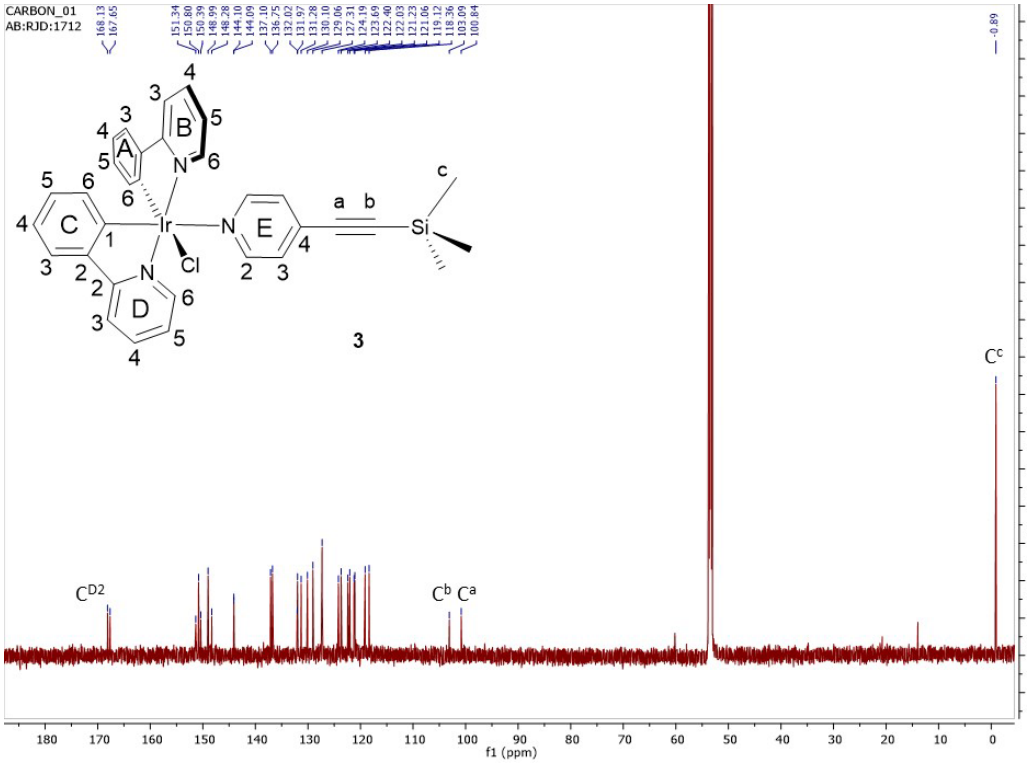

Figure S8a. $^{13}C\{^{1}H\}$ NMR spectrum of **3**, recorded in CD_2Cl_2 at 25°C.

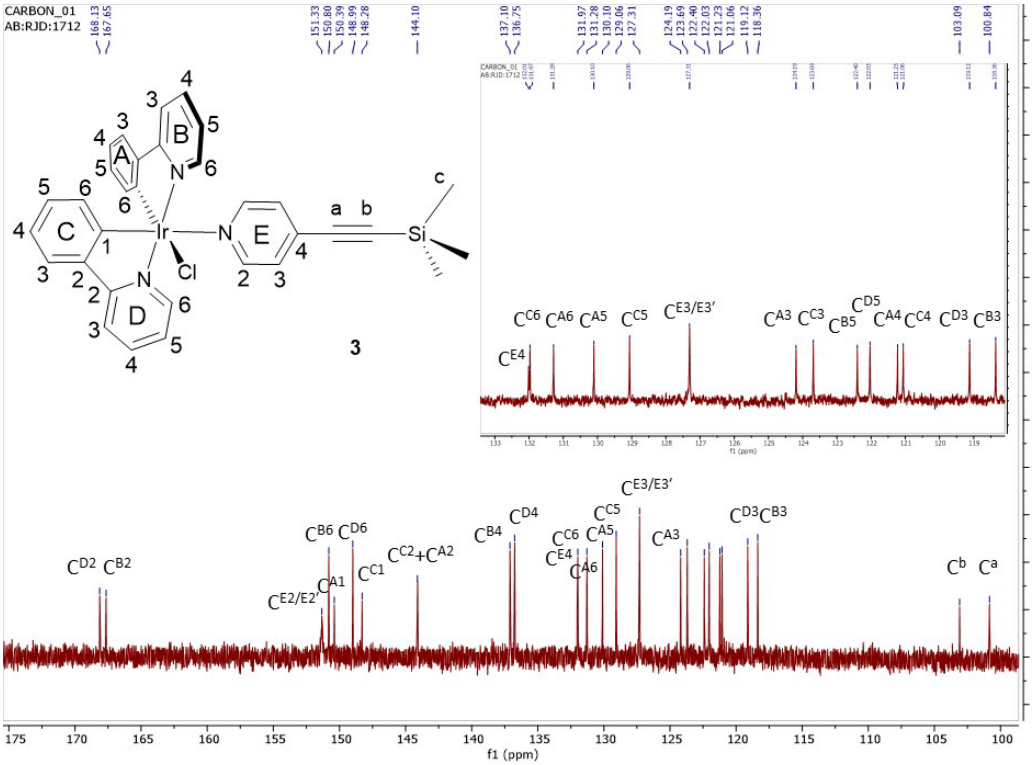

Figure S8b. $^{13}C\{^{1}H\}$ NMR spectrum of **3**, recorded in CD_2Cl_2 at 25°C.

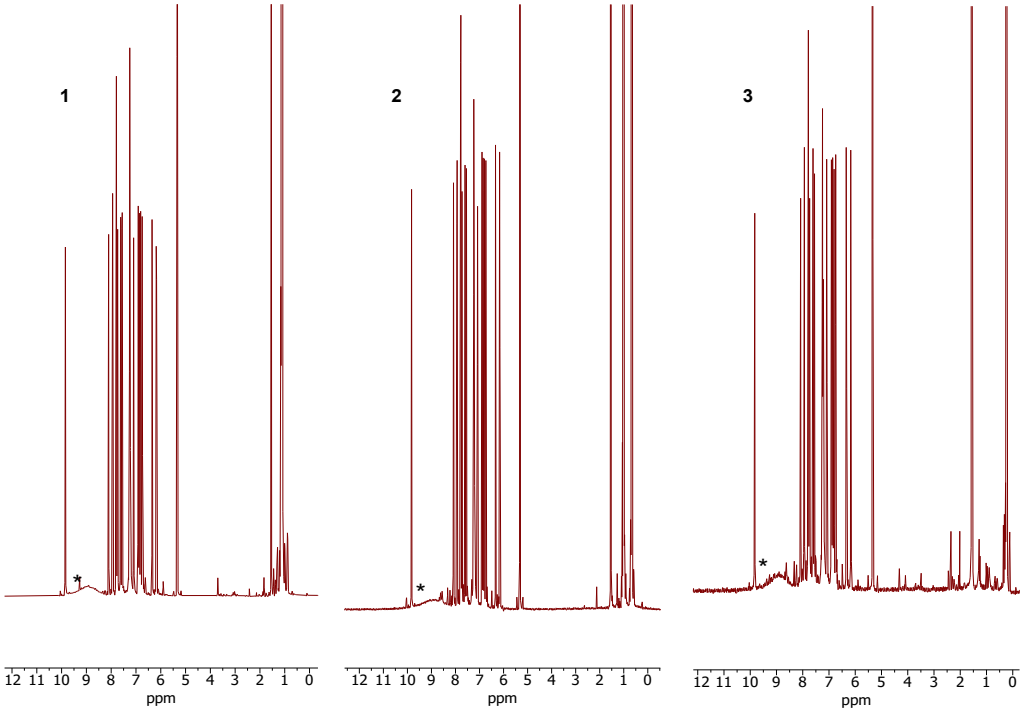

Figure S9. Broad peaks labelled as * are observed in ^{1}H spectra for protons at E2/E2′ positions of iridium complexes **1-3**, recorded in CD_2Cl_2 at 25°C.

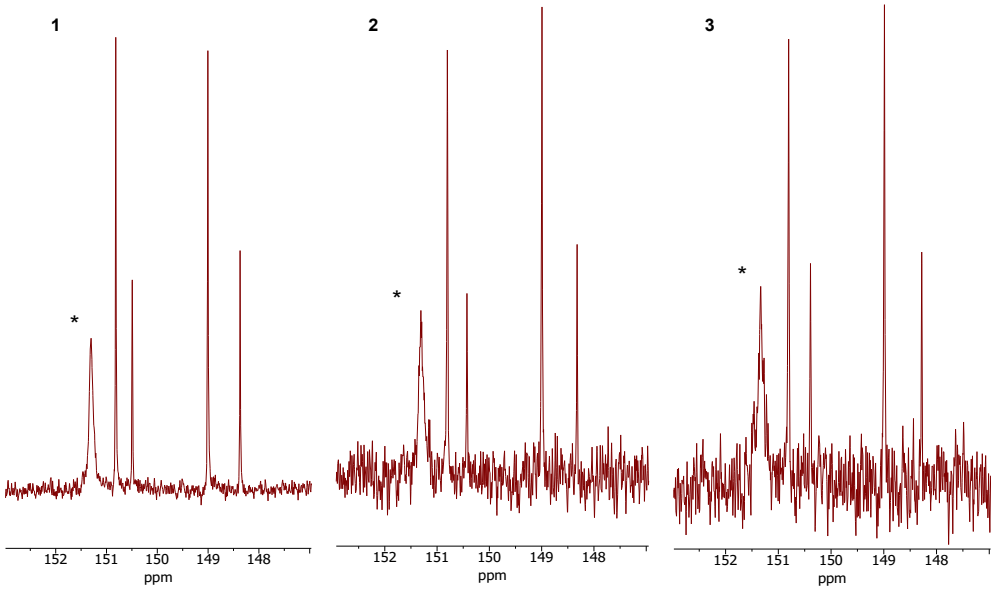

Figure S10. Broad peaks labelled as * are observed in $^{13}C\{^{1}H\}$ spectra for carbons at E2/E2′ positions of iridium complexes **1-3**, recorded in CD_2Cl_2 at 25°C.

S3. Crystallographic data

The X-ray single crystal data for compound **1** have been collected at 120.0(1)K using λMoKα radiation (λ = 0.71073Å) on a Bruker D8Venture (Photon100 CMOS detector, IμS-microsource, focusing mirrors) diffractometer equipped with a Cryostream (Oxford Cryosystems) open-flow nitrogen cryostat. The structure was solved by direct method and refined by full-matrix least squares on F^2 for all data using Olex2[S4] and SHELXTL[S5] softwares. All non-disordered non-hydrogen atoms were refined anisotropically, hydrogen atoms were placed in the calculated positions and refined in riding mode. Disordered atoms were refined in isotropic approximation with fixed SOF=0.5 and restrained (SADI) C-C distances. Crystal data and parameters of refinement are listed in Tables S1-S3. Crystallographic data for the structure have been deposited with the Cambridge Crystallographic Data Centre as supplementary publication CCDC-2143627.

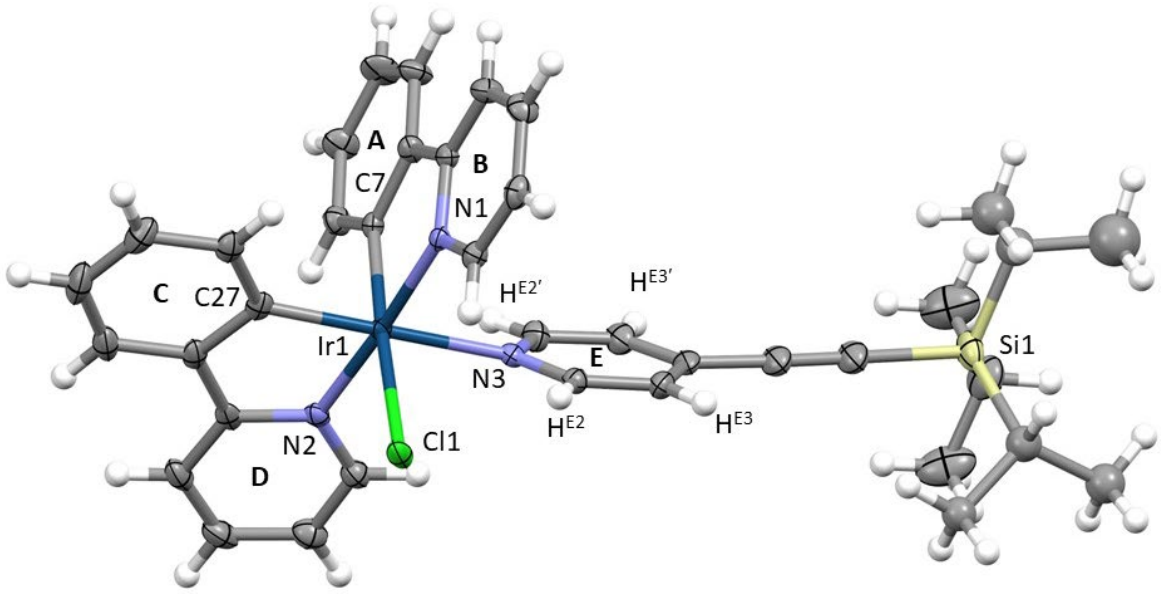

Figure S11. Crystal structure of complex **1** (Λ enantiomer) with the disorder removed for clarity and the thermal ellipsoids displayed at 50% probability.

Table S1. Crystal data and structure refinement for **1**.

Empirical formula	$C_{38}H_{41}ClIrN_3Si$
Formula weight	795.48
Temperature/K	120.0
Crystal system	monoclinic
Space group	$P2_1/c$
a/Å	14.3230(2)
b/Å	22.6945(4)
c/Å	11.3723(3)
β/°	104.7440(19)
Volume/Å^3	3574.88(12)
Z	4
ρ_{calc}g/cm^3	1.478
μ/mm^{-1}	3.873
F(000)	1592.0
Reflections collected	58858
Independent reflections	10427 [R_{int} = 0.0611]
Data/restraints/parameters	10427/28/401
Goodness-of-fit on F^2	1.021
Final R_1 index [≥2σ (I)]	0.0335
Final wR_2 index [all data]	0.0653
Largest diff. peak/hole / e Å^{-3}	1.39/-0.76

Table S2. Selected bond lengths for **1**.

Atom	Atom	Length/Å		Atom	Atom	Length/Å
Ir1	Cl1	2.4695(7)		C10	C11	1.372(5)
Ir1	N1	2.043(2)		C21	C22	1.369(4)
Ir1	N2	2.034(3)		C22	C23	1.376(5)
Ir1	N3	2.178(3)		C23	C24	1.376(5)
Ir1	C7	2.000(3)		C24	C25	1.389(4)
Ir1	C27	1.992(3)		C25	C26	1.459(5)
Si1	C47	1.837(4)		C26	C27	1.413(4)
Si1	C48	1.871(4)		C26	C31	1.401(4)
Si1	C51A	2.005(10)		C27	C28	1.402(4)
Si1	C51B	1.775(10)		C28	C29	1.393(5)
Si1	C54A	1.799(8)		C29	C30	1.384(5)
Si1	C54B	1.968(9)		C30	C31	1.380(5)
N1	C1	1.347(4)		C41	C42	1.374(4)
N1	C5	1.366(4)		C42	C43	1.391(5)
N2	C21	1.342(4)		C43	C44	1.400(5)
N2	C25	1.359(4)		C43	C46	1.433(5)
N3	C41	1.338(4)		C44	C45	1.375(4)
N3	C45	1.347(4)		C46	C47	1.199(5)
C1	C2	1.371(4)		C48	C49	1.523(6)
C2	C3	1.379(5)		C48	C50	1.524(6)
C3	C4	1.378(4)		C51A	C52A	1.532(5)
C4	C5	1.383(4)		C51A	C53A	1.530(5)
C5	C6	1.466(4)		C51B	C52B	1.532(5)
C6	C7	1.408(4)		C51B	C53B	1.531(5)
C6	C11	1.395(4)		C54A	C55A	1.533(5)
C7	C8	1.396(4)		C54A	C56A	1.529(5)
C8	C9	1.385(4)		C54B	C55B	1.532(5)
C9	C10	1.388(5)		C54B	C56B	1.530(5)

Table S3. Selected bond angles for **1**.

Atom	Atom	Atom	Angle/°		Atom	Atom	Atom	Angle/°
N1	Ir1	Cl1	96.26(7)		C6	C7	Ir1	114.5(2)
N1	Ir1	N3	85.41(9)		C8	C7	Ir1	128.2(2)
N2	Ir1	Cl1	86.09(7)		C8	C7	C6	117.3(3)
N2	Ir1	N1	176.33(10)		C9	C8	C7	121.3(3)
N2	Ir1	N3	97.49(10)		C8	C9	C10	120.5(3)
N3	Ir1	Cl1	88.52(7)		C11	C10	C9	119.7(3)
C7	Ir1	Cl1	176.37(8)		C10	C11	C6	120.2(3)
C7	Ir1	N1	80.42(11)		N2	C21	C22	123.0(3)
C7	Ir1	N2	97.30(11)		C21	C22	C23	118.6(3)
C7	Ir1	N3	89.76(10)		C22	C23	C24	119.4(3)
C27	Ir1	Cl1	93.83(8)		C23	C24	C25	119.8(3)
C27	Ir1	N1	96.79(11)		N2	C25	C24	120.4(3)
C27	Ir1	N2	80.21(12)		N2	C25	C26	113.7(3)
C27	Ir1	N3	176.58(11)		C24	C25	C26	125.9(3)
C27	Ir1	C7	88.04(11)		C27	C26	C25	114.6(3)
C47	Si1	C48	107.32(18)		C31	C26	C25	123.1(3)
C47	Si1	C51A	104.9(2)		C31	C26	C27	122.3(3)
C47	Si1	C54B	99.9(3)		C26	C27	Ir1	115.1(2)
C48	Si1	C51A	110.6(3)		C28	C27	Ir1	128.5(3)
C48	Si1	C54B	110.2(3)		C28	C27	C26	116.4(3)
C51B	Si1	C47	111.4(3)		C29	C28	C27	121.2(3)
C51B	Si1	C48	113.5(3)		C30	C29	C28	121.0(3)
C51B	Si1	C51A	9.3(4)		C31	C30	C29	119.8(3)
C51B	Si1	C54A	99.7(4)		C30	C31	C26	119.4(3)
C51B	Si1	C54B	113.6(4)		N3	C41	C42	123.3(3)
C54A	Si1	C47	111.9(3)		C41	C42	C43	119.4(3)
C54A	Si1	C48	113.1(3)		C42	C43	C44	117.6(3)
C54A	Si1	C51A	108.8(4)		C42	C43	C46	120.7(3)
C54A	Si1	C54B	15.1(4)		C44	C43	C46	121.7(3)
C54B	Si1	C51A	122.2(4)		C45	C44	C43	119.1(3)
C1	N1	Ir1	124.9(2)		N3	C45	C44	123.2(3)
C1	N1	C5	118.7(3)		C47	C46	C43	177.0(4)
C5	N1	Ir1	116.4(2)		C46	C47	Si1	178.3(3)
C21	N2	Ir1	124.7(2)		C49	C48	Si1	112.9(3)
C21	N2	C25	118.8(3)		C49	C48	C50	110.2(4)
C25	N2	Ir1	116.4(2)		C50	C48	Si1	111.4(3)
C41	N3	Ir1	120.1(2)		C52A	C51A	Si1	111.9(6)
C41	N3	C45	117.3(3)		C53A	C51A	Si1	113.4(6)
C45	N3	Ir1	122.1(2)		C53A	C51A	C52A	112.2(7)
N1	C1	C2	122.5(3)		C52B	C51B	Si1	114.1(7)
C1	C2	C3	119.2(3)		C53B	C51B	Si1	115.1(7)
C4	C3	C2	118.9(3)		C53B	C51B	C52B	107.6(8)
C3	C4	C5	120.1(3)		C55A	C54A	Si1	115.0(7)
N1	C5	C4	120.5(3)		C56A	C54A	Si1	116.5(6)
N1	C5	C6	112.9(3)		C56A	C54A	C55A	105.5(8)
C4	C5	C6	126.6(3)		C55B	C54B	Si1	109.4(7)
C7	C6	C5	115.7(3)		C56B	C54B	Si1	111.0(6)
C11	C6	C5	123.2(3)		C56B	C54B	C55B	112.3(8)
C11	C6	C7	121.1(3)					

Table S4. Comparison of $Ir(N^C)_2Cl(py\text{-}X)$ crystal structure data.

CSD Refcode	N^C	X	Enantiomer	Cl-Ir-N(Py)-C(Py)	Ir-N(Py)
This work **1**	ppy	$CCSi^iPr_3$	Λ	-37.4(2)	2.178(3)
EMOQUS (**A**)	ppy	$CHCH_2$	Λ	-19.2(4)	2.203(4)
GEXWAJ (**C**)	ppy	2′-py	Δ	20.8(6)	2.216(7)
QECZUX	piq	H	Λ	-27.8(4), 7.0(4)	2.219(2), 2.219(2)
POFJUQ	pq	H	Λ	-40.5(4)	2.221(5)
Reference S6.	btp	H	Λ	-38.6(5)	2.171(6)
Reference S6.	btp	BODIPY	Λ	-36.5(2)	2.183(3)
WEBDUF	F2ppy	H	Λ	-34.3(8)	2.18(1)
BUZXEC	F2ppy	FzaIr	Λ	-30.9(8)	2.183(9)
BUZXIG	F2ppy	FzaPt	Δ	19.4(7)	2.173(6)
BUZYED	F2ppy	FzaH	Λ	-38.9(9), -38.6(9)	2.18(1), 2.19(1)

piq = phenylisoquinoline
pq = phenylquinoline
btp = 2-(2'-pyridyl)benzothiophene
Fza = formazanate
BODIPY = boron-dipyrromethene = 4,4-difluoro-4-bora-3a,4a-diaza-*s*-indacene

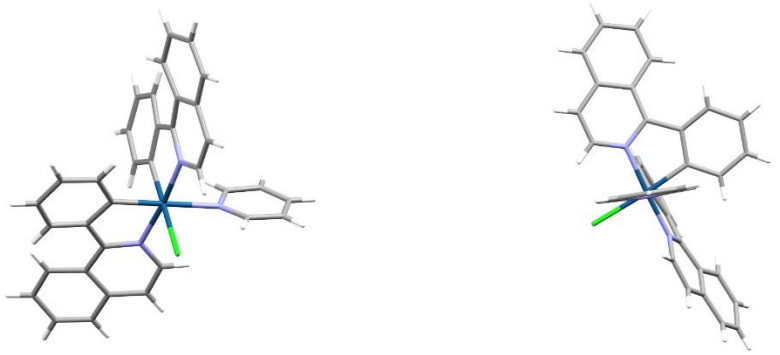

Min1

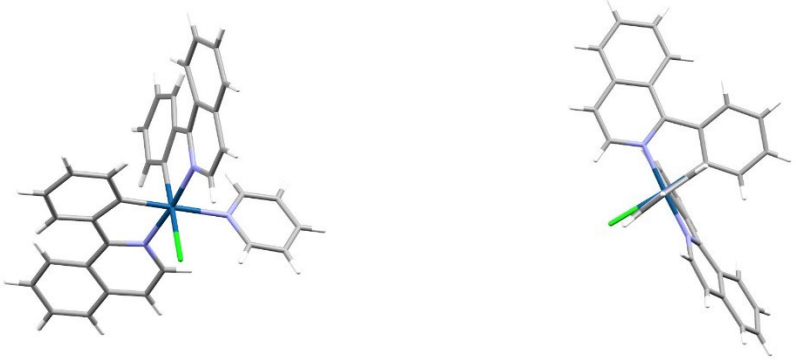

Min2

Figure S12. The two conformers (Min1 and Min2) located in the reported crystal structure of $Ir(piq)_2(py)Cl$ (CSD refcode QECZUX).[S7]

S4 Variable temperature NMR spectra

All variable temperature Nuclear Magnetic Resonance (VT NMR) spectra were recorded on a Varian DD2-500 spectrometer operating 499.53 MHz for ^{1}H. For simplicity, the frequency will be rounded to 500 MHz in all subsequent spectra.

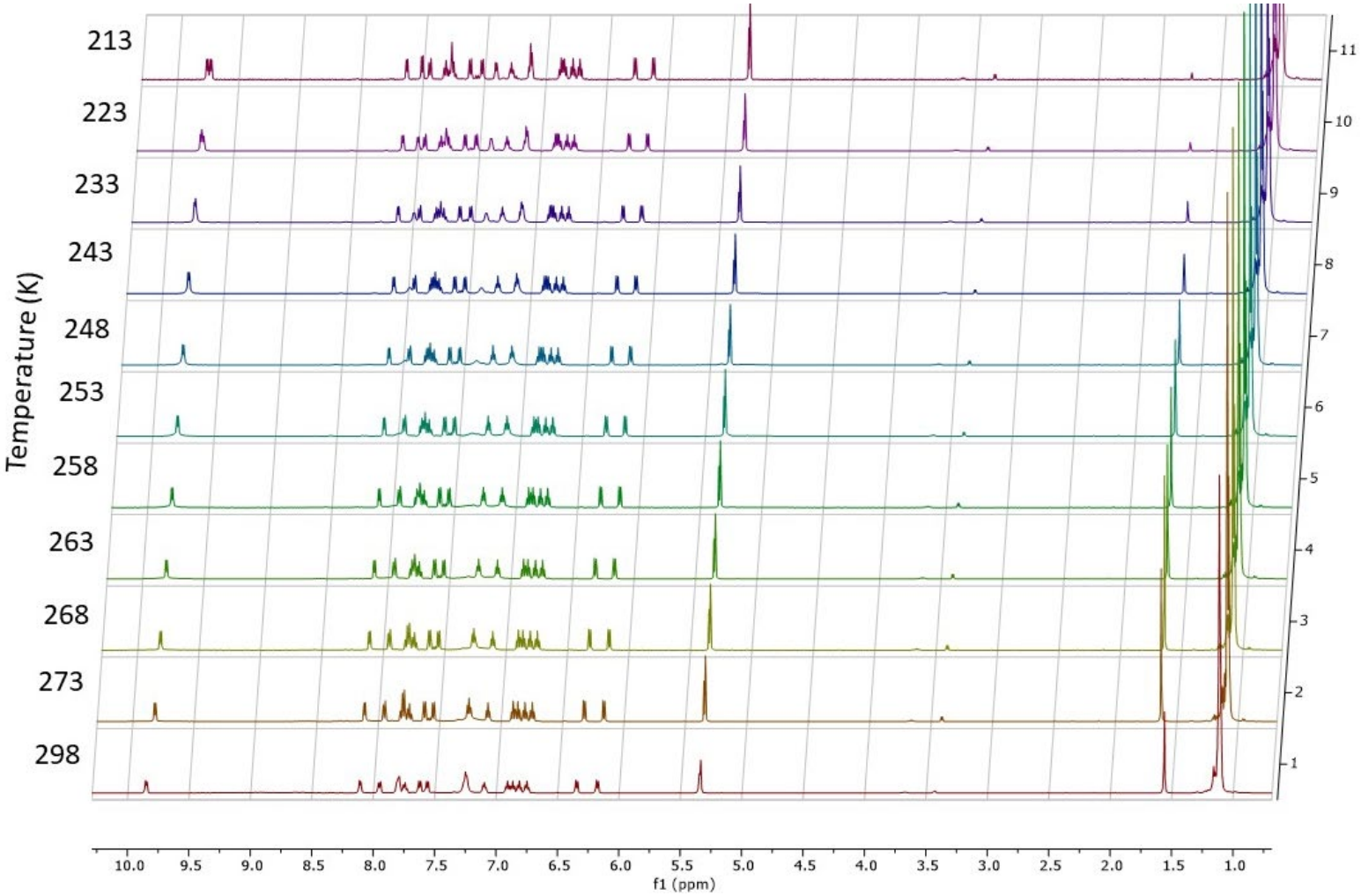

Figure S13. 500 MHz variable temperature ^{1}H NMR spectra of **1** recorded in DCM-d_2.

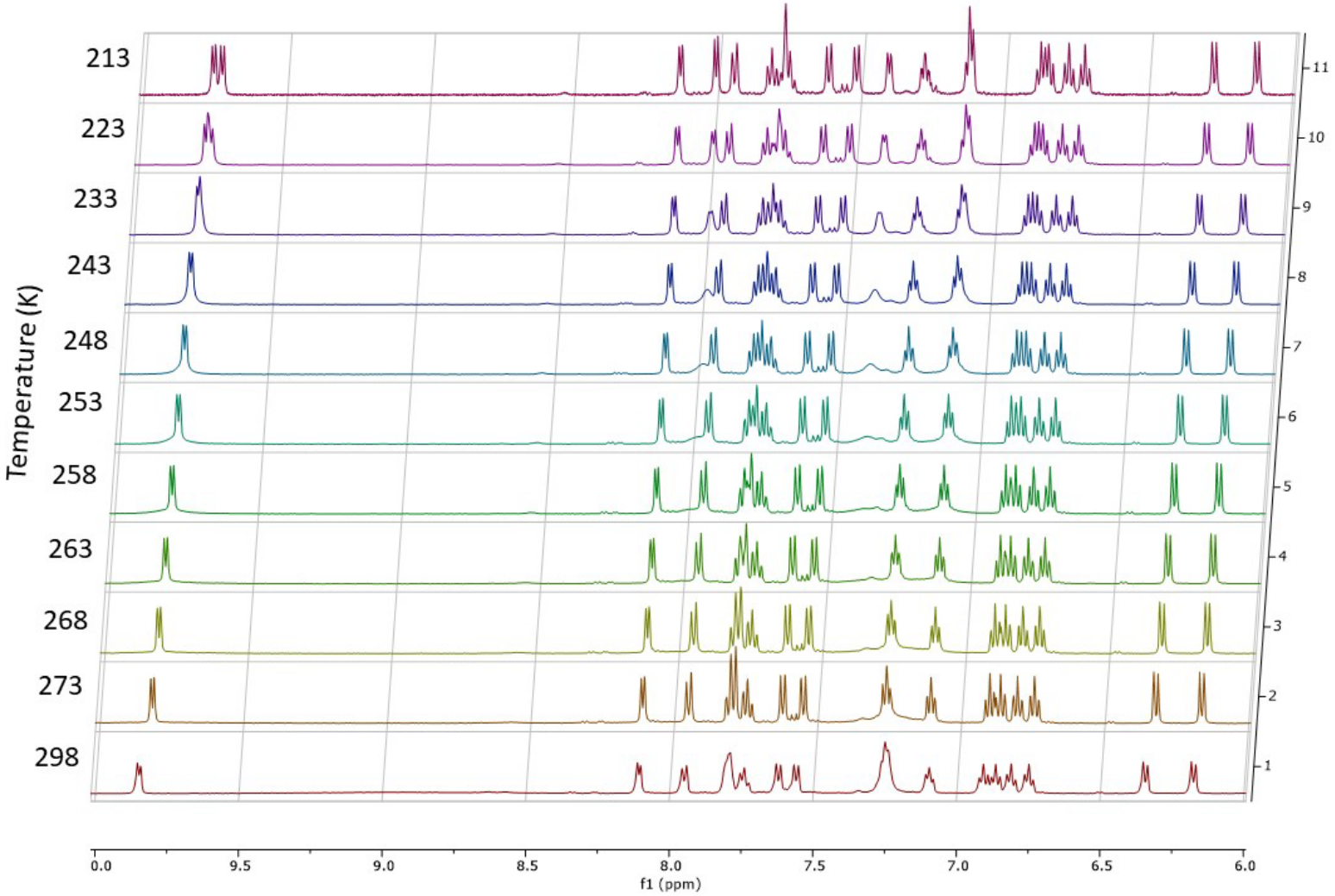

Figure S14. 500 MHz variable temperature ^{1}H NMR spectra (aromatic region) of **1** recorded in DCM-d_2.

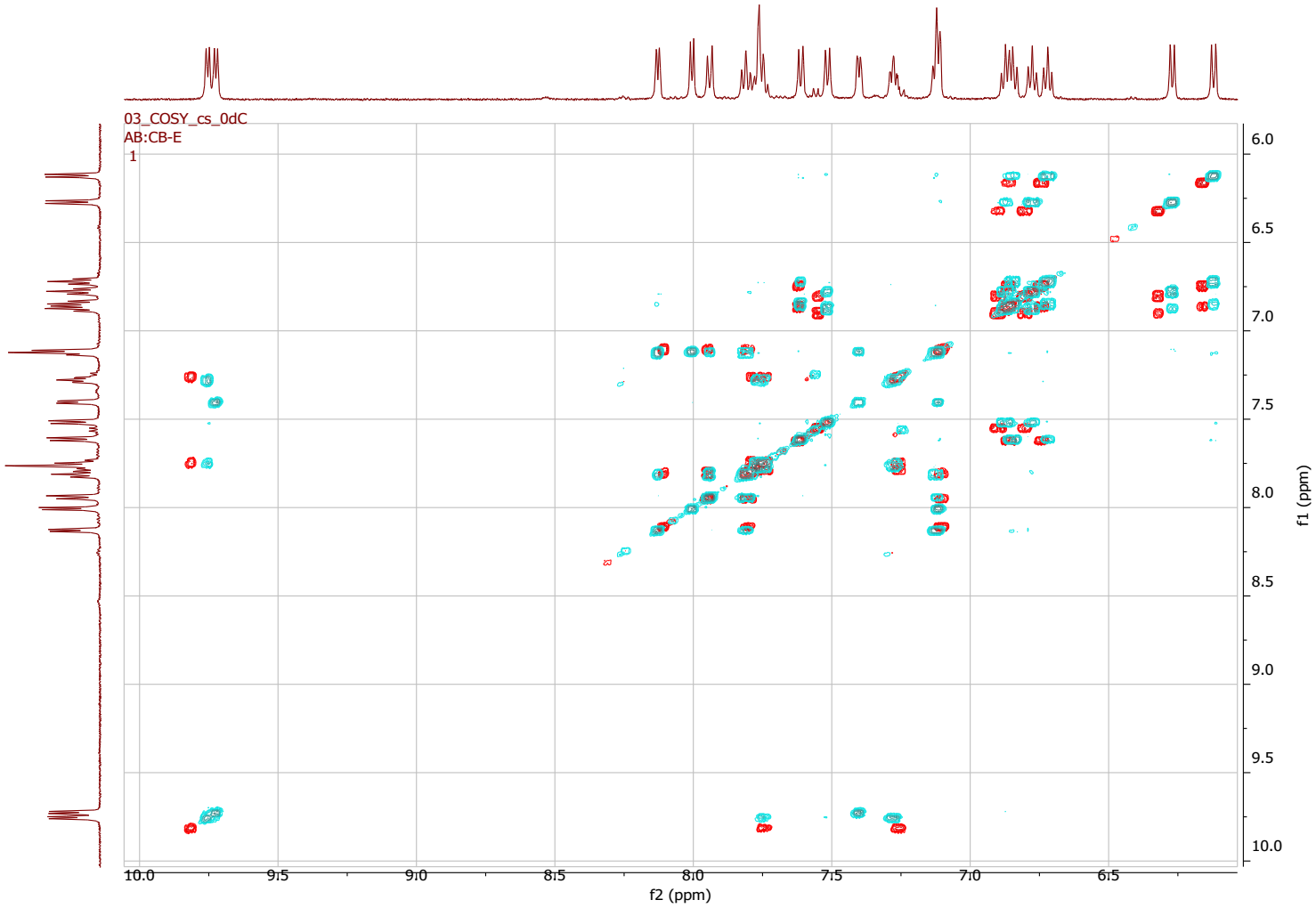

Figure S15. 500 MHz ^{1}H-^{1}H COSY NMR spectrum of **1** recorded in CD_2Cl_2, red = 273 K, blue = 213 K.

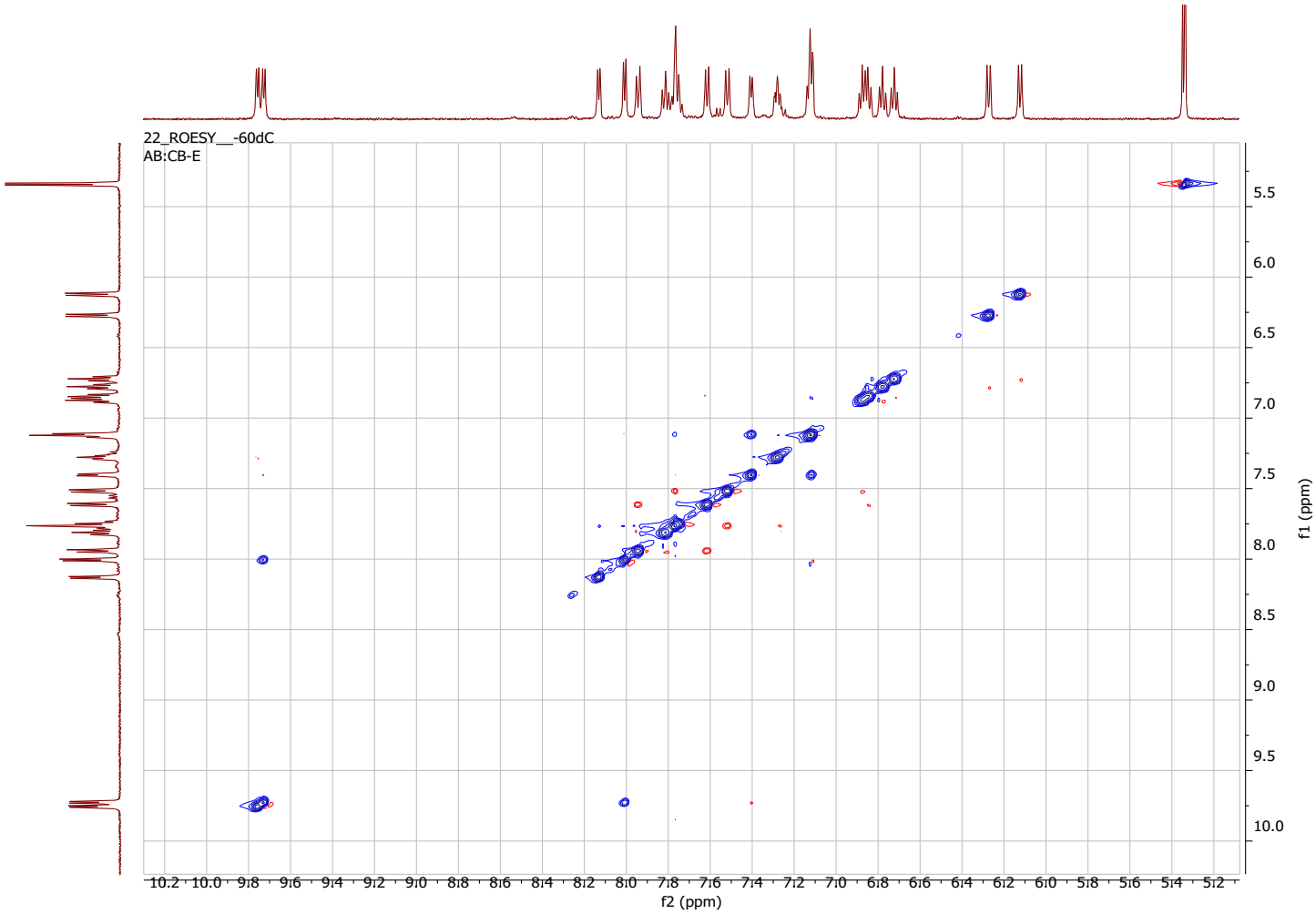

Figure S16. 500 MHz ^{1}H-^{1}H EASY-ROESY NMR spectrum of **1** recorded in CD_2Cl_2 at 213K. Red cross-peaks represent spatial proximity, while blue cross-peaks represents conformational (as in this case) or chemical exchange. Blue peaks can also be due to homonuclear scalar interactions, although this type of ROESY minimizes these contributions. The ^{1}H-^{1}H COSY could be used to identify these peaks.

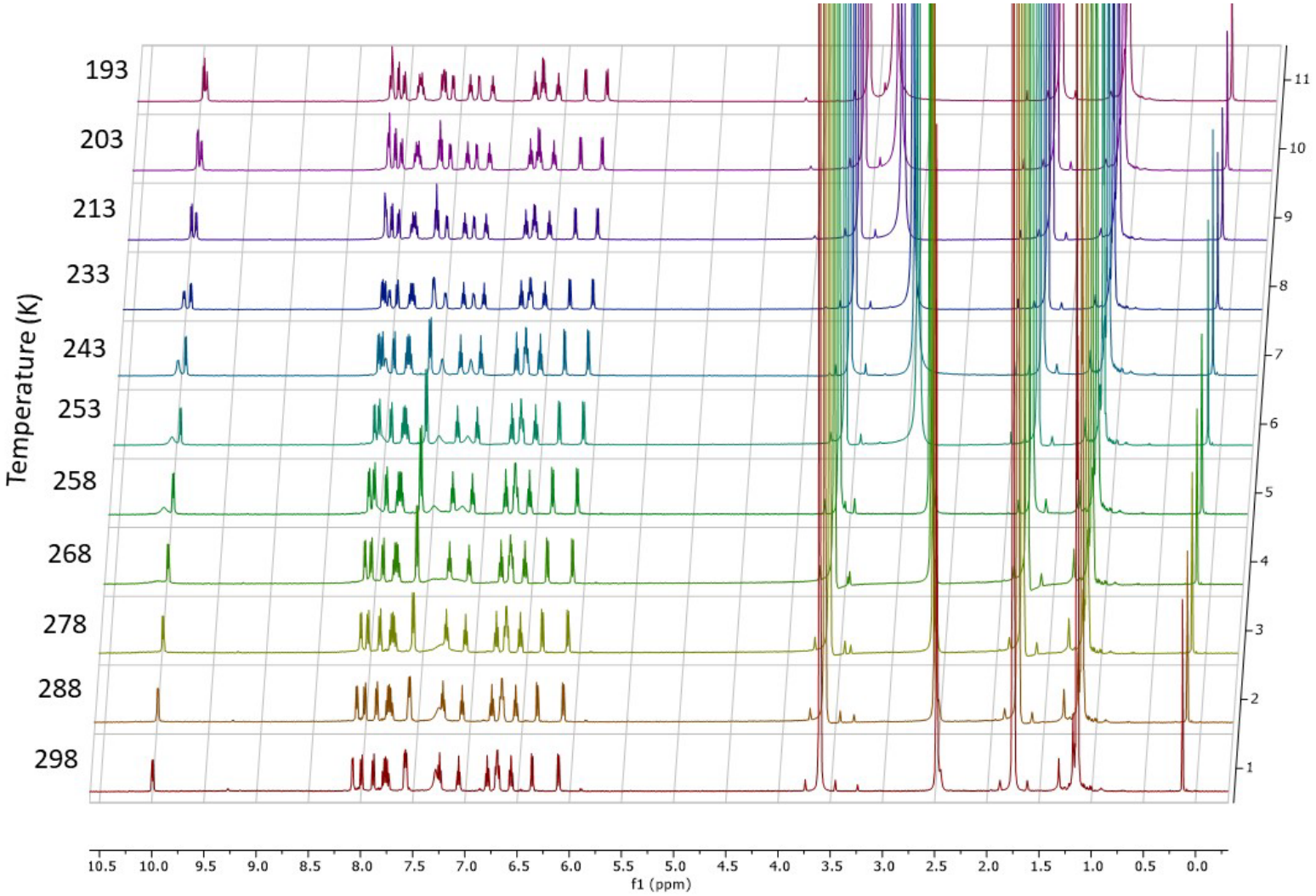

Figure S17. 500 MHz variable temperature ^{1}H NMR spectra of **1** recorded in THF-d_8.

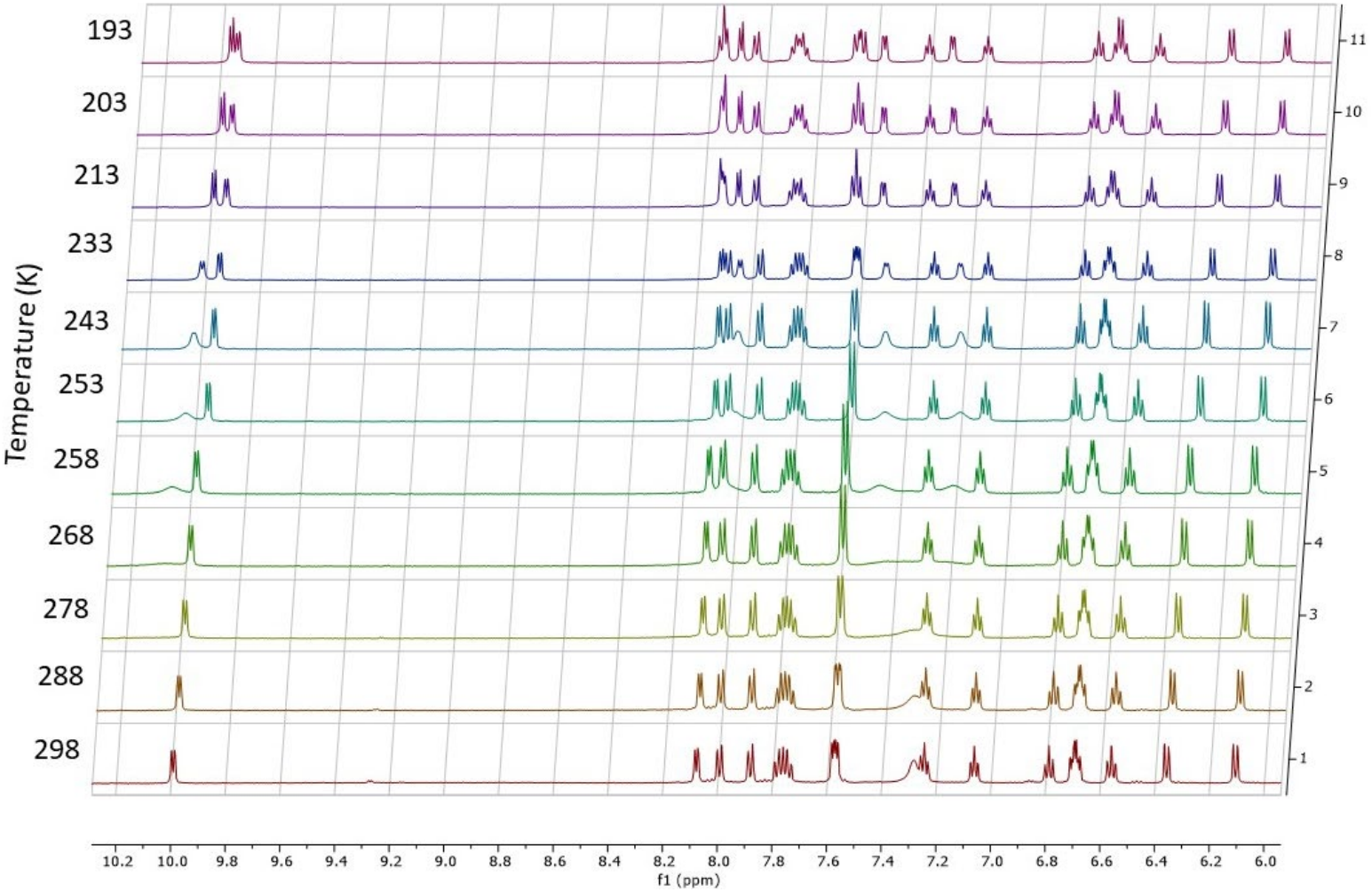

Figure S18. 500 MHz variable temperature ^{1}H NMR spectra of **1** recorded in THF-d_8.

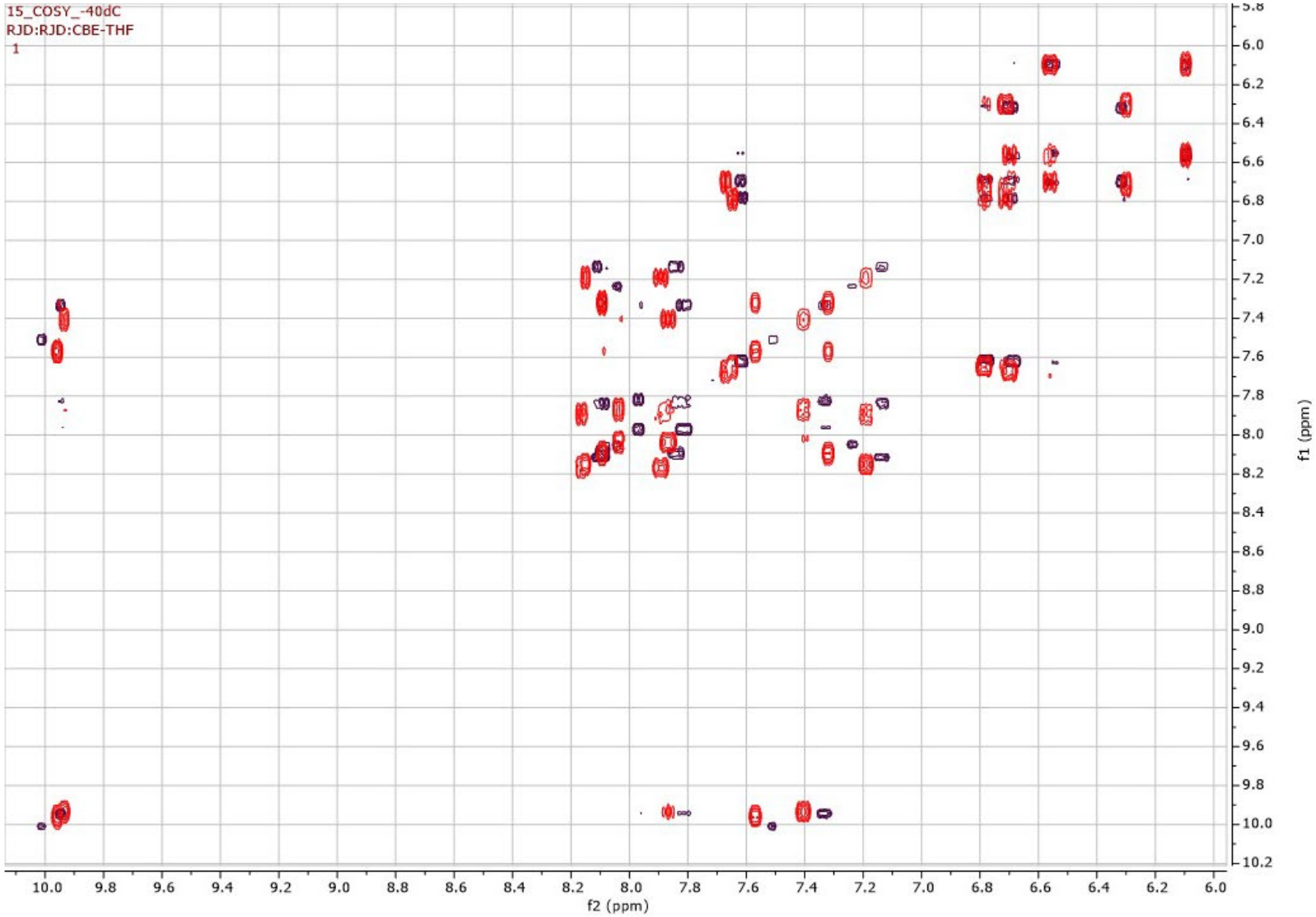

Figure S19. 500 MHz ^{1}H-^{1}H COSY NMR spectrum of **1** recorded in THF-d_8, red = 233 K, purple = 193 K.

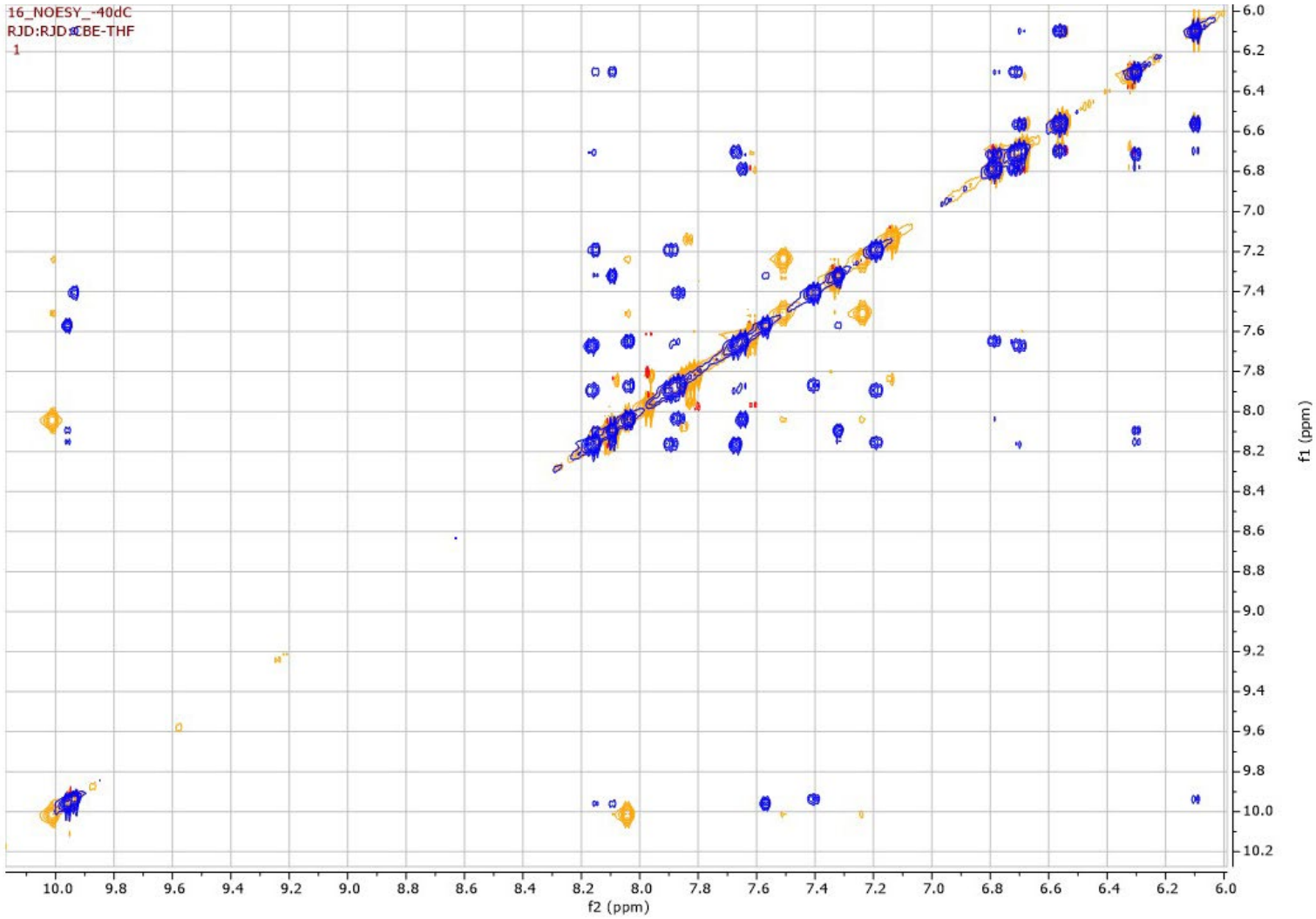

Figure S20. 500 MHz ^{1}H-^{1}H NOESY NMR spectrum of **1** recorded in THF-d_8, blue = 233 K, orange = 193 K. Because of the slow rotation of the complex with respect of the Larmor frequency, it is not possible to distinguish peaks due to proximity from peaks due to exchange. The EASY-ROESY presented in Figure S20 can differentiate between the two.

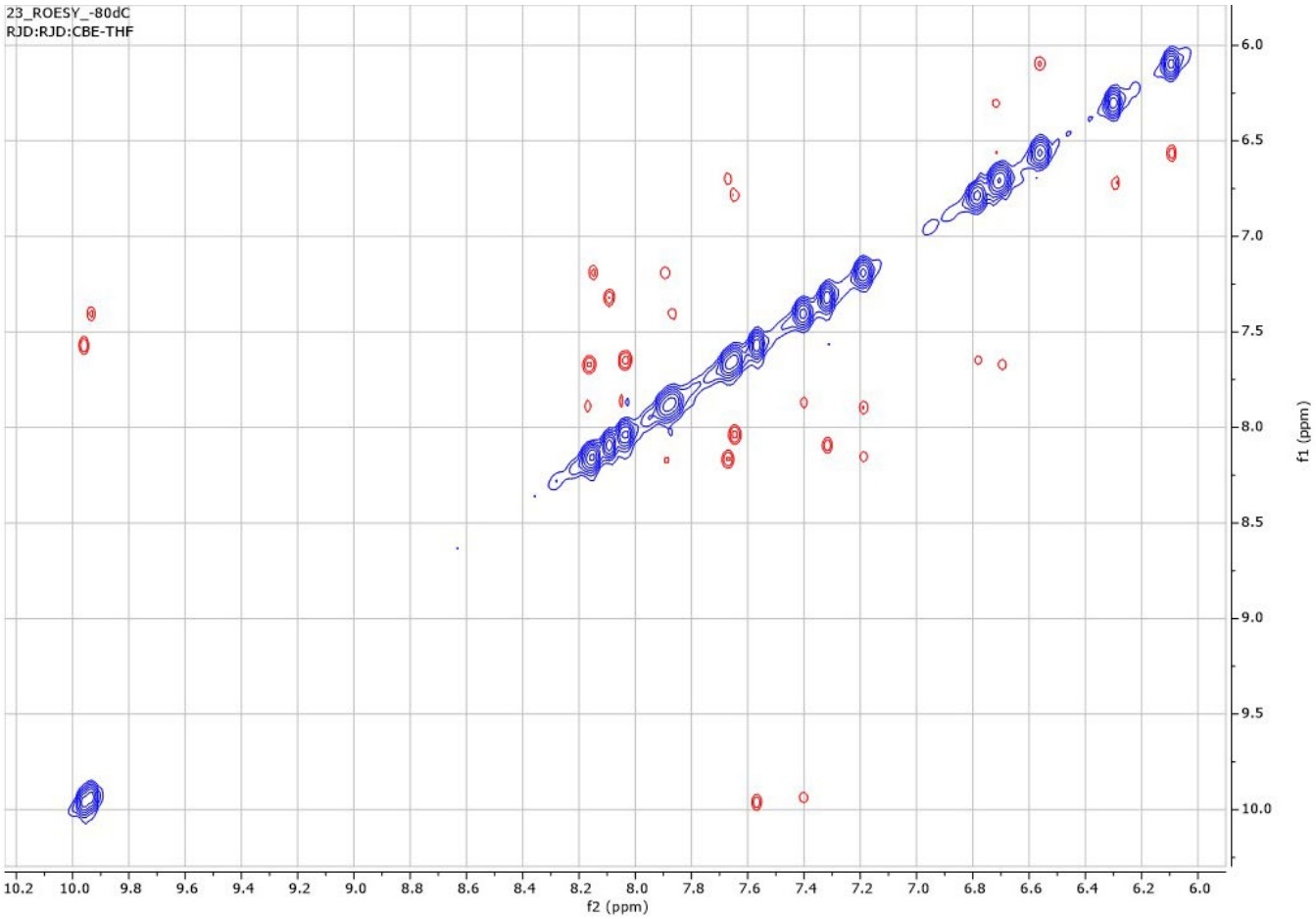

Figure S21. 500 MHz ^{1}H-^{1}H EASY-ROESY NMR spectrum of **1** recorded in THF-d_8 at 193K. Red cross-peaks represent spatial proximity.

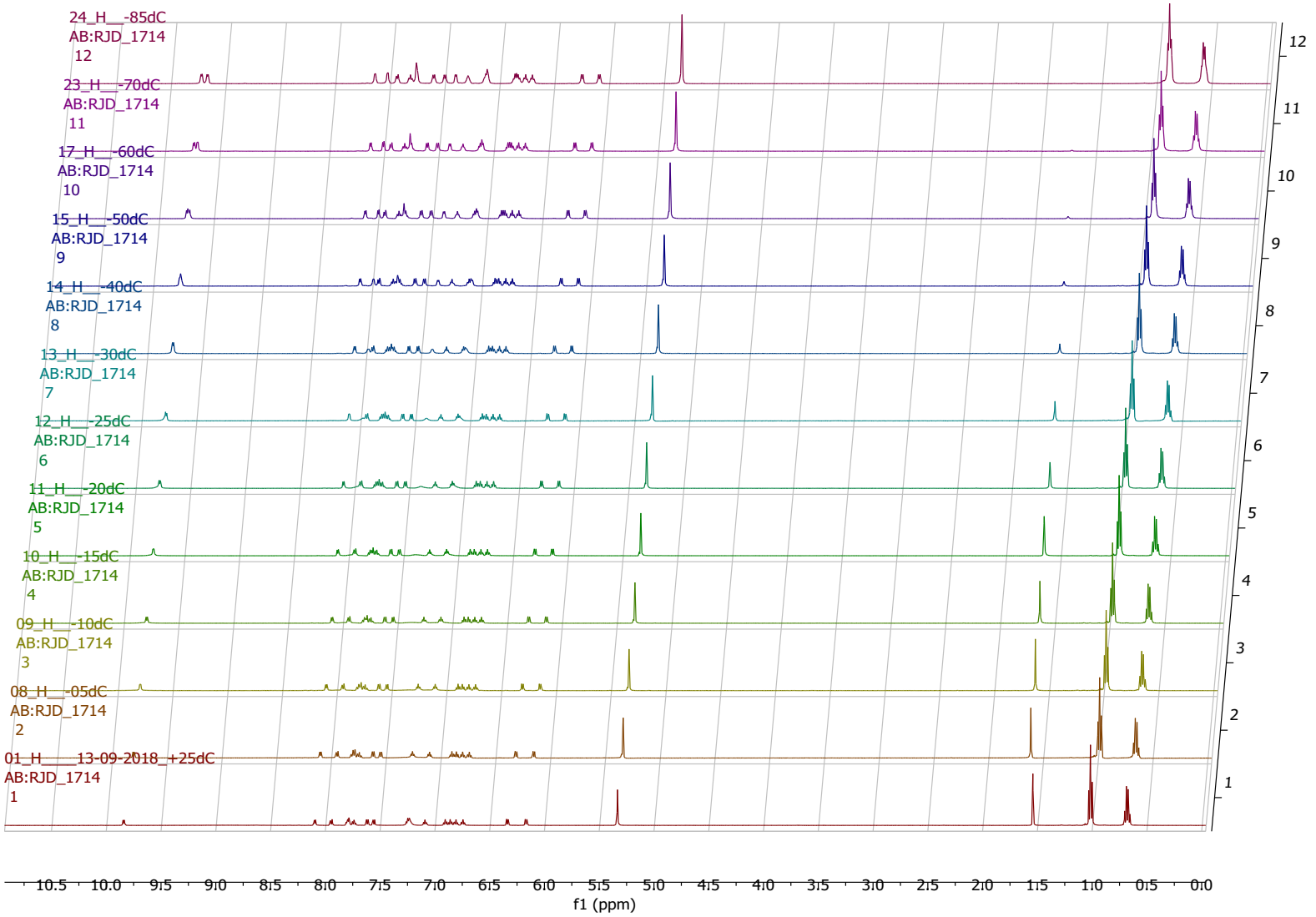

Figure S22. 500 MHz variable temperature ^{1}H NMR spectra of **2** recorded in CD_2Cl_2.

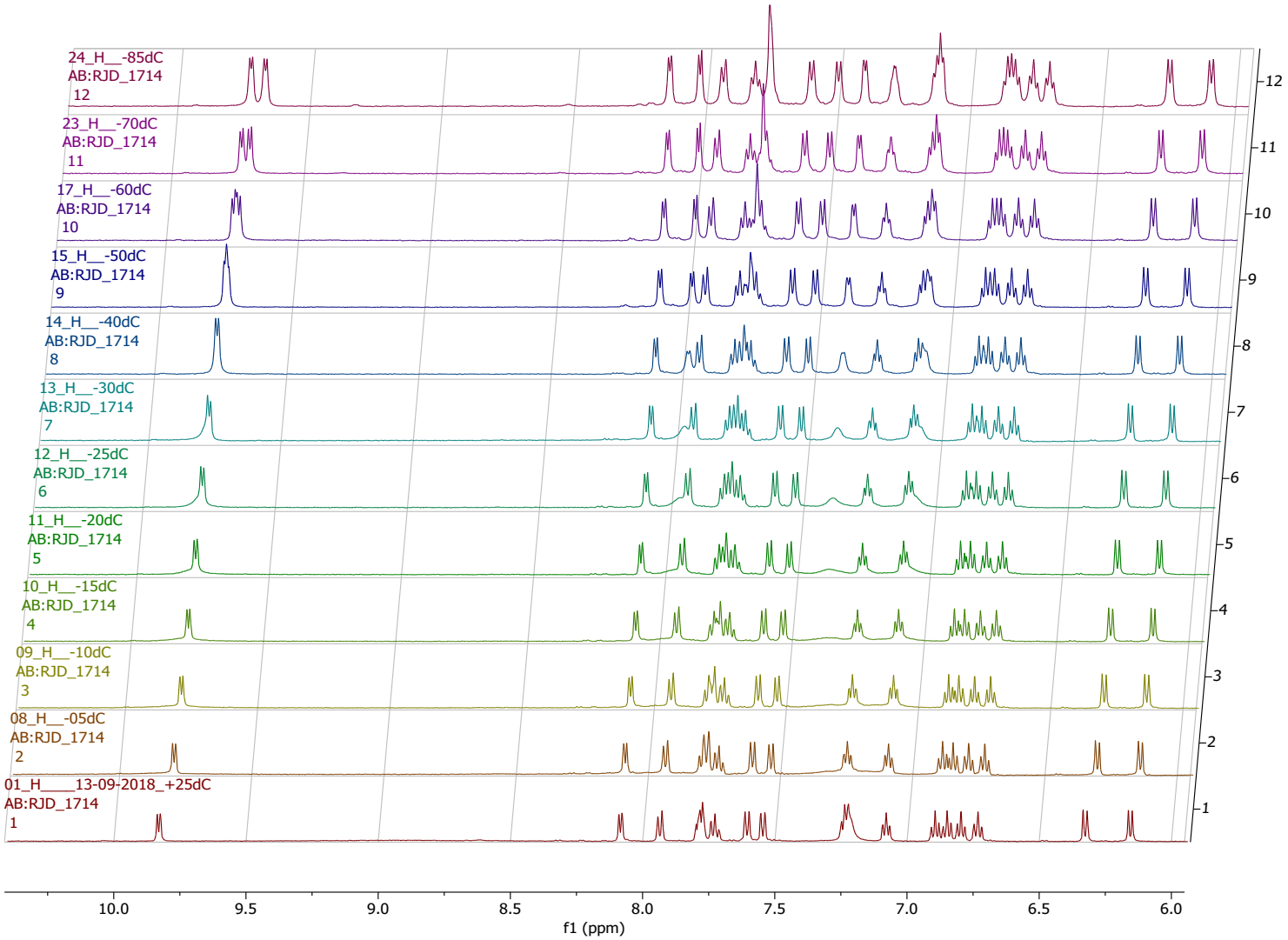

Figure S23. 500 MHz variable temperature ^{1}H NMR spectra (aromatic region) of **2** recorded in CD_2Cl_2.

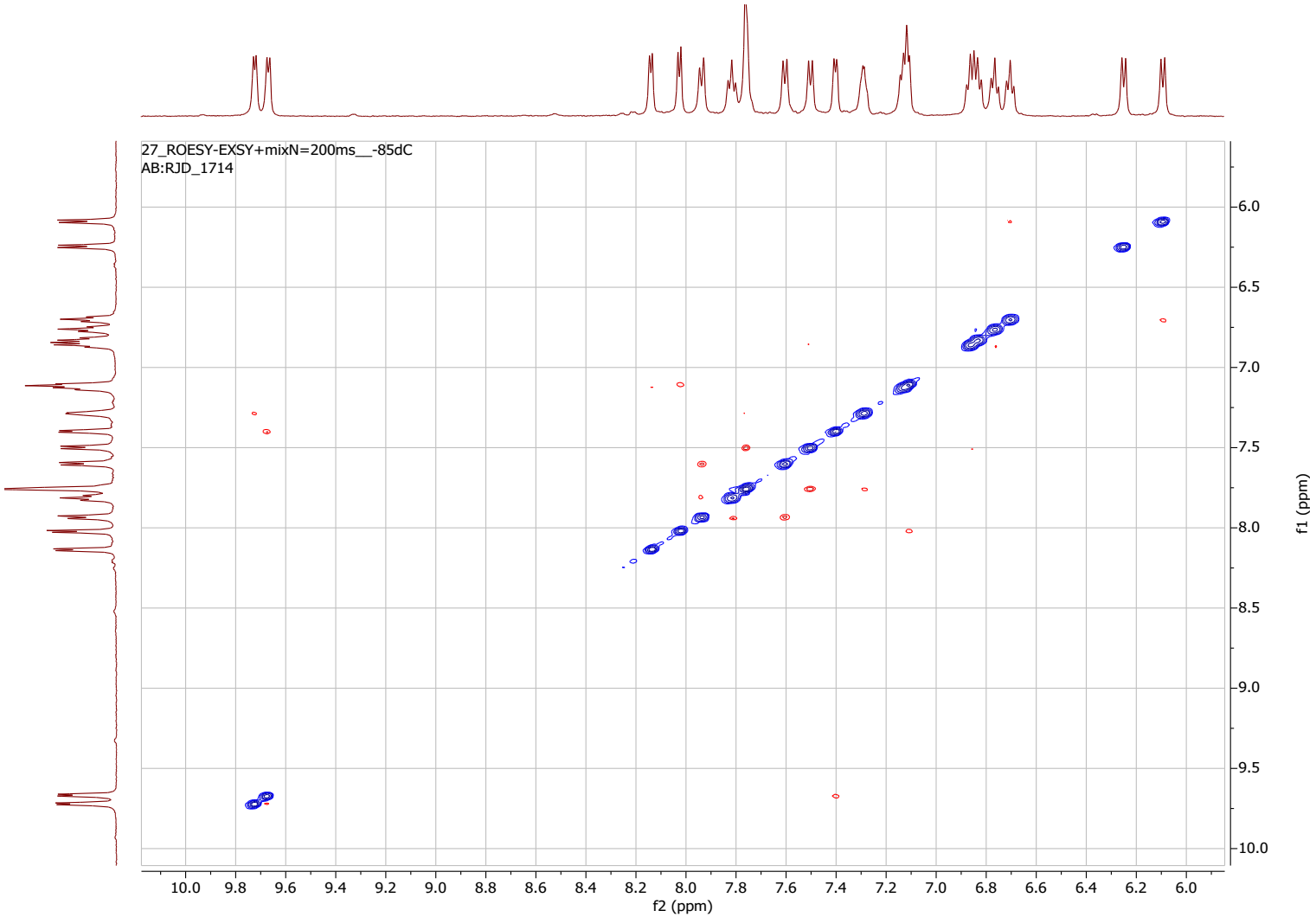

Figure S24. 500 MHz ^{1}H-^{1}H EASY-ROESY NMR spectrum of **2** recorded in CD_2Cl_2 at 188 K. Red cross-peaks indicate spatial proximity between the correlated spins.

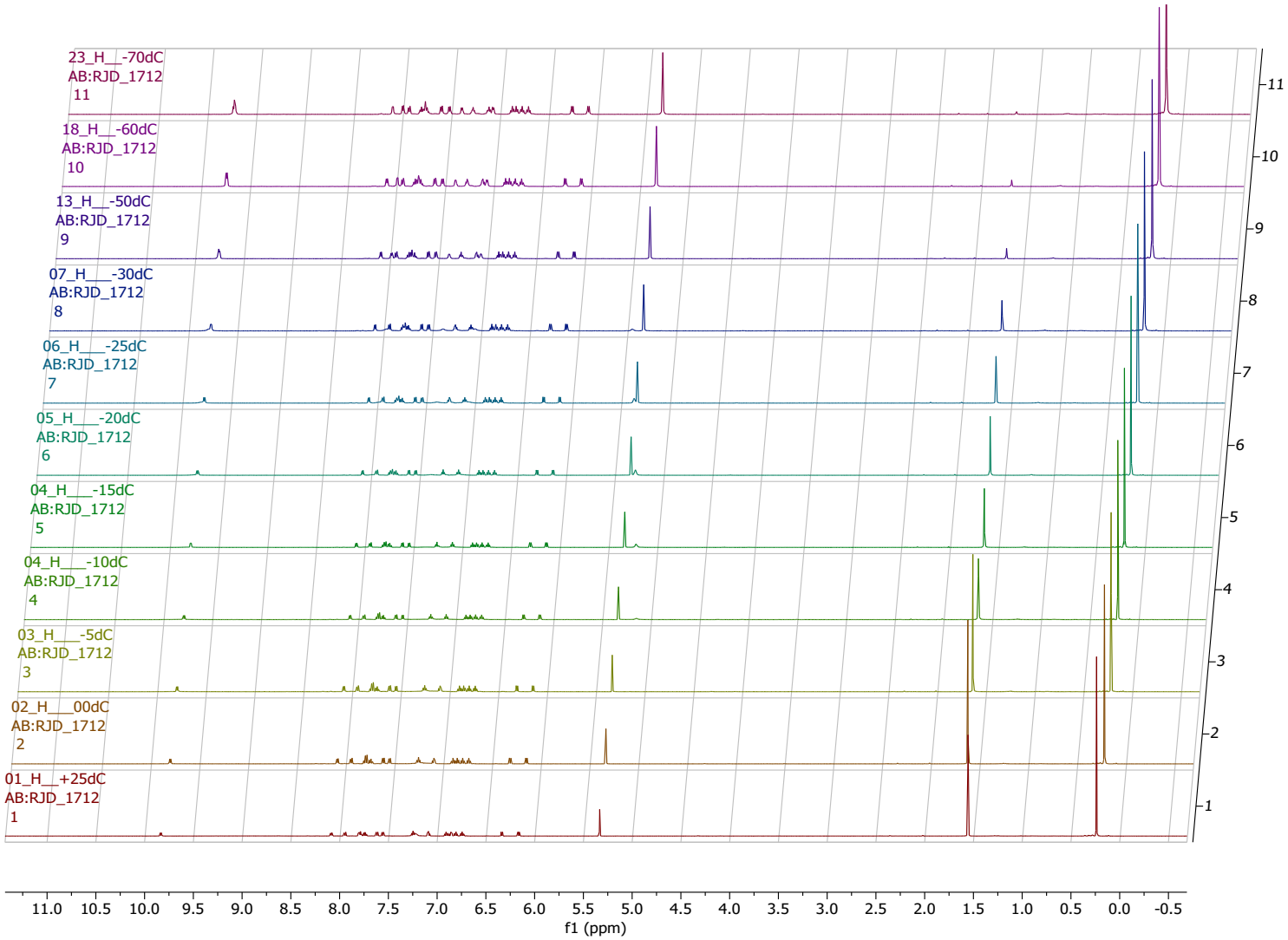

Figure S25. 500 MHz variable temperature ^{1}H NMR spectra of **3** recorded in CD_2Cl_2.

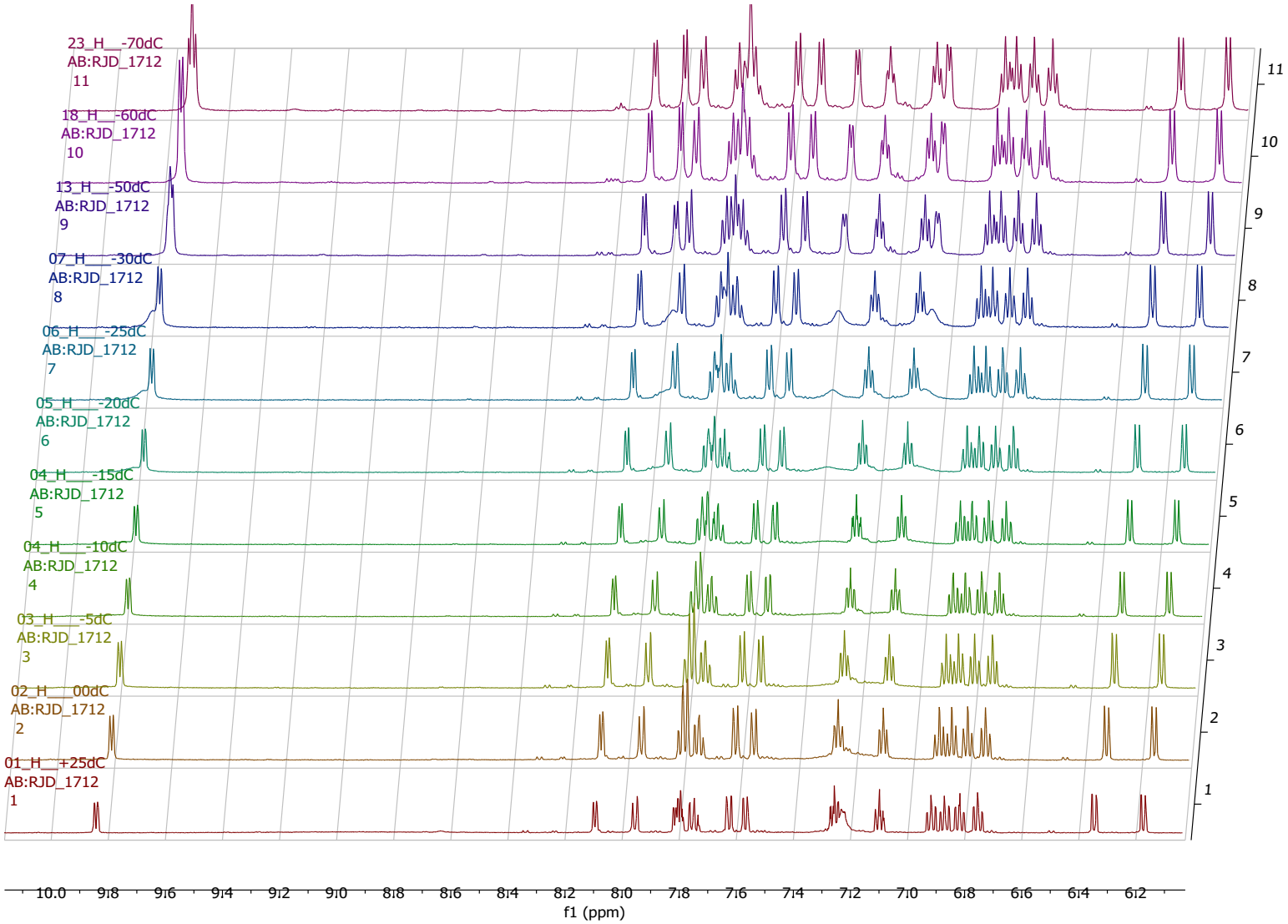

Figure S26. 500 MHz variable temperature ^{1}H NMR spectra (aromatic region) of **3** recorded in CD_2Cl_2.

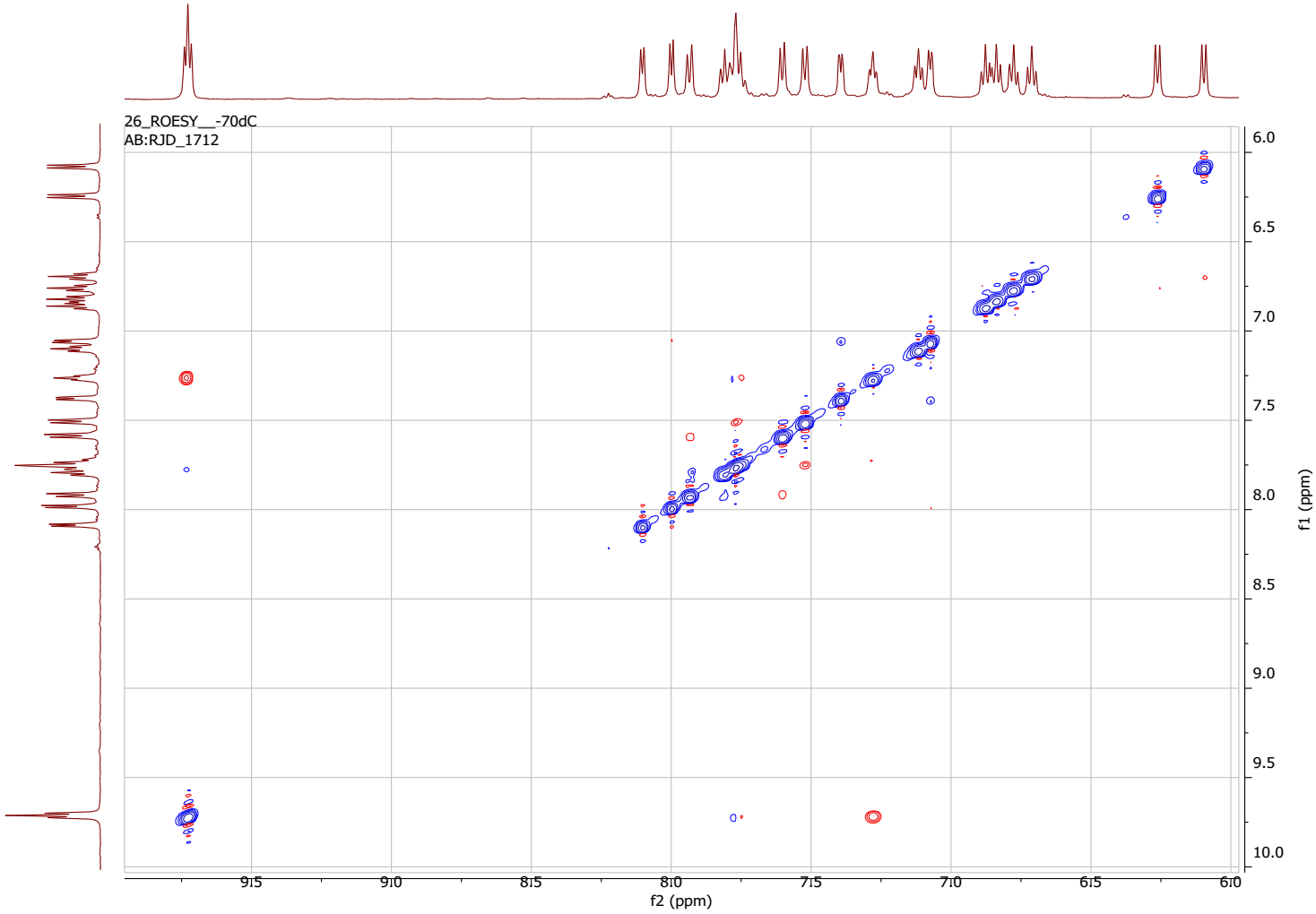

Figure S27. 500 MHz ^{1}H-^{1}H EASY-ROESY NMR spectrum of **3** recorded in CD_2Cl_2 at 203 K. Red cross-peaks represent spatial proximity, while blue and red cross-peaks represents COSY peaks.

S5. Solvent viscosity data

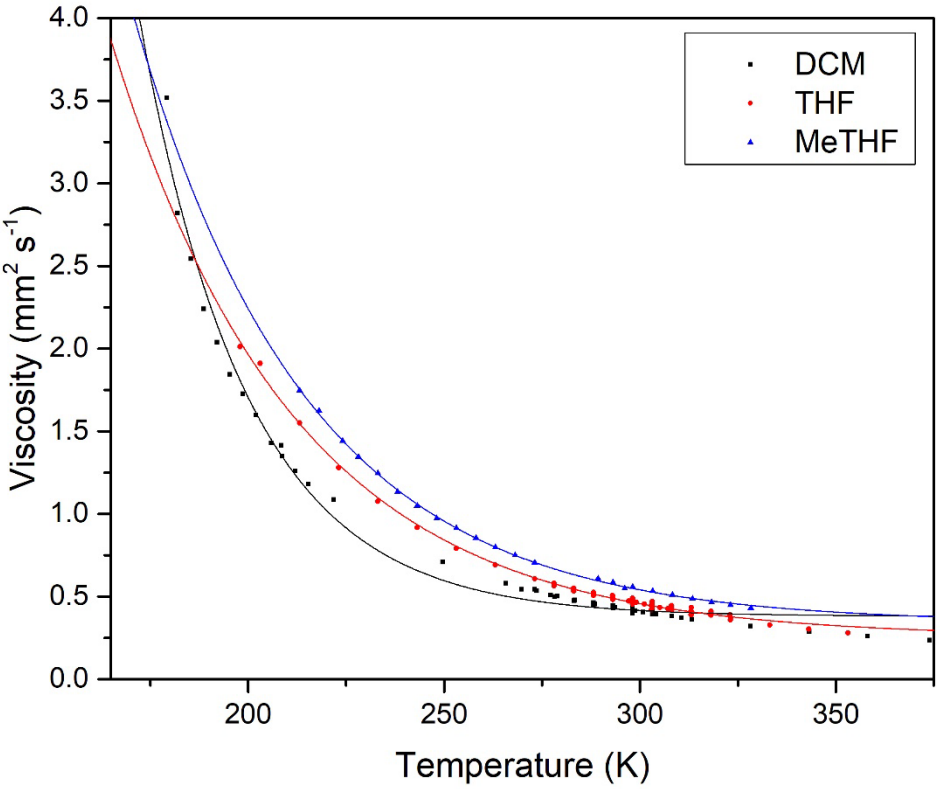

Figure S28. Plot of viscosity vs. temperature for DCM, THF and MeTHF. Data obtained from Wohlfarth and Wohlfahrt.[S8]

S6. Thermodynamic Parameter Calculations

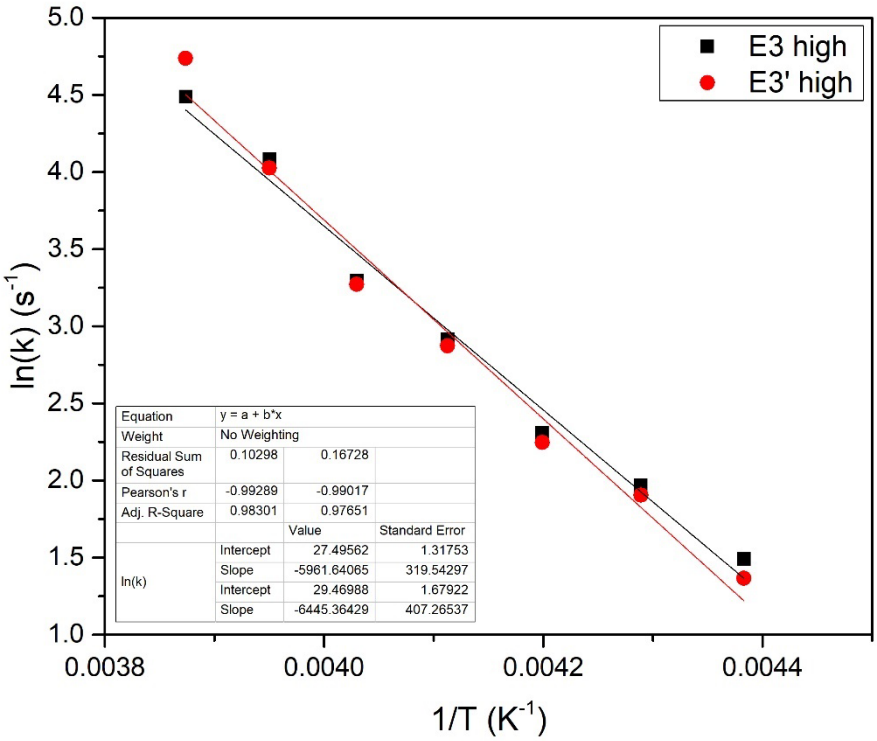

Figure S29. Arrhenius plot of the high E_a region for **1** recorded in THF-d_8 using the E3 and E3′ NMR signals.

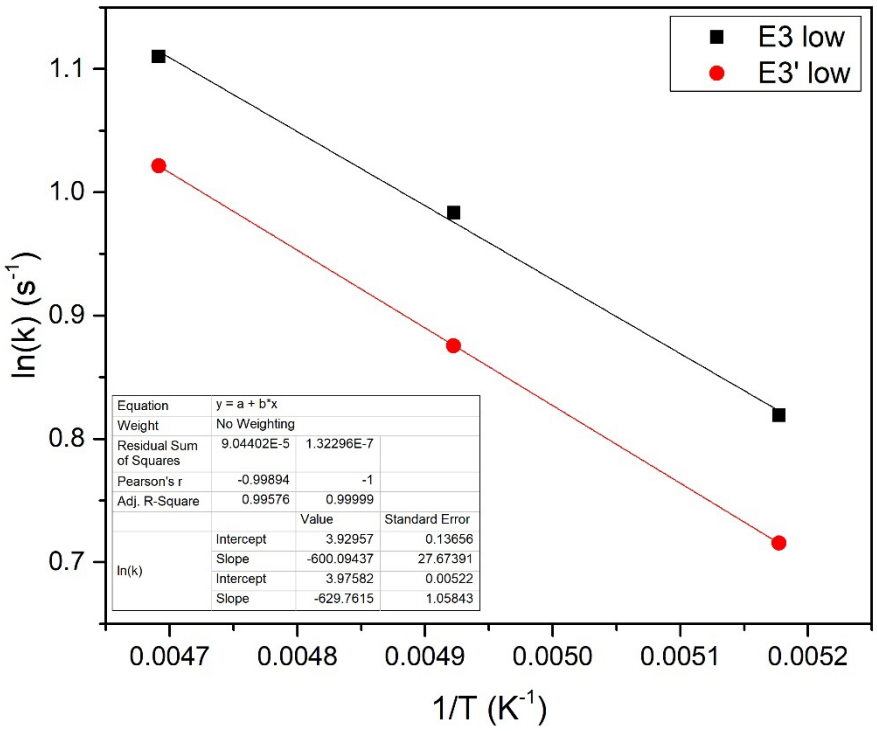

Figure S30. Arrhenius plot of the low E_a region for **1** recorded in THF-d_8 using the E3 and E3′ NMR signals.

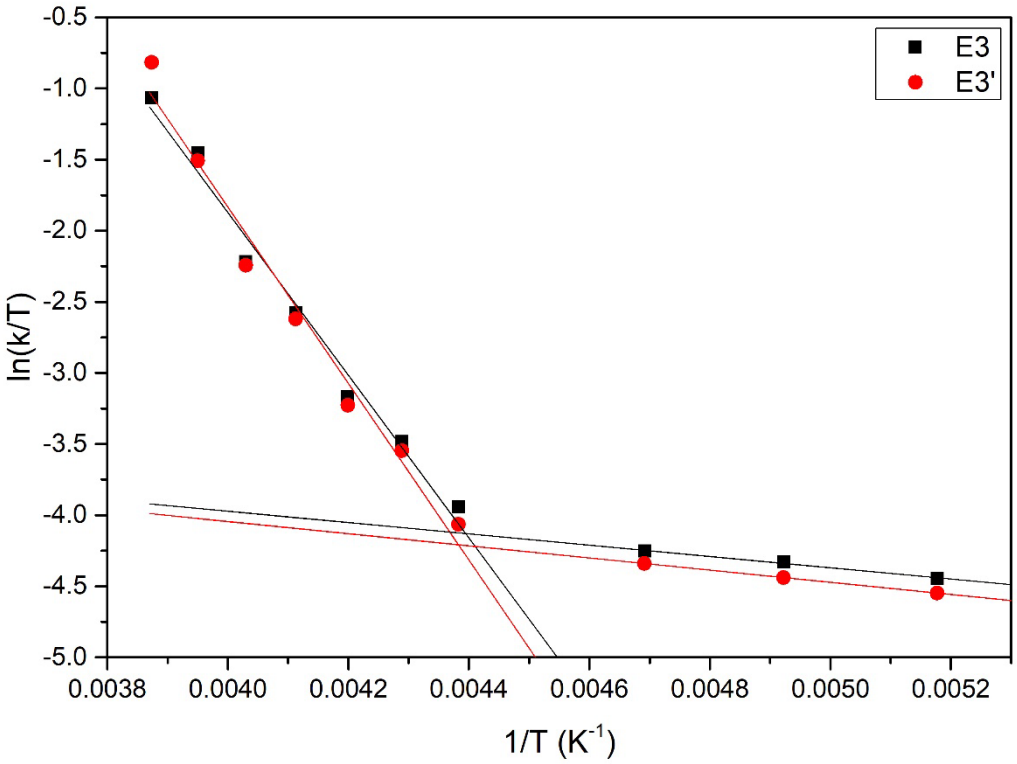

Figure S31. Eyring plot of **1** recorded in THF-d_8 using the E3 and E3′ NMR signals.

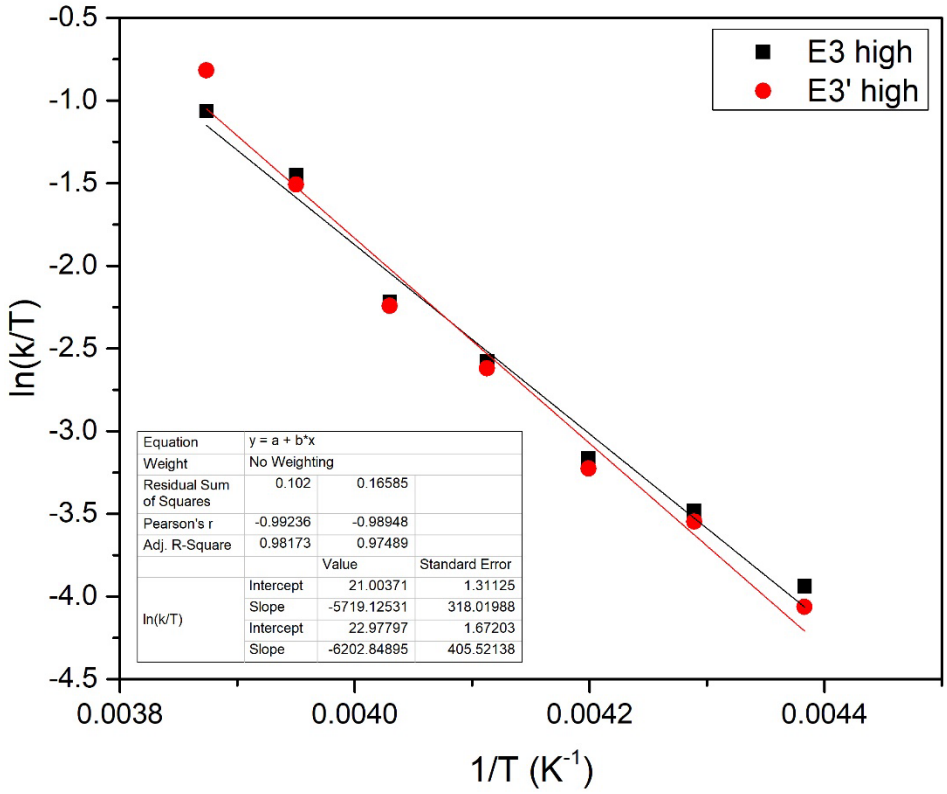

Figure S32. Eyring plot of the high E_a region for **1** recorded in THF-d_8 using the E3 and E3′ NMR signals.

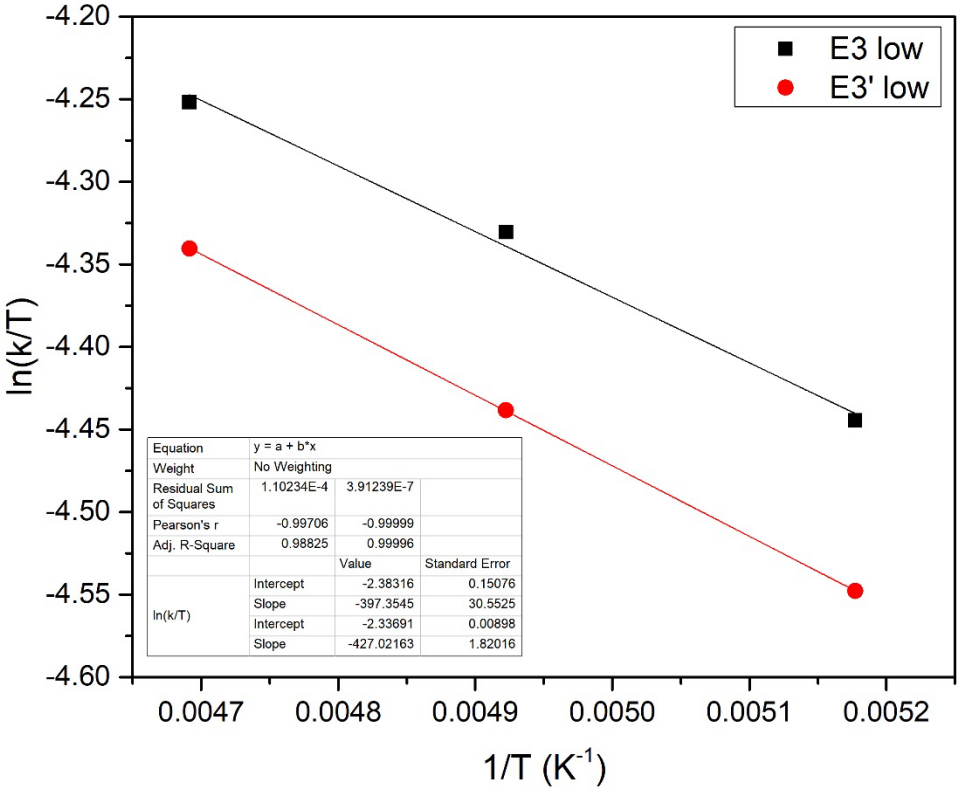

Figure S33. Eyring plot of the low E_a region for **1** recorded in THF-d_8 using the E3 and E3′ NMR signals.

S7. Cyclic Voltammetry

Cyclic (CV) and square wave voltammetry (SWV) of the iridium complexes **1**-**3** were carried out in dichloromethane (DCM) solutions containing a 0.1 M supporting electrolyte (tetrabutylammonium hexafluorophosphate, $TBAPF_6$) using a AutoLab 30 potentiostat with platinum working, platinum counter and platinum pseudo reference electrodes with a scan rate of 100 mV s^{-1}. The ferrocene/ferrocenium couple (FcH^+/FcH) was employed as the internal reference.

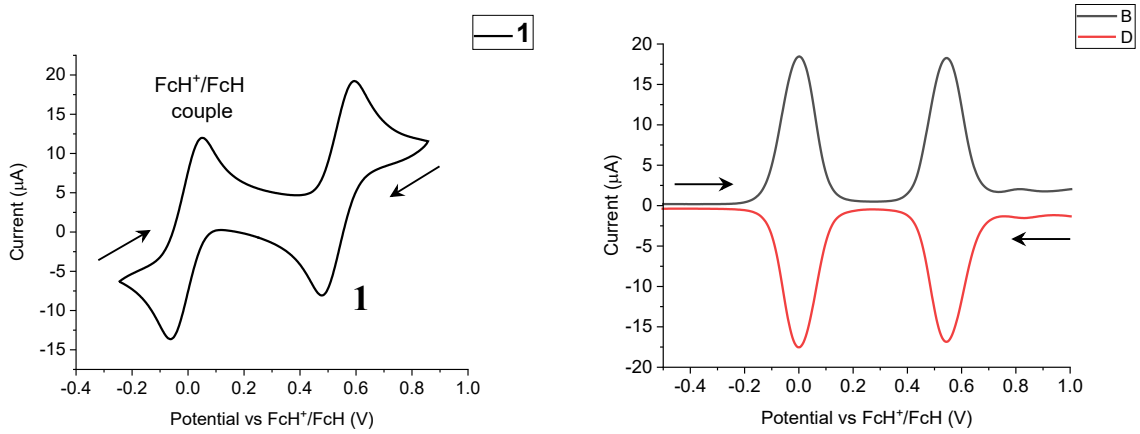

Figure S34. CV (left) and SWV (right) traces for **1**.

The electrochemical behaviours are identical for complexes **1**-**3** where each displays a single reversible oxidation wave attributed to the Ir(III)/Ir(IV) couple at 0.54 V with respect to the FcH^+/FcH couple at 0.00 V. The unsubstituted iridium complex $Ir(ppy)_2(py)Cl$ (**D**) was reported[S7] to have an oxidation potential at 0.54 V thus the ethynyl substitution in **1**-**3** had no impact on the oxidation potential with the substituent being some distance away from the iridium redox centre.

S8. Photophysical Measurements

Instrumentation: Unless specified, all photophysical measurements of **1**, **2**, and **3** were performed using dry DCM as the solvent. The UV-Visible spectra were measured on a Unicam UV2-100 spectrometer operated with the Unicam Vison software in quartz cuvettes with path length l = 1 cm.

Excitation and emission photoluminescence spectra were recorded on a Horiba Jobin Yvon SPEX Fluorolog 3-22 spectrofluorometer. Samples were degassed by repeated freeze-pump-thaw cycles using a turbomolecular pump until the pressure was stable in quartz cuvettes, l = 1 cm. The solutions had absorbance below 0.15 to minimise inner filter effects. T_1 energies were determined from the highest energy onsets of the emission spectra in MeTHF at 80 K.

Photoluminescence quantum yields (PLQYs) were measured in DCM following our previously reported method (see below).[S9] Quinine sulfate in 0.1 M H_2SO_4 (Φ_F: 0.546)[S10] as the reference, the emission spectra of quinine sulfate were collected by exciting the samples at 360 nm. The PLQY of each complex was measured in duplicate and determined by the following method:

1. The UV-vis absorbance spectrum was recorded in quartz cuvette with path length l = 2 cm (to improve spectrum signal-to-noise), recording the absorbance at the excitation wavelength.
2. The same sample solution was transferred to the quartz fluorescence cell (a standard 1 cm cell modified with a Teflon Young's tap) degassed via repeated freeze-pump-thaw cycles before the emission spectrum was recorded.
3. The fully corrected fluorescence spectrum was integrated and the integrated intensity (the area of the fluorescence spectrum) was recorded.
4. Steps 1 to 3 were repeated for five additional solutions with increasing concentrations (with absorbance ranging from 0.02 to 0.1).
5. The integrated fluorescence intensity was plotted verse absorbance, which resulted a linear plot with gradient X ($Grad_X$).
6. Steps 1, 3, 4 and 5 were repeated for the chosen standard (quinine sulfate).

7. Fluorescence quantum yield for each complex was calculated using the following equation

$$\Phi_X = \Phi_{ST}\left(\frac{Grad_X}{Grad_{ST}}\right)\left(\frac{\eta^2{}_X}{\eta^2{}_{ST}}\right)$$

Where ST and X denote standard and the measured complex, Φ is the fluorescence quantum yield, Grad the gradient from the plot of integrated fluorescence intensity vs. absorbance, and η the refractive index of the solvent.

Emission lifetimes were determined by using a custom spectrometer; measured by time-correlated single photon counting (TCSPC) using a pulsed diode laser (371 nm), made by IBH Ltd, running at 1 MHz. The fluorescence emission was collected at right angles to the excitation source. The emission wavelength was selected using a Horiba Jobin Yvon Triax 190 monochromator and detected by a cooled IBH TBX-04 PMT. Timing was achieved using an Ortec 567 time-to-amplitude converter and an E. G. & G Trumpcard pulse height analyser (PHA), and data was recorded using Maestro (ver.510) software. The data were transferred to a PC and analysed using non-linear regression to a single exponential decay, and the quality of fit established by reduced χ^2 and random residuals. The samples were degassed by repeated freeze-pump-thaw cycles in duplicates. The decay data were fitted to a single exponential function. Low temperature emission spectra and lifetime data were measured in a DN1704 optical cryostat (Oxford Instruments) with a ITC601 temperature controller (Oxford Instruments).

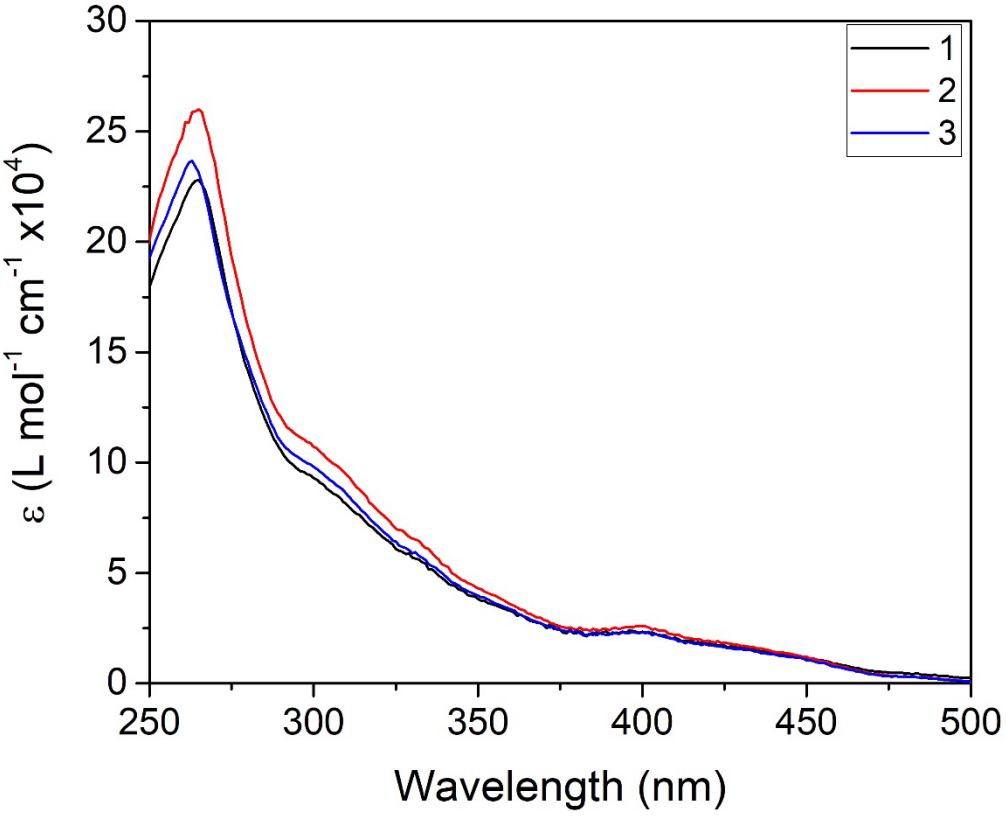

Figure S35. UV-Visible electronic absorbance spectra of **1**, **2** and **3** recorded in DCM.

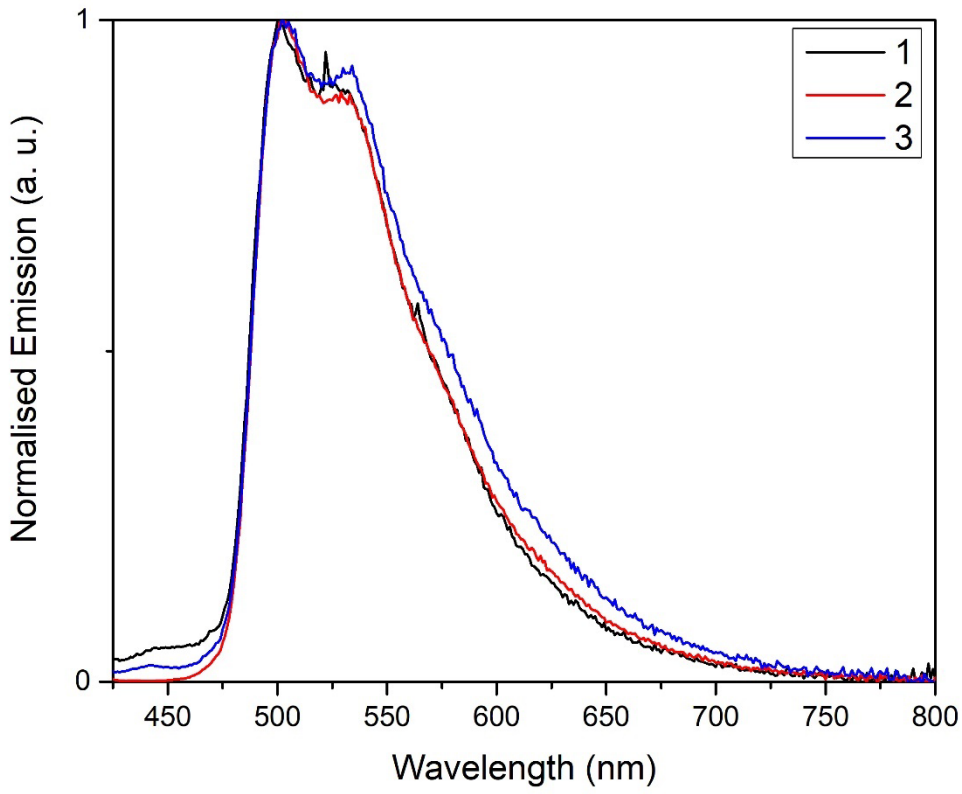

Figure S36. Emission spectra of **1**, **2**, and **3** recorded in DCM at room temperature.

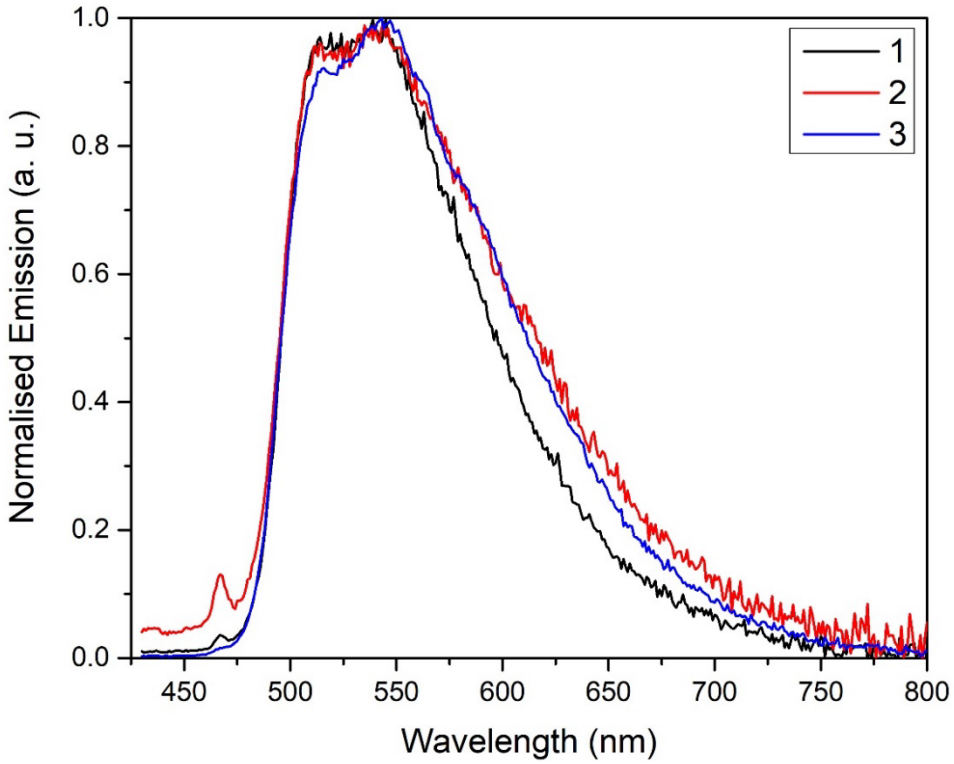

Figure S37. Emission spectra of **1**, **2**, and **3** recorded in MeTHF at room temperature.

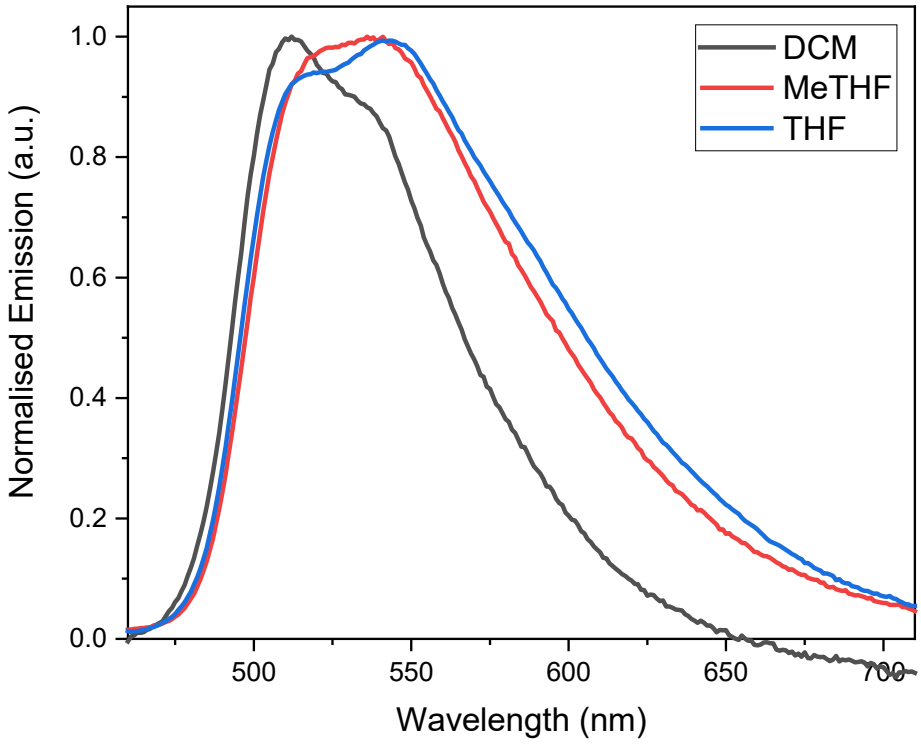

Figure S38. Room temperature emission spectra of **1** recorded in DCM, MeTHF and THF.

Table S5. Photophysical data for complexes **1**-**3**.

Compound	$\lambda_{Emission}$ (nm)		Lifetime[i]	T_1[i]	k_r[i]	k_{nr}[i]	PLQY[i]	Pure radiative lifetime
	DCM	MeTHF	(τ, μs)	(eV)	(10^5 s^{-1})	(10^7 s^{-1})	Φ	(τ_0, μs)
1	501, 525	514, 540	0.16	2.62	3.54	0.58	0.057	2.82
2	501, 529	514, 540	0.21	2.59	2.18	0.43	0.047	4.58
3	504, 532	515, 542	0.23	2.59	3.22	0.39	0.075	3.09

[i] Recorded in DCM

Variable Temperature emission

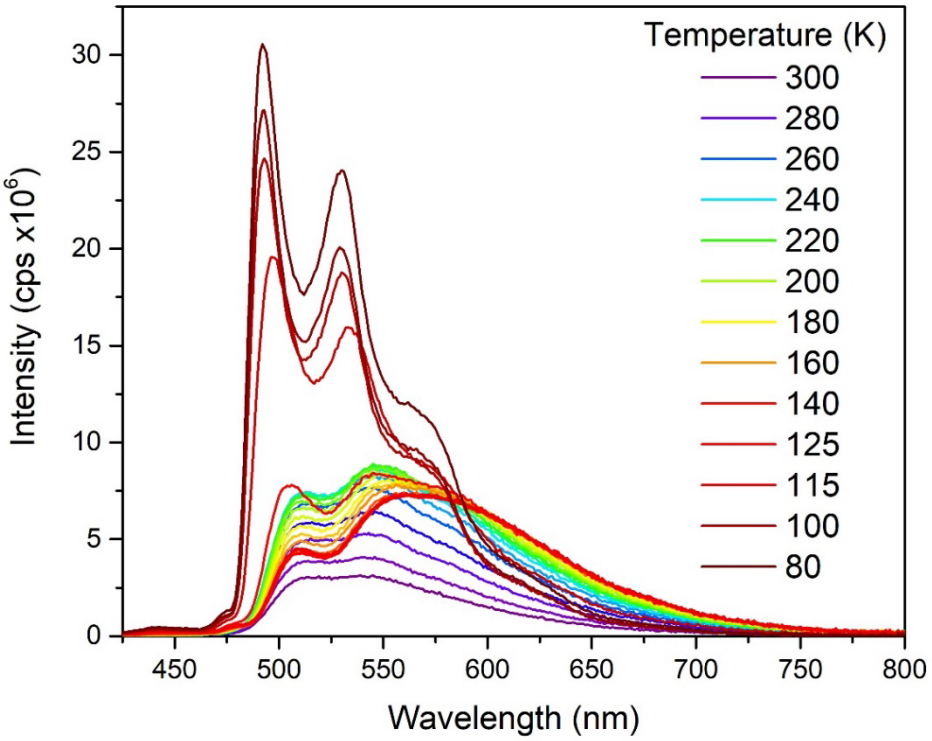

Figure S39. Variable temperature (80 – 300 K) emission spectra of **1** recorded in MeTHF.

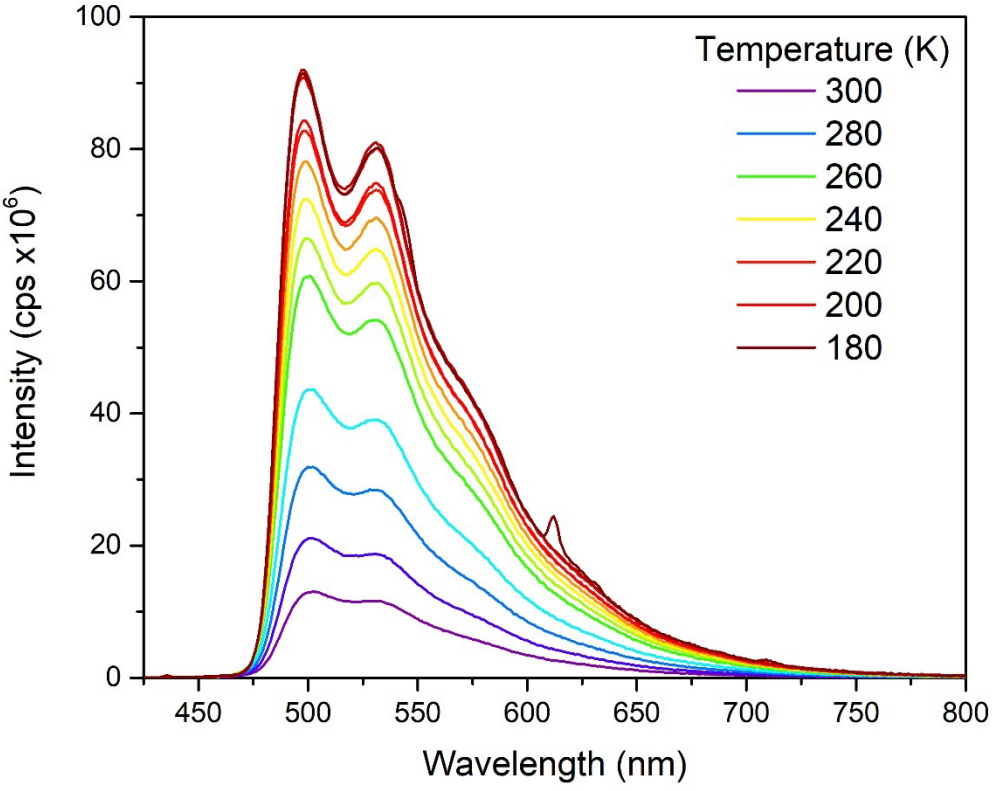

Figure S40. Variable temperature (180 – 300 K) emission spectra of **2** recorded in DCM. Note: the increase of vibronic band intensity as the temperature decreases.

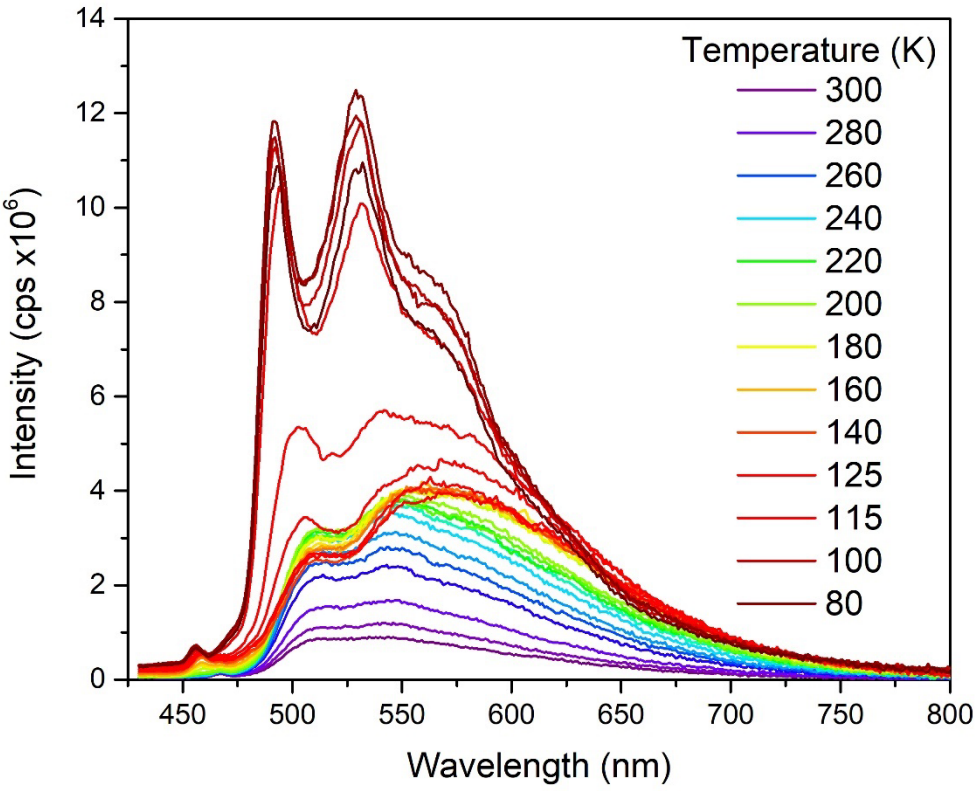

Figure S41. Variable temperature (80 – 300 K) emission spectra of **2** recorded in MeTHF.

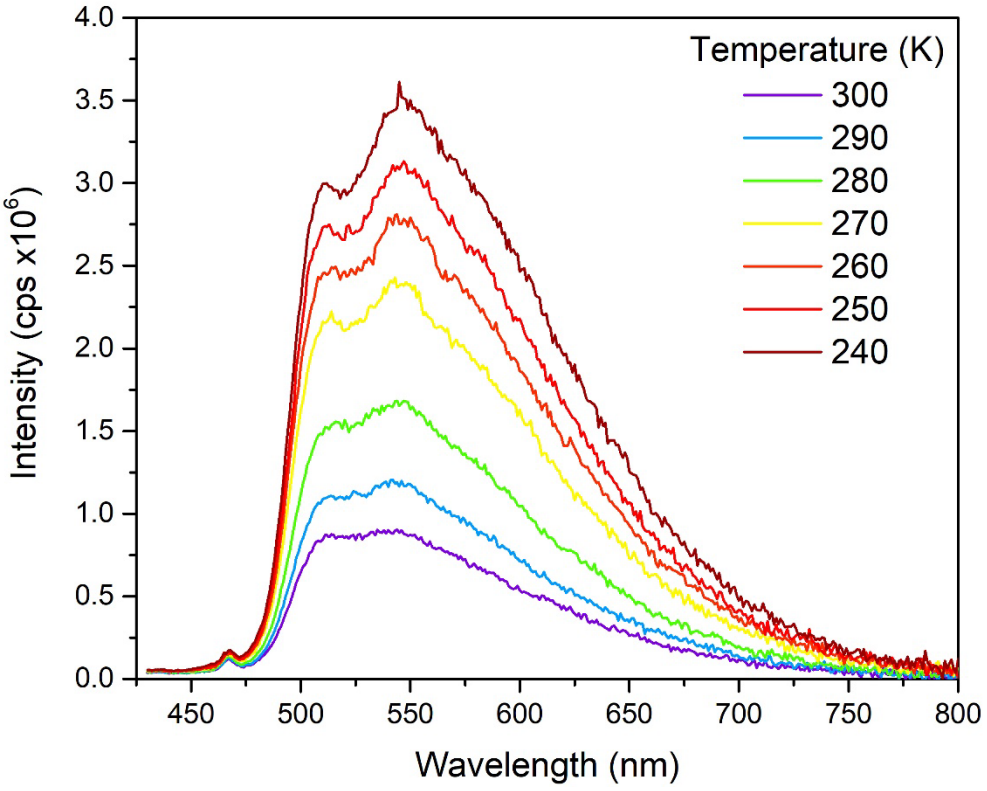

Figure S42. Variable temperature (240 – 300 K) emission spectra of **2** recorded in MeTHF. Note: the increase of vibronic band intensity as the temperature decreases.

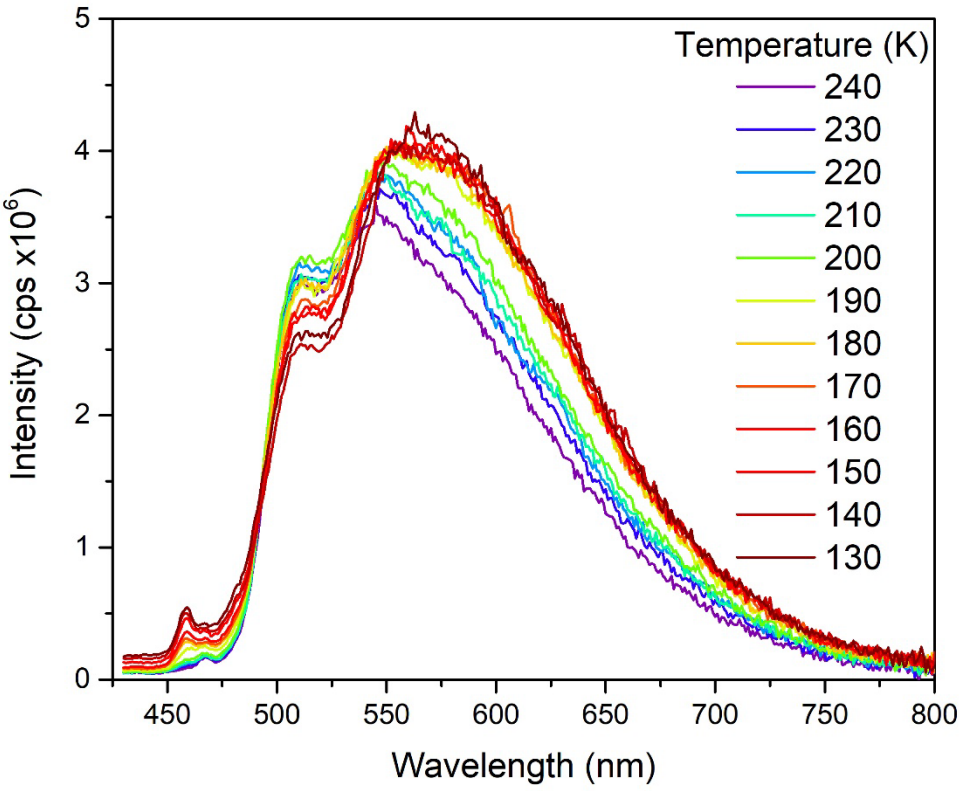

Figure S43. Variable temperature (130 – 240 K) emission spectra of **2** recorded in MeTHF. Note: the decrease of vibronic band intensity as the temperature decreases.

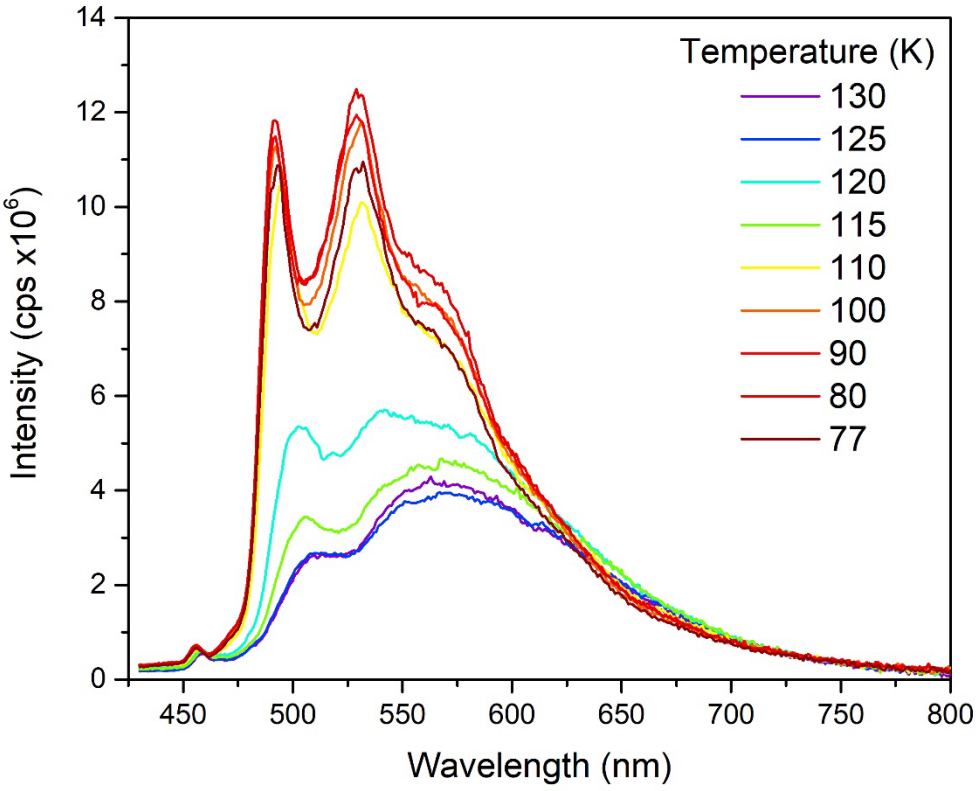

Figure S44. Variable temperature (77 – 130 K) emission spectra of **2** recorded in MeTHF. Note: the increase of vibronic band intensity as the temperature decreases.

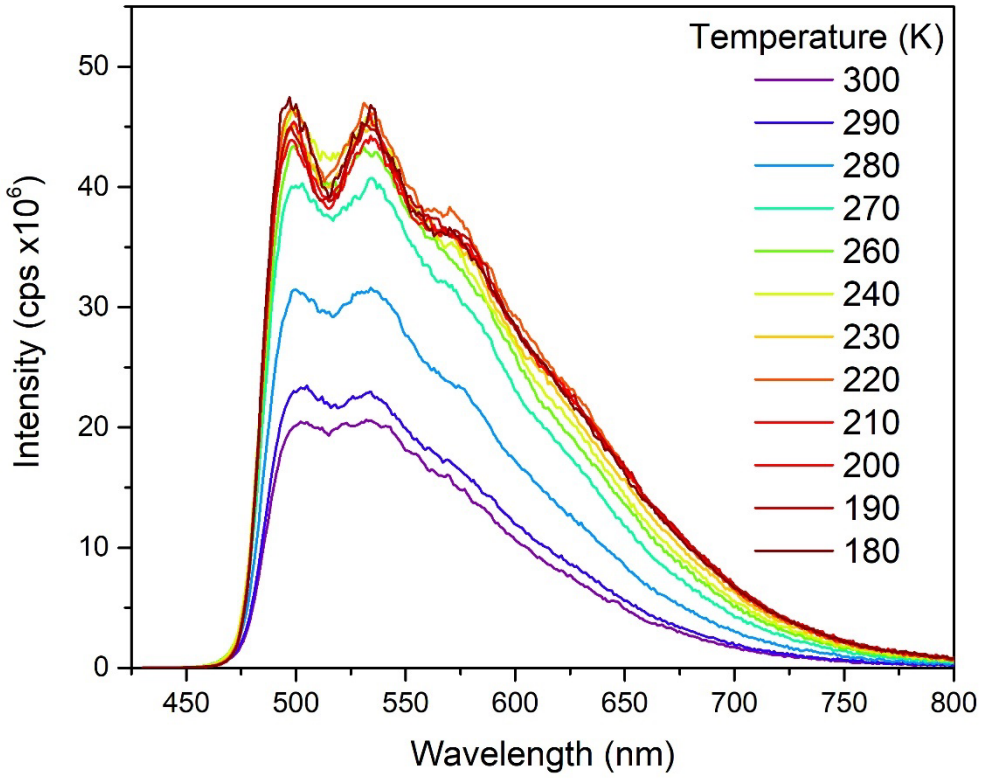

Figure S45. Variable temperature (180 – 300 K) emission spectra of **3** recorded in DCM. Note: the increase of vibronic band intensity as the temperature decreases.

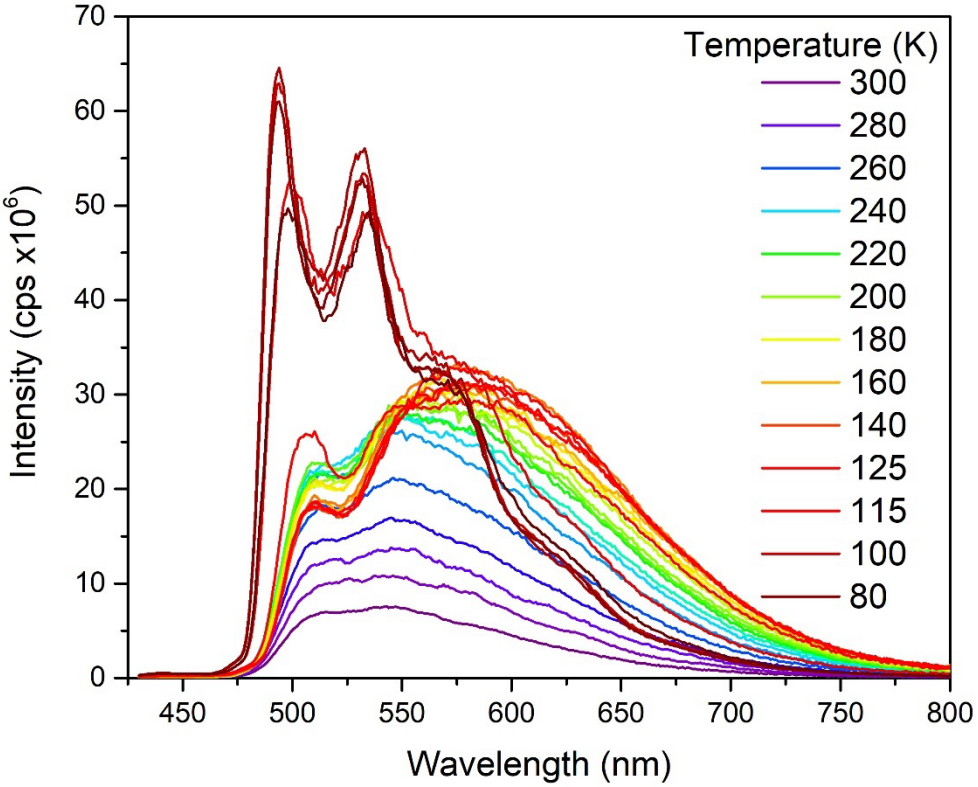

Figure S46. Variable temperature (80 – 300 K) emission spectra of **3** recorded in MeTHF.

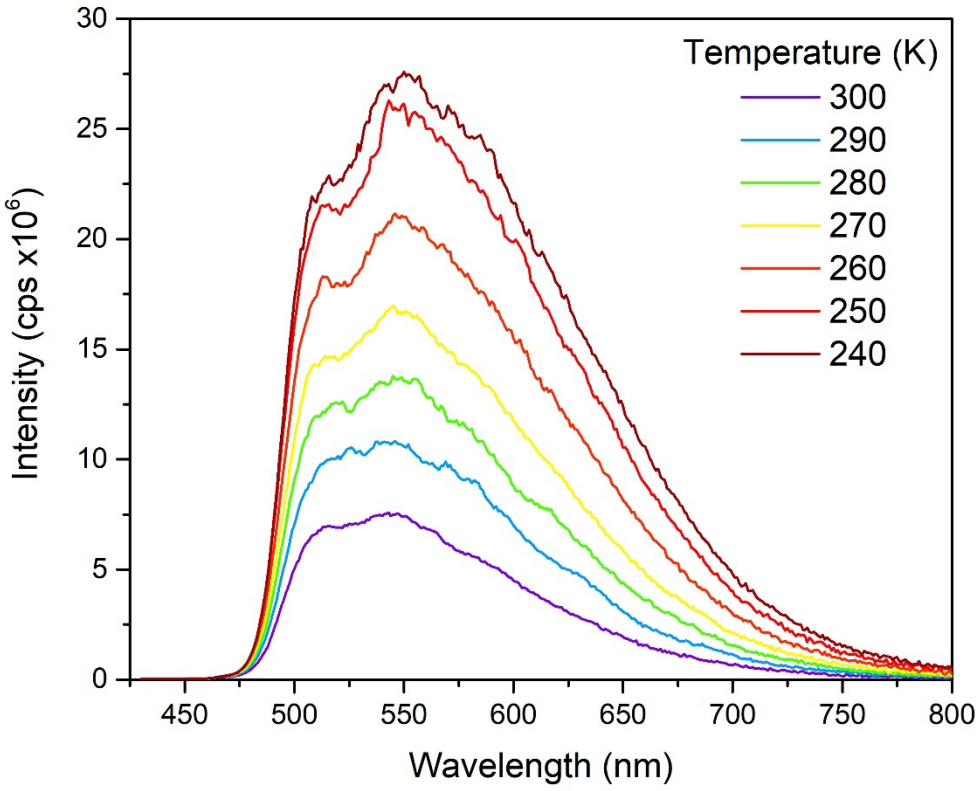

Figure S47. Variable temperature (240 – 300 K) emission spectra of **3** recorded in MeTHF. Note: the increase of vibronic band intensity as the temperature decreases.

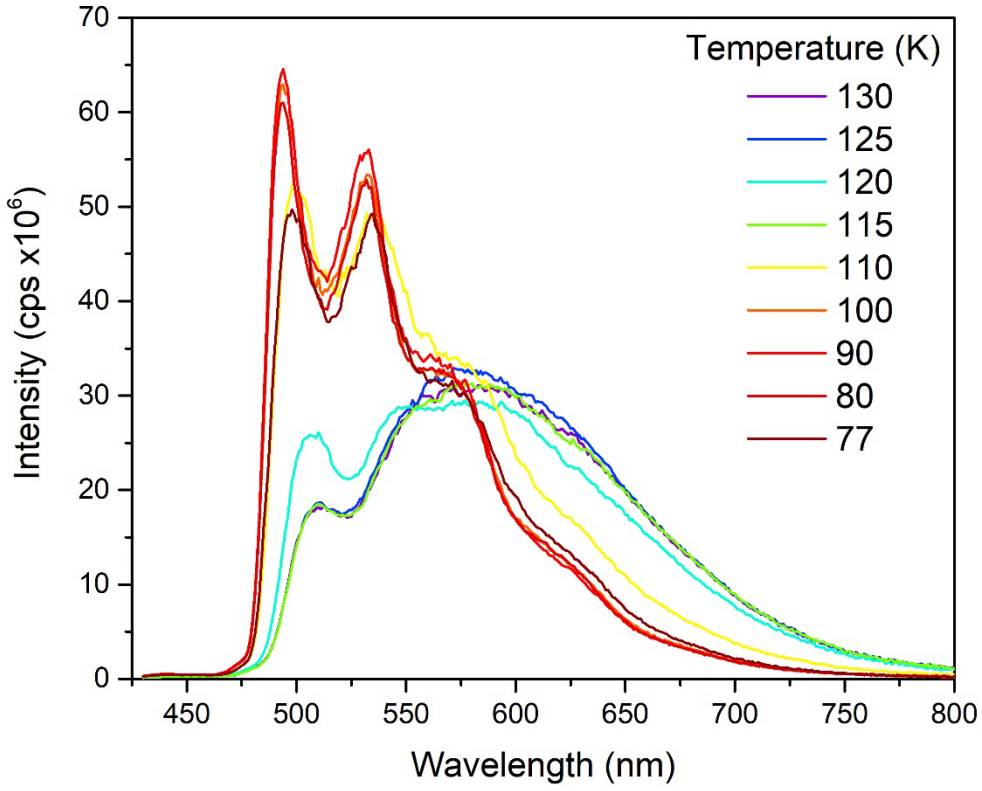

Figure S48. Variable temperature (77 – 130 K) emission spectra of **3** recorded in MeTHF. Note: the increase of vibronic band intensity as the temperature decreases.

S9. Computations

All hybrid-DFT calculations were carried out with the Gaussian 16 package.[S11] The model chemistry B3LYP[S12] with the pseudopotential (LANL2DZ)[S13] for iridium and 3-21G* basis set[S14] for all other atoms was initially selected on the basis of good agreements between experimental and computed data in related iridium complexes elsewhere.[S15] The IEF-PCM solvation model[S16] was applied using tetra-hydrofuran (THF) as solvent.

The Ir-N(pyridine) bond rotation conformers in **1** were examined by fixing the Cl-Ir-N(py)-C(py) dihedral angle at 1° intervals in clockwise (and anticlockwise) steps and then optimising each geometry at the ground state (S_0). Two minima (Min1 and Min2) and two rotational barriers (transition states, TS1 and TS2) were predicted by the VT NMR data for **1**. However, the expected second rotation barrier TS2 and the second minimum Min2 were not located at B3LYP/LANL2DZ:3-21G*/IEF-PCM which indicated that the optimised geometry was different to the experimental geometry at this model chemistry. Other model chemistries were then explored for a better agreement between experimental and optimised geometries with selected bond values listed in Table S6. The agreement between the experimental X-ray determined geometry and the optimised geometry with the hybrid-DFT functional PBE0[17] (instead of B3LYP) is excellent. The PBE0 functional was also preferred over the B3LYP functional in cationic iridium complex $[Ir(N^C)_2(N^N)]^+$ systems elsewhere recently as the latter functional gave barrier energies that are too low.[S18] It is noted here that dual phosphorescence of cationic iridium complex $[Ir(N^C)_2(N^N)]^+$ systems have been reported.[S19] The two emission bands are assigned from ^{3}LC and ^{3}MLCT excited states instead in these cationic systems.

The rotation energy plot at PBE0/LANL2DZ:3-21G*/IEF-PCM in Figure 3 shows the two minima (Min1 and Min2) and two rotational barriers (TS1 and TS2) in agreement with VT NMR data for **1**. Full geometry optimisations of Min1 and Min2 were confirmed as true minima with no imaginary frequencies. Transition state (TS) geometries, TS1 and TS2, were also located (using the OPT=QST3 command) and each TS contained one imaginary frequency from frequency calculations. The rotational conformers in **1** were also explored at the triplet excited state (T_1) at PBE0/LANL2DZ:3-21G*/IEF-PCM (Figure 6) and at B3LYP/LANL2DZ:3-21G*/IEF-PCM where Min1, Min2, TS1 and TS2 conformers of **1** at T_1 were present at both model chemistries.

The rotational conformer procedures for S_0 and T_1 states were applied at PBE0/LANL2DZ:3-21G*/IEF-PCM and B3LYP/LANL2DZ:3-21G*/IEF-PCM to the simpler complex **D** where no Min2 and TS2 geometries were located. These findings suggest that the second rotational barrier TS2 and the second minimum Min2 do not exist for complex **D**. Excited state geometries of the Min2 conformer responsible for broad emissions were found for complexes **A** and **C** but not for complexes **B** and **D**.

Simulated emission spectra for related iridium complexes were recently shown to be in good agreement with experimental emission data.[S20] Some AH calculations did not proceed for some complexes in the recent study so VH calculations were carried out instead. Adiabatic (AH) and vertical Hessian (VH) methods at B3LYP were employed with a fixed FWHH broadening value of 1000 cm^{-1}. Here, AH for **1** at B3LYP/LANL2DZ:3-21G*/IEF-PCM gave the desired simulated vibronic spectra. The FWHH broadening value applied for the simulated vibronic spectra was scaled according to the selected temperature T in K with the equation FWHH(cm^{-1}) = 600 cm^{-1} + 2T. For example at T = 130 K, FWHH = 600 + 260 = 860 cm^{-1}. For the simulated broad emission spectra of **1** at B3LYP/LANL2DZ:3-21G*/IEF-PCM, the AH calculation did not proceed thus the VH calculation was employed instead along with a fixed FWHH broadening value of 3000 cm^{-1} at all temperatures in accord with observed broad emission bands from deconvolution analyses of the observed dual emissions for **1**. The simulated emission spectra were analysed with GaussView[S21] and the vibration figures were generated using Gabedit.[S22]

The natural transition orbitals (NTOs) for T_1 conformers of **1** were obtained by time-dependent DFT (TD-DFT) calculations at B3LYP/LANL2DZ:3-21G*/IEF-PCM. NTO figures and orbital contributions for **1** were generated with the aid of Gabedit[S20] and Multiwfn[S23] packages, respectively.

Table S6. Comparison of key bond parameters in optimised and experimental geometries for **1**. All optimised geometries contain the Min1 conformation at the ground state (S_0).

Functional/ pseudopotential:basis	Ir-Cl	Ir-C(ppy) Ring A	Ir-N(ppy) Ring B	Ir-C(ppy) Ring C	Ir-N(ppy) Ring D	Ir-N(py) Ring E
BP86/ LANL2DZ:3-21G*	2.536	2.012	2.053	2.018	2.048	2.202
CAM/ LANL2DZ:3-21G*	2.525	2.009	2.059	2.015	2.056	2.203
M06/ LANL2DZ:3-21G*	2.533	2.001	2.056	2.009	2.050	2.203
M062X/ LANL2DZ:3-21G*	2.560	1.987	2.063	1.995	2.057	2.224
B3LYP/SDD	2.628	2.020	2.077	2.030	2.076	2.237
B3LYP/LANL2DZ	2.622	2.016	2.069	2.025	2.068	2.224
B3LYP/LANL2DZ:6-31G(d)	2.589	2.014	2.081	2.014	2.076	2.290
B3LYP/LANL2DZ:3-21G*	2.559	2.017	2.065	2.022	2.063	2.228
PBE0/SDD	2.575	2.000	2.052	2.013	2.052	2.192
PBE0/LANL2DZ	2.567	1.998	2.045	2.009	2.043	2.176
PBE0/LANL2DZ:6-31G(d)	2.529	1.995	2.055	1.998	2.050	2.232
PBE0/LANL2DZ:3-21G*	2.502	1.996	2.041	2.003	2.037	2.175
Experimental	2.470	2.000	2.043	1.993	2.033	2.178

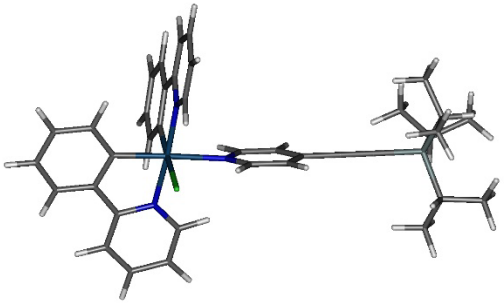

S_0 Min1

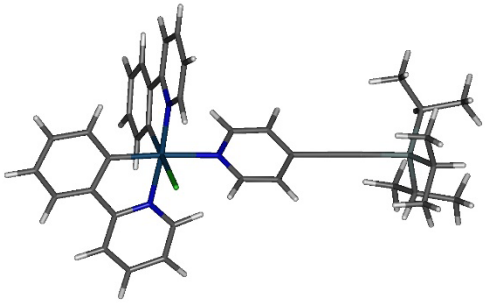

S_0 Min2

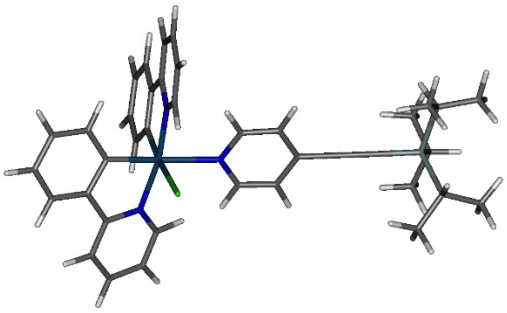

S_0 TS1

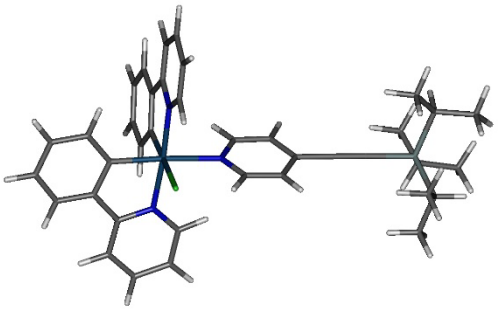

S_0 TS2

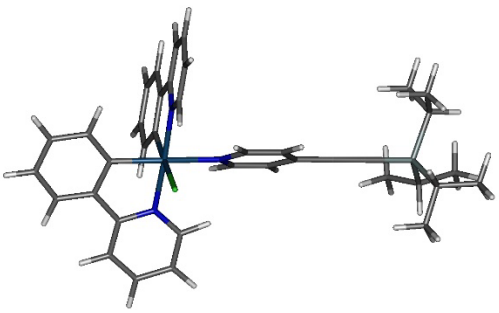

T_1 Min1

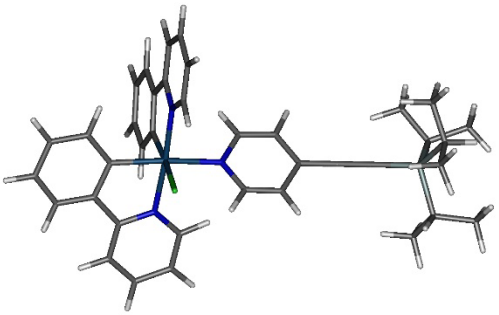

T_1 Min2

Figure S49. Optimised geometries for **1**.

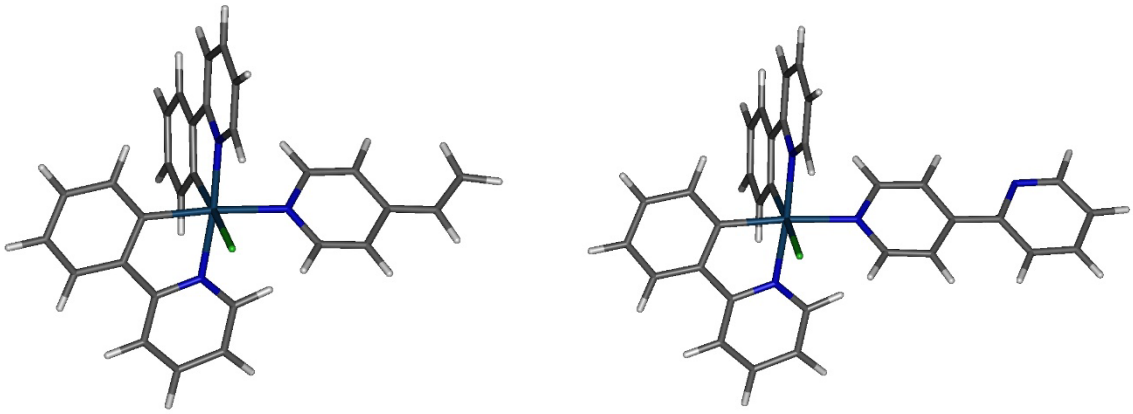

Figure S50. Optimised T_1 Min2 geometries for **A** and **C**. Broad phosphorescent emissions are expected from these conformers for complexes **A** and **C**. No T_1 Min2 geometries could be located for **B** and **D**.

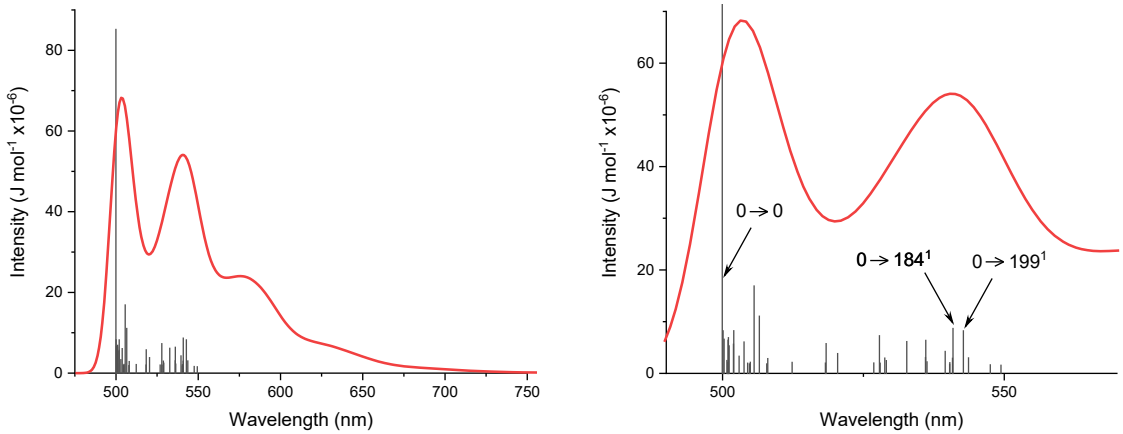

Figure S51. Calculated vibronic spectrum for Min1 conformer of **1** $S_0 \leftarrow T_1$ (Adiabatic Hessian, AH) at B3LYP/LANL2DZ:3-21G*/IEF-PCM(THF). Temperature = 0 K. FWHH = 600 cm^{-1}.

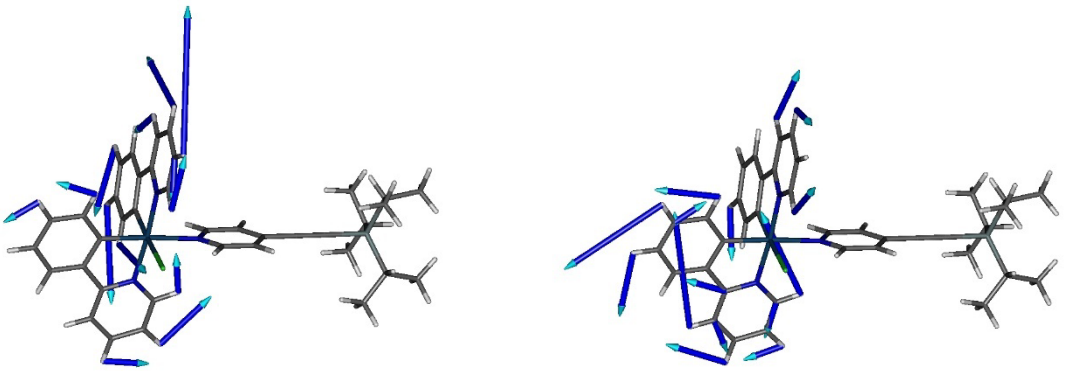

Vibration mode 184; 1495 cm^{-1} Vibration mode 199; 1511 cm^{-1}

Figure S52. Vibrations mainly responsible for the observed vibronic emission bands after 0-0 band at 510 nm.

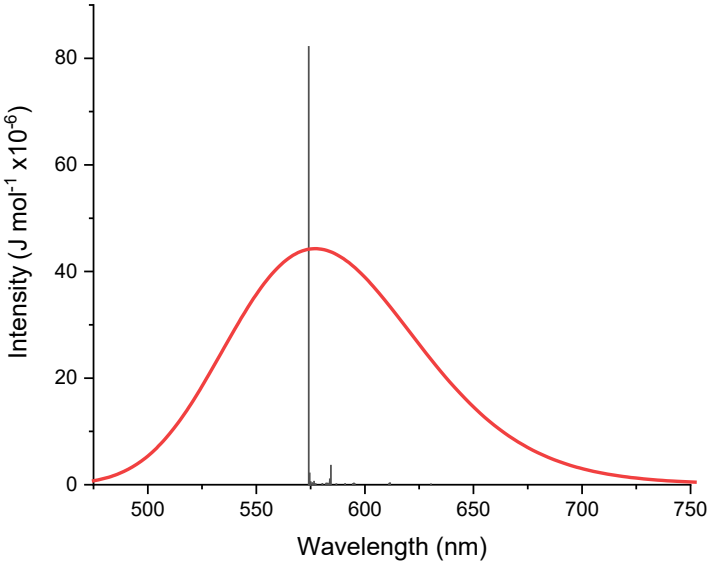

Figure S53. Calculated vibronic spectrum for Min2 conformer of 1 $S_0 \leftarrow T_1$ (Vertical Hessian, VH) at B3LYP/LANL2DZ:3-21G*/IEF-PCM(THF). Temperature = 0 K. FWHH = 3000 cm^{-1}.

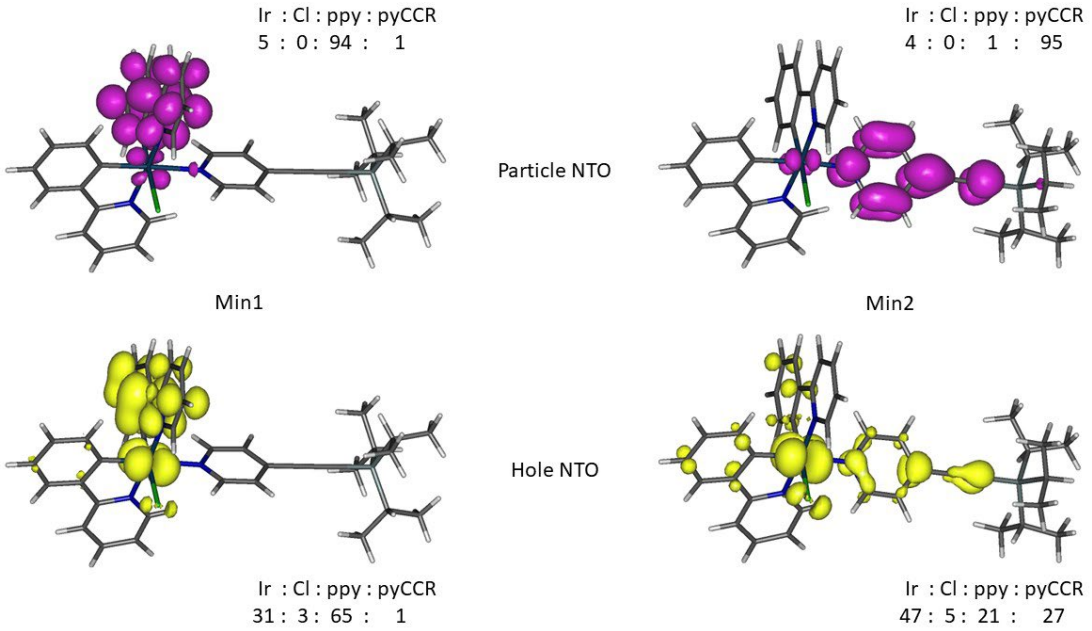

Figure S54. Particle (purple) and hole (yellow) NTOs for T_1 conformers (Min1 and Min2) of **1** with orbital contributions (%).

S10. Cartesian coordinates

Optimised geometries of **1**

S_0 Min1
E(PBE0/LANL2DZ:3-21G*/PCM-THF) = -2476.722271 a.u.
G(PBE0/LANL2DZ:3-21G*/PCM-THF) = -2476.095093 a.u.
NIMAG = 0

Ir	-2.427907	0.073614	-0.353547
N	-2.838411	2.023013	0.070529
N	-2.145679	-1.920639	-0.683150
C	-1.900023	2.983856	0.239151
C	-2.018442	-2.476744	-1.910612
H	-0.870709	2.667295	0.148530
H	-2.095110	-1.784103	-2.740057
C	-2.235979	4.300162	0.508517
C	-1.813315	-3.837735	-2.074827
C	-3.586685	4.644178	0.602715
C	-1.736504	-4.650586	-0.941836
H	-3.880809	5.666142	0.811392
H	-1.576968	-5.718031	-1.040480
C	-4.550339	3.662735	0.418958
C	-1.869255	-4.078075	0.316921
H	-5.602527	3.908197	0.478737
H	-1.815571	-4.690817	1.207291
C	-4.169666	2.344909	0.148479
C	-2.076767	-2.702195	0.440936
C	-2.638179	0.192009	2.701479
C	-5.247219	-1.124669	-0.601947
C	-2.601893	-0.405055	3.962365
C	-6.637506	-1.017948	-0.565824
H	-2.744161	0.204091	4.850176
H	-7.249826	-1.894672	-0.756057
C	-2.387668	-1.781046	4.094906
C	-7.253399	0.207026	-0.286099
C	-2.212846	-2.561369	2.957335
C	-6.469688	1.328675	-0.043189
C	-2.245667	-1.966543	1.689155
C	-5.072202	1.224185	-0.079141
C	-2.455532	-0.569314	1.535922
C	-4.429499	-0.009871	-0.362384
H	-1.454484	5.037595	0.637566
H	-2.361424	-2.238325	5.077775
H	-2.050579	-3.629834	3.062764
H	-1.718293	-4.248484	-3.071637
H	-8.334969	0.282090	-0.259249
H	-6.949175	2.279080	0.171469
H	-2.810468	1.260990	2.623708
H	-4.794486	-2.086546	-0.820756
C	0.474198	0.181369	-1.441178
C	0.399965	0.319620	0.883343
C	1.859412	0.181426	-1.433047
H	-0.096519	0.157499	-2.361381
C	1.781473	0.333077	0.965226
H	-0.216755	0.356305	1.772029
C	2.547283	0.256852	-0.210870
H	2.404497	0.126413	-2.366419
H	2.265496	0.394817	1.931277
C	3.965457	0.255149	-0.159542
C	5.184927	0.252384	-0.103368
Cl	-2.411703	0.690078	-2.777856
N	-0.260358	0.245356	-0.301856
Si	7.030468	0.241890	-0.028304
C	7.597233	1.837479	-0.876077
H	7.154490	1.829772	-1.885509
C	7.601394	-1.272796	-1.007396
H	8.701043	-1.314990	-0.937285
C	7.556459	0.187296	1.794579
H	7.570335	1.231973	2.147300
C	8.985001	-0.387247	1.952703
H	9.286110	-0.361311	3.008885
H	9.019798	-1.432148	1.619937
H	9.724540	0.180502	1.375978
C	7.211791	-1.139036	-2.497393
H	7.534403	-2.029386	-3.054313
H	6.122363	-1.051625	-2.603017
H	7.675842	-0.260527	-2.961850
C	9.134751	1.893351	-1.023411
H	9.431461	2.800955	-1.566697
H	9.617762	1.923552	-0.038540
H	9.524226	1.026483	-1.572067
C	6.577552	-0.600749	2.693966
H	6.908112	-0.553540	3.740703
H	5.560682	-0.197020	2.631947
H	6.542327	-1.657083	2.400858
C	7.088350	3.095740	-0.138940
H	7.387729	4.002234	-0.682383
H	5.995035	3.094262	-0.048946
H	7.517723	3.153724	0.869647
C	7.023603	-2.584244	-0.429902
H	7.346043	-3.441128	-1.037361
H	7.355390	-2.755691	0.600779
H	5.926340	-2.556416	-0.438515

S_0 Min2
E(PBE0/LANL2DZ:3-21G*/PCM-THF) = -2476.722020 a.u.
G(PBE0/LANL2DZ:3-21G*/PCM-THF) = -2476.093824 a.u.
NIMAG = 0

Ir	2.400428	-0.061137	-0.327364
N	2.681888	-2.031686	0.118483
N	2.267781	1.943942	-0.666097
C	1.687623	-2.906819	0.397050
C	2.103227	2.493857	-1.892412
H	0.682724	-2.509882	0.387336
H	2.047551	1.785286	-2.709793
C	1.937604	-4.239579	0.678703
C	2.022318	3.865938	-2.068022
C	3.258968	-4.692521	0.671178
C	2.113596	4.697486	-0.948983
H	3.486185	-5.730303	0.885230
H	2.055485	5.774203	-1.058126
C	4.279961	-3.797162	0.386257
C	2.279993	4.131471	0.308257
H	5.310894	-4.125738	0.375995
H	2.352860	4.757825	1.187762
C	3.985643	-2.458377	0.110521
C	2.356623	2.742882	0.444925
C	2.724331	-0.170854	2.719386
C	5.290126	0.919849	-0.694595
C	2.828554	0.440172	3.968729
C	6.666888	0.701731	-0.745741
H	2.950195	-0.171590	4.857808
H	7.335309	1.529557	-0.964030
C	2.779760	1.833580	4.090442
C	7.197402	-0.573079	-0.519598
C	2.628948	2.616913	2.952280
C	6.341912	-1.631640	-0.238877
C	2.524761	2.007867	1.693794
C	4.957918	-1.415025	-0.186477
C	2.564643	0.592697	1.552699
C	4.401453	-0.130056	-0.418561
H	1.112832	-4.905280	0.897279
H	2.861753	2.300557	5.065663
H	2.595070	3.698052	3.047709
H	1.892330	4.271606	-3.062939
H	8.268850	-0.735320	-0.562224
H	6.755497	-2.620294	-0.064153
H	2.767697	-1.253114	2.651914
H	4.904744	1.917749	-0.877388
C	-0.501250	-0.787034	-1.162860
C	-0.428773	0.583051	0.719912
C	-1.884742	-0.825397	-1.126285
H	0.067427	-1.276847	-1.943604
C	-1.810276	0.596182	0.810719
H	0.185021	1.119221	1.431399
C	-2.574240	-0.124643	-0.122417
H	-2.428862	-1.387399	-1.874248
H	-2.294153	1.157630	1.599294
C	-3.991614	-0.141755	-0.057876
C	-5.211186	-0.161061	-0.006094
Cl	2.284469	-0.704764	-2.743885
N	0.233358	-0.102027	-0.247308
Si	-7.056722	-0.209376	0.050395
C	-7.507200	-1.855366	0.872312
H	-7.012023	-2.644182	0.282727
C	-7.650452	-0.178169	-1.745461
H	-8.753036	-0.177186	-1.728741
C	-7.668996	1.274565	1.062041
H	-7.644973	0.963724	2.119722
C	-9.131292	1.634582	0.704685
H	-9.480588	2.461965	1.337354
H	-9.204324	1.958312	-0.341050
H	-9.811986	0.787430	0.848939
C	-7.174676	-1.441776	-2.498456
H	-7.511817	-1.409004	-3.543531
H	-6.078054	-1.497440	-2.499599
H	-7.567111	-2.358968	-2.042836
C	-9.030496	-2.115211	0.842469
H	-9.256020	-3.099920	1.274338
H	-9.564320	-1.362649	1.436477
H	-9.428686	-2.093622	-0.179838
C	-6.775366	2.527086	0.917987
H	-7.151202	3.332978	1.563303
H	-5.736999	2.314393	1.196254
H	-6.781829	2.894476	-0.115401
C	-6.982310	-1.940158	2.322363
H	-7.209619	-2.925141	2.752311
H	-5.896814	-1.787848	2.366604
H	-7.463263	-1.181403	2.953074
C	-7.170944	1.087379	-2.490961
H	-7.499818	1.058084	-3.538916
H	-7.568642	2.002434	-2.036759
H	-6.074891	1.146218	-2.481573

S_0 TS1
E(PBE0/LANL2DZ:3-21G*/PCM-THF) = -2476.699450 a.u.
G(PBE0/LANL2DZ:3-21G*/PCM-THF) = -2476.070376 a.u.
NIMAG = 1

Ir	-2.414142	0.094969	-0.210081
N	-3.018169	2.051242	0.156723
N	-2.192812	-1.904161	-0.511457
C	-2.315451	3.048078	0.744404
C	-2.101778	-2.474759	-1.739457
H	-1.354080	2.790323	1.148870
H	-2.081099	-1.776266	-2.567891
C	-2.788190	4.342827	0.869348
C	-2.023652	-3.848230	-1.896058
C	-4.054307	4.646070	0.367576
C	-2.047322	-4.661456	-0.758561
H	-4.448934	5.653348	0.427616
H	-1.986991	-5.739395	-0.853132
C	-4.810724	3.624707	-0.183440
C	-2.157699	-4.076545	0.495448
H	-5.812239	3.818089	-0.543733
H	-2.192333	-4.689244	1.386762
C	-4.300959	2.324261	-0.260727
C	-2.238923	-2.685399	0.615401
C	-2.808854	0.234359	2.832066
C	-5.105565	-1.242239	-0.812586
C	-2.844328	-0.356230	4.094778
C	-6.450084	-1.189037	-1.177485
H	-3.020558	0.260125	4.971492
H	-6.991785	-2.111977	-1.362457
C	-2.658826	-1.735386	4.246153
C	-7.108650	0.037849	-1.309715
C	-2.447429	-2.525666	3.123078
C	-6.417606	1.213570	-1.048236
C	-2.412082	-1.936454	1.851454
C	-5.067960	1.161717	-0.671555
C	-2.581500	-0.534732	1.679781
C	-4.372375	-0.067894	-0.569981
H	-2.171808	5.091528	1.349372
H	-2.685352	-2.185776	5.232168
H	-2.310088	-3.596438	3.240313
H	-1.947411	-4.270377	-2.889616
H	-8.152185	0.071665	-1.602589
H	-6.933383	2.164939	-1.133104
H	-2.965940	1.304491	2.742971
H	-4.629440	-2.211652	-0.724984
C	0.543452	-0.908275	-0.468024
C	0.577281	1.253249	0.327684
C	1.926342	-0.966291	-0.487235
H	-0.027396	-1.757332	-0.800208
C	1.961710	1.276863	0.338173
H	0.046541	2.133833	0.633556
C	2.677567	0.144316	-0.074916
H	2.418842	-1.868611	-0.825369
H	2.480184	2.169986	0.661107
C	4.095998	0.125921	-0.081803
C	5.316532	0.110362	-0.090755
Cl	-2.052126	0.713419	-2.602554
N	-0.158199	0.184033	-0.061184
Si	7.163735	0.078966	-0.089922
C	7.659336	-1.705706	-0.480723
H	7.172525	-2.339605	0.278494
C	7.708094	0.558565	1.657255
H	8.810378	0.588989	1.662041
C	7.785734	1.288529	-1.414193
H	7.803840	0.728641	-2.363930
C	9.228714	1.759682	-1.111474
H	9.586435	2.415207	-1.917189
H	9.259981	2.331295	-0.175492
H	9.927597	0.919691	-1.023006
C	7.243931	-0.498606	2.685252
H	7.553032	-0.203804	3.697432
H	6.149371	-0.585654	2.678741
H	7.670542	-1.486481	2.473367
C	9.187212	-1.913828	-0.375764
H	9.440210	-2.968338	-0.551568
H	9.712294	-1.316520	-1.131931
H	9.570921	-1.632838	0.613255
C	6.868166	2.516642	-1.608294
H	7.257425	3.151888	-2.415765
H	5.845298	2.218150	-1.863863
H	6.828148	3.122639	-0.694899
C	7.157095	-2.152214	-1.871487
H	7.410742	-3.206464	-2.047459
H	6.069466	-2.040318	-1.961226
H	7.631171	-1.557951	-2.663331
C	7.178229	1.952062	2.062682
H	7.483098	2.189886	3.091139
H	7.561730	2.740421	1.404534
H	6.081525	1.971792	2.021143

S_0 TS2
E(PBE0/LANL2DZ:3-21G*/PCM-THF) = -2476.721900 a.u.
G(PBE0/LANL2DZ:3-21G*/PCM-THF) = -2476.092205 a.u.
NIMAG = 1

Ir	2.404492	-0.059883	-0.334034
N	2.669131	-2.026029	0.133308
N	2.277624	1.941487	-0.702321
C	1.663946	-2.895219	0.391006
C	2.111397	2.473917	-1.935764
H	0.661671	-2.493706	0.350036
H	2.058888	1.754087	-2.743525
C	1.901827	-4.226646	0.689071
C	2.025982	3.843335	-2.130420
C	3.221411	-4.684065	0.720009
C	2.114355	4.690225	-1.022977
H	3.439062	-5.720741	0.948897
H	2.052174	5.765159	-1.146565
C	4.252880	-3.795592	0.451437
C	2.283015	4.141697	0.241866
H	5.282272	-4.128760	0.467232
H	2.353160	4.780131	1.112847
C	3.970590	-2.458459	0.156140
C	2.364253	2.755485	0.397402
C	2.737153	-0.124587	2.713526
C	5.301450	0.898033	-0.697015
C	2.851682	0.505076	3.953097
C	6.677935	0.673474	-0.723515
H	2.976979	-0.093564	4.850567
H	7.352853	1.493402	-0.951428
C	2.809049	1.900108	4.053309
C	7.199811	-0.597732	-0.460007
C	2.653165	2.666202	2.903737
C	6.335971	-1.646407	-0.167784
C	2.537332	2.038627	1.655936
C	4.952253	-1.423555	-0.140271
C	2.573099	0.621751	1.536178
C	4.404818	-0.141647	-0.408961
H	1.069329	-4.888247	0.890159
H	2.899707	2.382063	5.020450
H	2.623684	3.748797	2.982777
H	1.894853	4.234825	-3.130866
H	8.271094	-0.764953	-0.483145
H	6.742874	-2.632500	0.035024
H	2.776128	-1.207978	2.662193
H	4.922256	1.892891	-0.907539
C	-0.522877	-0.553649	-1.275894
C	-0.420507	0.381443	0.854784
C	-1.906888	-0.573358	-1.239934
H	0.038123	-0.893608	-2.138025
C	-1.801124	0.395112	0.956945
H	0.205587	0.745402	1.657958
C	-2.581013	-0.093562	-0.104743
H	-2.462815	-0.954894	-2.086591
H	-2.272212	0.779100	1.852434
C	-3.998234	-0.102970	-0.034835
C	-5.217646	-0.116186	0.022102
Cl	2.313595	-0.729230	-2.745668
N	0.227496	-0.089993	-0.242195
Si	-7.062455	-0.161049	0.104208
C	-7.491291	-0.737630	1.856098
H	-6.971646	-1.698477	2.004220
C	-7.627498	-1.432768	-1.176777
H	-8.730077	-1.441683	-1.170420
C	-7.720306	1.584909	-0.245359
H	-7.705209	2.122769	0.717061
C	-9.184553	1.543472	-0.745320
H	-9.560556	2.565232	-0.891977
H	-9.249056	1.021290	-1.708084
H	-9.849174	1.036735	-0.035824
C	-7.125454	-2.845757	-0.800381
H	-7.444143	-3.575111	-1.557633
H	-6.028460	-2.863895	-0.755324
H	-7.516776	-3.170804	0.171255
C	-9.008183	-0.978333	2.028586
H	-9.219506	-1.365484	3.034768
H	-9.565722	-0.040652	1.910248
H	-9.392085	-1.702173	1.298614
C	-6.852169	2.381804	-1.244970
H	-7.256461	3.395985	-1.367902
H	-5.814115	2.460497	-0.902874
H	-6.849816	1.900292	-2.230331
C	-6.984559	0.251413	2.928732
H	-7.194128	-0.137385	3.934523
H	-5.903637	0.418288	2.842971
H	-7.491900	1.220038	2.832507
C	-7.149075	-1.068681	-2.600079
H	-7.458498	-1.843838	-3.314661
H	-7.565049	-0.111992	-2.936992
H	-6.054025	-0.997856	-2.630211

T_1 Min1
E(PBE0/LANL2DZ:3-21G*/PCM-THF) = -2476.626589 a.u.
G(PBE0/LANL2DZ:3-21G*/PCM-THF) = -2476.002503 a.u.
NIMAG = 0

Ir	2.449568	-0.045717	-0.408871
N	2.673536	-2.038551	-0.046322
N	2.303487	1.974427	-0.702834
C	1.651938	-2.924469	-0.044898
C	2.284397	2.572733	-1.915400
H	0.665290	-2.514628	-0.209443
H	2.392861	1.912314	-2.766319
C	1.868333	-4.277462	0.161927
C	2.133117	3.944568	-2.042089
C	3.173163	-4.730070	0.366415
C	1.991120	4.718519	-0.888750
H	3.369440	-5.782676	0.532081
H	1.864766	5.792241	-0.959906
C	4.221998	-3.820181	0.343898
C	2.017077	4.100478	0.354918
H	5.241575	-4.153256	0.484600
H	1.913896	4.683195	1.260483
C	3.964133	-2.465414	0.125879
C	2.179425	2.716741	0.440762
C	2.603934	-0.260012	2.636036
C	5.355663	0.953522	-0.359079
C	2.522631	0.297185	3.911239
C	6.725646	0.735738	-0.235784
H	2.625898	-0.337129	4.785371
H	7.417318	1.565288	-0.339961
C	2.309646	1.670686	4.071067
C	7.218296	-0.548569	0.026211
C	2.184503	2.493428	2.955393
C	6.340784	-1.620478	0.160045
C	2.263669	1.940692	1.672649
C	4.964086	-1.408040	0.032558
C	2.462162	0.547710	1.501514
C	4.450886	-0.111359	-0.240485
H	1.027962	-4.958899	0.158740
H	2.246302	2.097824	5.065453
H	2.026238	3.557825	3.092296
H	2.123530	4.392037	-3.027154
H	8.285758	-0.710014	0.126205
H	6.735848	-2.611136	0.358865
H	2.773567	-1.325988	2.526588
H	4.988018	1.955313	-0.554335
C	-0.436338	0.460086	-1.333566
C	-0.368287	-0.546204	0.808436
C	-1.798588	0.448825	-1.330777
H	0.116736	0.840445	-2.182725
C	-1.728251	-0.582458	0.872155
H	0.239321	-0.877015	1.642842
C	-2.537055	-0.089903	-0.215059
H	-2.335882	0.848149	-2.183417
H	-2.211092	-0.971228	1.761590
C	-3.924864	-0.116111	-0.175727
C	-5.160699	-0.145524	-0.129004
Cl	2.477749	-0.586025	-2.773640
N	0.334297	-0.055695	-0.291953
Si	-6.979832	-0.179031	-0.057780
C	-7.607488	-0.742341	-1.761481
H	-7.147579	-0.058582	-2.494713
C	-7.618650	1.576757	0.284317
H	-8.717500	1.531592	0.364369
C	-7.523254	-1.398682	1.300316
H	-7.515731	-2.399640	0.836803
C	-8.960837	-1.115168	1.795440
H	-9.261392	-1.864457	2.541486
H	-9.016249	-0.127976	2.271462
H	-9.690301	-1.140029	0.977589
C	-7.249604	2.520816	-0.882350
H	-7.591130	3.544184	-0.671279
H	-6.160060	2.548475	-1.016860
H	-7.705243	2.196979	-1.826275
C	-9.141525	-0.636118	-1.903207
H	-9.453906	-0.913710	-2.919995
H	-9.642846	-1.318798	-1.205442
H	-9.499660	0.381792	-1.703769
C	-6.559392	-1.435288	2.507365
H	-6.874220	-2.208827	3.222321
H	-5.532098	-1.647361	2.190594
H	-6.559484	-0.472651	3.033517
C	-7.142442	-2.176558	-2.094499
H	-7.438305	-2.451376	-3.116703
H	-6.052622	-2.269379	-2.011338
H	-7.602079	-2.899326	-1.407493
C	-7.051447	2.140600	1.605354
H	-7.383672	3.177798	1.756068
H	-7.376571	1.550737	2.470694
H	-5.954044	2.133645	1.578296

T_1 Min2
E(PBE0/LANL2DZ:3-21G*/PCM-THF) = -2476.629057 a.u.
G(PBE0/LANL2DZ:3-21G*/PCM-THF) = -2476.004087 a.u.
NIMAG = 0

Ir	-2.385152	0.066994	-0.337723
N	-2.626446	2.041035	0.162876
N	-2.280488	-1.922529	-0.758317
C	-1.609763	2.883767	0.458724
C	-2.089890	-2.419412	-2.003133
H	-0.616362	2.458915	0.447093
H	-2.008931	-1.682788	-2.791990
C	-1.834289	4.217017	0.759317
C	-2.019152	-3.783547	-2.230260
C	-3.144277	4.699842	0.754022
C	-2.148187	-4.659409	-1.149204
H	-3.348053	5.739306	0.982109
H	-2.098821	-5.730870	-1.302597
C	-4.186696	3.832040	0.460523
C	-2.337542	-4.146083	0.126617
H	-5.210045	4.182484	0.461317
H	-2.435145	-4.806750	0.977768
C	-3.920310	2.492518	0.167023
C	-2.397707	-2.763939	0.317171
C	-2.738364	0.075236	2.693060
C	-5.309234	-0.873205	-0.574280
C	-2.846697	-0.577071	3.919267
C	-6.680219	-0.625999	-0.617091
H	-2.956276	0.002875	4.829834
H	-7.370205	-1.441269	-0.809793
C	-2.816797	-1.975448	3.987986
C	-7.175283	0.666948	-0.413495
C	-2.676344	-2.726818	2.826857
C	-6.297244	1.716052	-0.162618
C	-2.562016	-2.078316	1.590953
C	-4.919318	1.472022	-0.124506
C	-2.582998	-0.660664	1.511713
C	-4.403199	0.170804	-0.345507
H	-0.995776	4.859238	0.994014
H	-2.904640	-2.473676	4.946772
H	-2.655743	-3.809805	2.888483
H	-1.866960	-4.149639	-3.236988
H	-8.243134	0.851828	-0.446282
H	-6.691151	2.713906	-0.000305
H	-2.767210	1.158576	2.658201
H	-4.944883	-1.881892	-0.738001
C	0.462814	0.988956	-1.034033
C	0.428748	-0.755022	0.582408
C	1.820171	1.019670	-1.018649
H	-0.111651	1.601171	-1.718463
C	1.785137	-0.771414	0.642419
H	-0.165514	-1.419290	1.196916
C	2.578570	0.139738	-0.155666
H	2.346566	1.698690	-1.679560
H	2.284273	-1.469191	1.304728
C	3.960531	0.159014	-0.104301
C	5.198018	0.176079	-0.053204
Cl	-2.391215	0.775561	-2.691582
N	-0.298525	0.123913	-0.229310
Si	7.020545	0.205044	0.008903
C	7.559308	2.002483	-0.286729
H	7.110201	2.302622	-1.248178
C	7.697784	-0.887649	-1.388545
H	8.797608	-0.897378	-1.308814
C	7.596197	-0.407424	1.717091
H	7.571777	0.470778	2.384129
C	9.048320	-0.938997	1.683626
H	9.368122	-1.234505	2.692826
H	9.119613	-1.823056	1.037612
H	9.753948	-0.187362	1.311071
C	7.311200	-0.306186	-2.767195
H	7.677620	-0.956876	-3.573758
H	6.218976	-0.237340	-2.857726
H	7.733534	0.694878	-2.918303
C	9.092315	2.148198	-0.406158
H	9.362019	3.187977	-0.639162
H	9.580849	1.883946	0.540378
H	9.502719	1.505676	-1.195464
C	6.666150	-1.482549	2.322590
H	7.003038	-1.750460	3.334045
H	5.630842	-1.128165	2.380335
H	6.678424	-2.394331	1.712512
C	7.020526	2.950727	0.806265
H	7.289435	3.991998	0.579602
H	5.928688	2.884069	0.887114
H	7.453561	2.698691	1.783315
C	7.183773	-2.339769	-1.275477
H	7.548527	-2.943336	-2.118811
H	7.517534	-2.817716	-0.346706
H	6.086334	-2.355669	-1.294583

S11. References

S1. R. Davidson, Y.-T. Hsu, G. C. Griffiths, C. Li, D. Yufit, R. Pal and A. Beeby, *Inorg. Chem.*, 2018, **57**, 14450-14462.

S2. T. A. Zeidan, S. V. Kovalenko, M. Manoharan, R. J. Clark, I. Ghiviriga and I. V. Alabugin, *J. Am. Chem. Soc.*, 2005, **127**, 4270-4285.

S3. M. S. Lowry, W. R. Hudson, R. A. Pascal and S. Bernhard, *J. Am. Chem. Soc.*, 2004, **126**, 14129-14135.

S4. O. V. Dolomanov, L. J. Bourhis, R. J. Gildea, J. A. K. Howard and H. Puschmann, *J. Appl. Cryst.,* 2009, **42**, 339-341.

S5. G. M. Sheldrick, SHELXTL: Suite of Programs for Crystal Structure Analysis, Tammanstrasse 4: Gottingen, 1998.

S6. G. D. Sutton, C. Jiang, G. Liu and T. S. Teets, *Dalton Trans.*, 2023, **52**, 3195-3202.

S7. C. Jiang and T. S. Teets, *Inorg. Chem.*, 2022, **61**, 8788-8796.

S8. C. Wohlfarth and B. Wohlfahrt, Pure Organic Liquids – C5, Landolt-Börnstein – Group IV Physical Chemistry 18B, M. D. Lechner (Ed.), Springer Materials, 2002, pp 206-254. DOI: 10.1007/10639283_6

S9. R. Davidson, Y.-T. Hsu, T. Batchelor, D. Yufit and A. Beeby, *Dalton Trans.*, 2016, **45**, 11496-11507.

S10. W. H. Melhuish, *J. Phys. Chem.*, 1961, **65**, 229-235.

S11. M. J. Frisch, G. W. Trucks, H. B. Schlegel, G. E. Scuseria, M. A. Robb, J. R. Cheeseman, G. Scalmani, V. Barone, G. A. Petersson, H. Nakatsuji, X. Li, M. Caricato, A. V. Marenich, J. Bloino, B. G. Janesko, R. Gomperts, B. Mennucci, H. P. Hratchian, J. V. Ortiz, A. F. Izmaylov, J. L. Sonnenberg, D. Williams-Young, F. Ding, F. Lipparini, F. Egidi, J. Goings, B. Peng, A. Petrone, T. Henderson, D. Ranasinghe, V. G. Zakrzewski, J. Gao, N. Rega, G. Zheng, W. Liang, M. Hada, M. Ehara, K. Toyota, R. Fukuda, J. Hasegawa, M. Ishida, T. Nakajima, Y. Honda, O. Kitao, H. Nakai, T. Vreven, K. Throssell, J. A. Montgomery, Jr., J. E. Peralta, F. Ogliaro, M. J. Bearpark, J. J. Heyd, E. N. Brothers, K. N. Kudin, V. N. Staroverov, T. A. Keith, R. Kobayashi, J. Normand, K. Raghavachari, A. P. Rendell, J. C. Burant, S. S. Iyengar, J. Tomasi, M. Cossi, J. M. Millam, M. Klene, C. Adamo, R. Cammi, J. W. Ochterski, R. L. Martin, K. Morokuma, O. Farkas, J. B. Foresman, and D. J. Fox, Gaussian 16, Revision B.01, Gaussian, Inc., Wallingford CT, 2016.

S12. a) A. D. Becke, *J. Chem. Phys.,* 1993, **98**, 5648-5652; b) C. Lee, W. Yang and R. G. Parr, *Phys. Rev. B,* 1988, **37**, 785-789.

S13. a) T. H. Dunning Jr. and P. J. Hay in *Modern Theoretical Chemistry*, (Ed:. H. F. Schaefer III) Vol. 3, Plenum, New York, 1976; b) P. J. Hay and W. R. Wadt, *J. Chem. Phys.,* 1985, **82**, 270-283; c) W. R. Wadt and P. J. Hay, *J. Chem. Phys.,* 1985, **82**, 284-298; d) P. J. Hay and W. R. Wadt, *J. Chem. Phys.,* 1985, **82**, 299-310.

S14. a) G. A. Petersson, M. A. Al-Laham, *J. Chem. Phys.* **1991**, *94*, 6081–6090; b) G. A. Petersson, A. Bennett, T. G. Tensfeldt, M. A. Al-Laham, W. A. Shirley, J. Mantzaris, *J. Chem. Phys.* **1988**, *89*, 2193–2218.

S15. a) H. A. Al-Attar, G. C. Griffiths, T. N. Moore, M. Tavasli, M. A. Fox, M. R. Bryce and A. P. Monkman, *Adv. Funct. Mater.,* 2011, **21**, 2376-2382; b) M. Tavasli, T. N. Moore, Y. Zheng, M. R. Bryce, M. A. Fox, G. C. Griffiths, V. Jankus, H. A. Al-Attar and A. P. Monkman, *J. Mater. Chem*., 2012, **22**, 6419-6428; c) Y. Zheng, A. S. Batsanov, M. A. Fox, H. A. Al-Attar, K. Abdullah, V. Jankus, M. R. Bryce, A. P. Monkman, *Angew. Chem. Int. Ed*., 2014, **53**, 11616–11619; d) H. Benjamin, Y. Zheng, A. S. Batsanov, M. A. Fox, H. A. Al-Attar, A. P. Monkman and M. R. Bryce, *Inorg. Chem.,* 2016, **55**, 8612-8627; e) H. Benjamin, M. A. Fox, A. S. Batsanov, H. A. Al-Attar, C. Li, Z. Ren, A. P. Monkman and M. R. Bryce, *Dalton Trans.,* 2017, **46**, 10996-11007; f) A. M'hamedi, M. A. Fox, A. S. Batsanov, H. A. Al-Attar, A. P. Monkman, M. R. Bryce, *J. Mater. Chem. C,* 2017, **5**, 6777–6789; g) D. G. Congrave, Y.-T. Hsu, A. S. Batsanov, A. Beeby and M. R. Bryce, *Dalton Trans.,* 2018, **47**, 2086–2098; h) H. Benjamin, Y. Zheng, V. N. Kozhevnikov, J. S. Siddle, L. J. O'Driscoll, M. A. Fox, A. S. Batsanov, G. C. Griffiths, F. B. Dias, A. P. Monkman and M. R. Bryce, *Dalton Trans.,* 2020, **49**, 2190-2208; i) R. M. Edkins, Y.-T. Hsu, M. A. Fox, D. Yufit, A. Beeby and R. J. Davidson, *Organometallics*, 2022, **41**, 2487-2493; j) R. Davidson, Y.-T. Hsu, M. A. Fox, J. A. Aguilar D. Yufit, and A. Beeby, *Inorg. Chem.,* 2023, **62**, 2793-2805; k) A. M'hamedi, A. S. Batsanov, M. A. Fox, J. A. Aguilar and M. R. Bryce, *Eur. J. Inorg. Chem.,* 2023, **26**, e202300423.

S16. J. Tomasi, B. Mennucci and E. Cancès, *J. Mol. Struct. (Theochem),* 1999, **464**, 211-226.

S17. C. Adamo and V. Barone, *J. Chem. Phys.,* 1999, **110**, 6158-6170.

S18. I. Soriano-Diaz, E. Ortí and A. Giussani*, Inorg. Chem*., 2024, **63**, 16600-16604.

S19. a) S. DiLuzio, V. Mdluli, T. U. Connell, J. Lewis, V. VanBenschoten and S. Bernhard, *J. Am. Chem. Soc.,* 2021, **143**, 1179-1194; b) P. A. Scattergood, A. M. Ranieri, L.

Charalambou, A. Comia, D. A. W. Ross, C. R. Rice, S. J. O. Hardman, J.-L. Heully, I. M. Dixon, M. Massi, F. Alary and P. I. P. Elliott, *Inorg. Chem.*, 2020, **59**, 1785-1803; c) P. Kumar, M. Pérez-Escribano, D. M. E. van Raamsdonk and D. Escudero, *J. Phys. Chem. A*, 2023, **127**, 7241-7255.

S20. C. F. R. Mackenzie, S. -Y. Kwak, S. Kim and E. Zysman-Colman*, Dalton Trans*., 2023, **52**, 4112-4121.

S21. R. Dennington, T. Keith and J. Millam, Semichem Inc., Shawnee Mission, KS, 2019. GaussView, Version 6.

S22. A. R. Allouche, *J. Comput. Chem*., 2011, **32**, 174-182.

S23. T. Lu and F. Chen, *J. Comput. Chem*., 2012, **33**, 580-592.